Modification of the Electronic Properties of the TCNQ Anion Radical Salts by Cation Design and Carrier Doping

Thesis
Submitted to the Graduate School of Chemical Sciences and Engineering
Hokkaido University

In Fulfillment of the Requirement
for the Degree of Doctor of Science

Hiroyuki Kubota

March, 2015

Acknowledgement

I would like to express my gratitude to all the people who kindly support my study and my life as a doctoral course student of the Solid-State Chemistry Laboratory, Graduate School of Chemical Sciences and Engineering, Hokkaido University.

First of all, I wish to extend my sincere appreciation for Professor Tamotsu Inabe for accepting me, even though I once stopped my study. Without his supervision, I could not have finished my work. I am very glad that I was able to study under such a great, broad-minded professor.

Secondly, I would like to express my deep gratitude to Associate Professor Jun Harada, for giving much time for the X-ray crystal structural analysis, revising CIF file, and doing theoretical calculation.

I also appreciate Dr. Yukihiro Takahashi, for relieving me from many troubles, encouraging me when I felt down, giving me many important advices about the measurements, presentation, and the attitude to the study.

To Dr. Hiroyuki Hasegawa, thank you for giving your time for discussing my study, semiconductor meeting, and good leisure with other laboratory members. All of them are my precious experience.

I appreciate Professor Kazuki Sada, for giving important advices as sub-adviser and as chief-examiner of my thesis. I remember your kind and considerate regard for individual students.

To Professor Takanori Suzuki, I would like to express my gratitude for your kind advice about the synthesis and about the development of my study, and for the important pointing out in the preliminary examination. I owe the improvement of my thesis to your encouragement.

To Professor Toshihiro Shimada, thank you for your understanding about my study, and for making a new apparatus for the IR measurement in high temperature region. Even though I regret not having successfully summarized the IR data, the unit for controlling the temperature will become useful in future works.

I tender my cordial thanks to Professor Yukio Hinatsu and Associate Professor Makoto Wakeshima for the support of SQUID measurement.

I would like to express a special thanks to Mr. Tetsuzo Habu, for processing glassware, to Mr. Kazuhiko Matsudaira, Mr. Shingo Mukai, Mr. Yusuke Kawamura, for manufacturing and processing metal apparatus, and to Dr. Etsuo Kuramoto and his family members, for giving me a new PC and many kinds of convenient software for my study.

To my former and current mates, Dr. Derrick Ethelbhert Yu, Dr. Hiromi Minemawari, Dr. Manabu Ishikawa, Shingo Sasaki, Rena Obara, Ai Kukino, Hideyuki Sugawara, Masachika Nagare, Satoshi Yamashita, Yukari Yamada, Shigeki Sakamoto, Ryuta Ikeda, Akihiro Kakizaki, Sho Miyauchi, Tetsuro Miyahira, Kumpei Yamada, Kotaro Tajima, Ryora Ando, Yusuke Miki, Dr. Yukari Takahashi, Yukihisa Sakurada, Takahisa Sasaki, Yasuhiro Tanaka, Momoko Noda, Tatsuya Nakatsugawa, Marie Fukusaku. Saori Matsuo, Naoko Watanabe, Takahiro Takano, Kei hayakawa, Shinya Takao, Taku Ando, Masaaki Yokoyama, Dr. Jose Judy Fe Fernandez, Yu Kudo, Yuki Nakagawa, Sumire Kobayashi, Shunsuke Ashidate, Tsuyoshi Osaki, Yusuke Takita, Yuki Nakajima, Katsuya Takayama, and Ms. Shoko Demachi, Kazuki Ito, Shota Sato, Takafumi Shimojo, Tomohiro Mikasa, Masaki Otani, Hirotaka Kitahara, Masashi Kurokawa, Sarasa Matsuno, Atsuki Kimura, Hideaki Oyamaguchi, Keisuke Kobayashi, Takuro Shimada, Mika Takehisa, Azusa Oka, Tomomi Nakata, Rin Noutsuka, Naho Yoneyama, and Ms Yoshie Kosuge, I was very glad to share the laboratory life with you. I hope I can see you again the other day, in my next life stage.

To Dr. Giancarlo Soriano Lorena, thank you for talking to me in English every day. Owing to you, I was able to improve my English skill, and I believe I was able to exploit it in the international conference and writing my thesis.

To Seiya Yokokura, thank you for giving your time to help me when I was in trouble. Especially, in the initial term of my doctoral course, almost all the skill for physical measurements was lost. Your kind explanation about the instruments has lead to the recovery of my knowledge.

To my previous colleagues, Gaku Hijii, Jun Suzuki, Yousuke Watanabe, Yousuke Kawakami, Taketo Ito, Hiroki Nakamata, thank you for your visiting Sapporo, and encouraging me. I owe what I am to you.

Finally, to my wife and our parents, thank you for permitting me to come back to Hokkaido University, and for supporting my study life.

Hiroyuki Kubota

Contents

Chapter 1. General Introduction

1.1. Organic electronics

Conventionally, it has been considered that electrical conductivity and magnetism are inherent physical properties in metals, and that all the organic compounds are insulators which do not possess such properties. In 1950's, however, a highly conductive charge transfer complex, composed of aromatic compound perylene and bromine, was discovered by H. Akamatsu, H. Inokuchi, and Y. Matsunaga [1]. Owing to this discovery, the established concept that regards organic materials are insulating was exploded and the possibility of attaining metallic physical properties for even organic materials was proposed. Since then, organic conductors and organic magnets have been successively developed. As the investigation progressed, it proved that the electronic functions of organic crystals can be modified from insulating to superconductive, metallic or semiconducting, and that the spin function can be modified from diamagnetic to paramagnetic, ferromagnetic, or antiferromagnetic [2-5].

Organic electronics is a discipline of designing, synthesizing, and applying the organic compounds which own the charge transport electronic functions. Organic compounds possess many advantages which are not observed for inorganic compounds; flexibility, solubility in solvents, and feasibility of purification, and tuning of the orientation of the component anisotropic molecules. If organic molecules can take the place of inorganic electronics, low cost, light weight, and large area devices or products will be feasible [6].

1.2. The guidelines for designing conducting organic crystals

To obtain a conductive organic crystal, it is necessary to understand why general

organic compounds are insulators. The reason will be explained by using the energy band diagram. In the case of metal, the conduction band is partially occupied (Cu, for example) or overlapped with the valence band (Zn and Pb, for example), as described in Figure 1.2.1 [7]. Thus there is no band gap at the Fermi level. The electrons in partially occupied conduction band or higher levels of the overlapped conduction band can easily be promoted to the higher empty levels, therefore the current easily flows in metals. On the other hand, there are two following principal reasons why organic crystals have insulating behaviors.

(i) Since there is a rather large energy difference between the highest occupied molecular orbital (HOMO) and the lowest unoccupied molecular orbital (LUMO) in general organic compounds, the valence band composed of HOMOs and the conduction band composed of LUMOs do not overlap at all. In addition, most of organic compounds have closed-shell electronic structure. Thus the valence bands are filled with electrons and there is no electron in the conduction bands, as described in Figure 1.2.2.

(ii) The intermolecular overlaps of the molecular orbitals are extremely small, i.e. the width of the band which consists of these orbitals is narrow. This is because the HOMOs of organic molecules are completely localized within the molecular framework. (This is also the reason why the valence bands and the conduction bands do not overlap.)

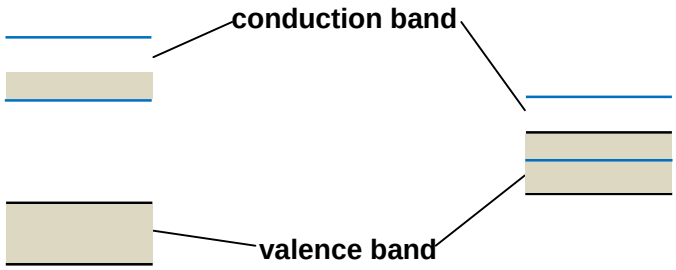

Figure 1.2.1. The energy band diagram of metals. The left one describes a partially occupied conduction band, and the right one describes a conduction band overlapped with the valence band.

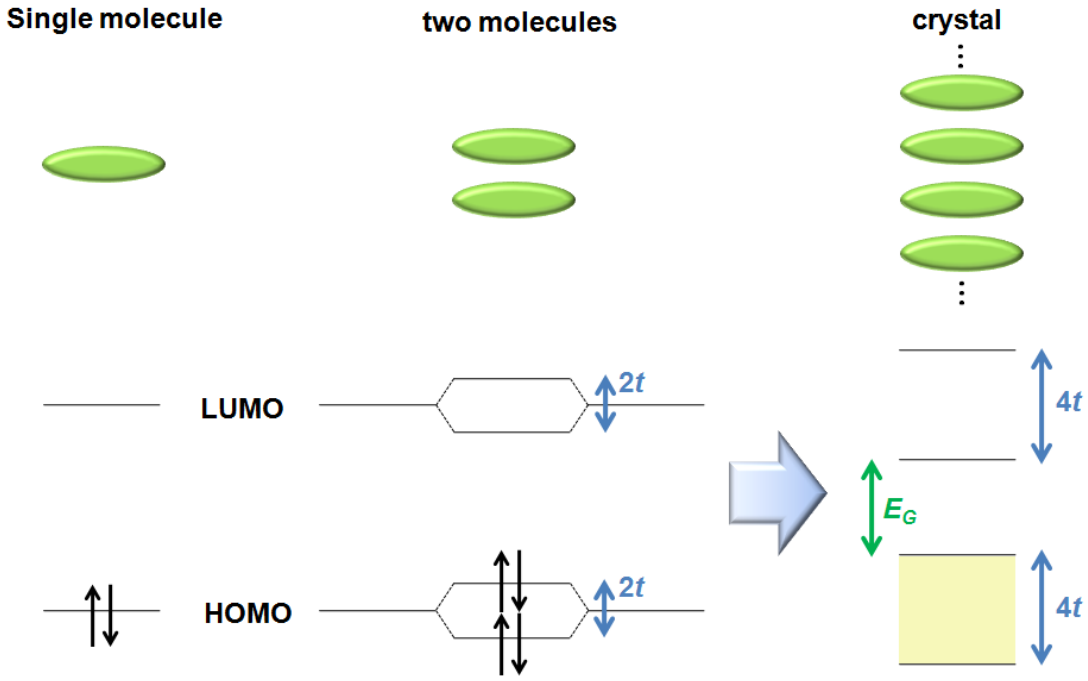

Figure 1.2.2. The energy band diagram of organic crystal.

These two features must be changed to obtain a conductive organic crystal. Initially, electrons in HOMO are required to move into LUMO in a certain way. To attain this for single-component organic crystal, designing an open-shell electronic structure, i.e. a neutral radical is considered to be effective. However, radical electrons tend to form

σ-bonds between adjacent two neutral radical molecules. If some bulky substituents are introduced to prevent the extinction of the radicals, the degree of freedom of the radical electrons will decrease, leading to a non-conducting state. To stabilize the neutral radicals without bulky substituents, the neutral radicals with hetero atoms-included ring structure and with both electron-donating substituent and electron-accepting substituent were designed [8]. Even if these attempts go successfully, the repulsion energy will be generated between an already-existed radical electron in a certain orbital and a new-coming radical electron in the crystal. This energy is called on-site Coulomb repulsion energy (*U*) [9], described in Figure 1.2.3. Since this repulsion is generally larger than the transfer energy of electron for most of the general organic compounds. As a result, metallic crystals have not been obtained by this method.

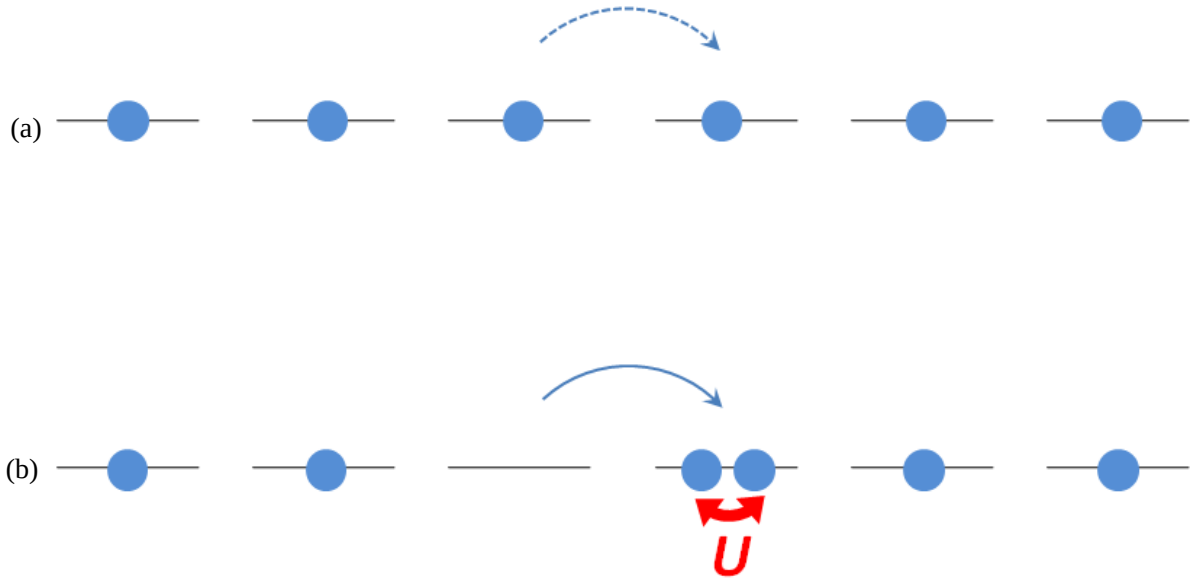

Figure 1.2.3. The model of the on-site Coulomb repulsion in an array of neutral radicals. The blue filled circles describe the electrons, and each horizontal line means the singly occupied molecular orbital (SOMO) of the single neutral radical. (a) The state before the electron transfer, and (b) the state after the electron transfer. The on-site Coulomb repulsion (*U*) operates between the two electrons occupied in the same molecular orbital, which requires extra energy for electron transfer.

As discussed above, it is quite difficult to attain a metallic state in single-component organic crystals. Thus, two-component crystal design will be more effective for the design of conductors. This method focuses on the charge transfer interaction, and was initially proposed by R. S. Mulliken [10]. The charge transfer is performed by the electron movement from one component to the other component. The former component is called (electron) donor, and the latter is called (electron) acceptor, and the complex which consists of a donor component and an acceptor component is called a charge transfer (CT) complex. As a result of the CT complex formation, the donor (or acceptor) molecules will be (fractionally) charged or neutral. Possible patterns of electron transportation between the same kind of molecules (for the case where donor (or acceptor) molecules are assembled in an array) are described as following schemes (Schemes1.1-3).

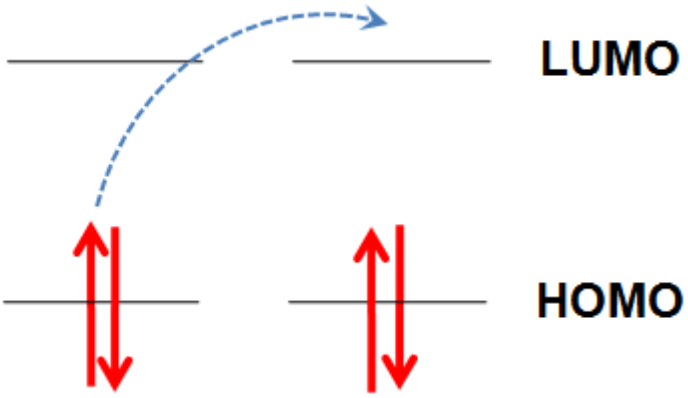

Scheme 1.1. Electron transportation between closed-shell molecules

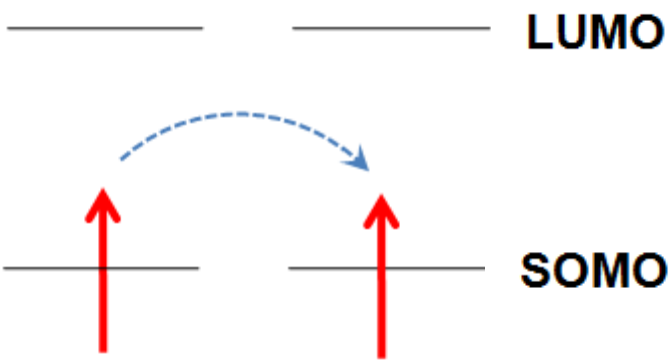

Scheme 1.2. Electron transportation between radicals

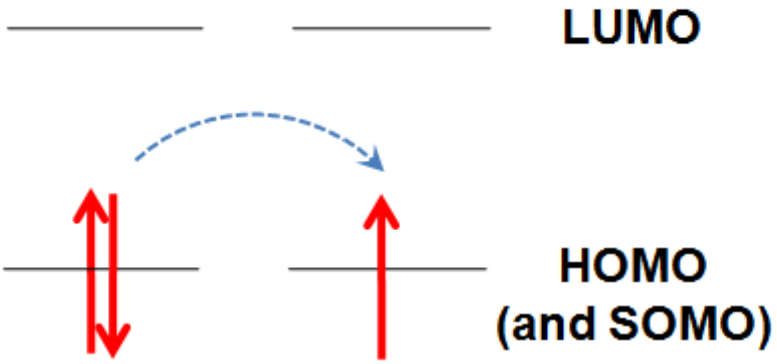

Scheme 1.3. Electron transportation between closed-shell molecule and radical

In the case of Scheme 1.1 (when the component is neutral), an electron must move from the HOMO of one molecule to energetically higher LUMO of another molecule. In this case, transport of electrons costs large energy.

In the case of Scheme 1.2 (when the component is fully charged), an electron is transported from one HOMO (strictly speaking, there is only one electron in the orbital. Thus the orbital should be called singly occupied molecular orbital (SOMO)) to another HOMO (SOMO). In this case, it becomes much easier to transport an electron because it is transportation between the same energy levels. However, the Coulomb repulsion

will be generated as described in Figure 1.2.3.

In the case of Scheme 1.3 (when the component is fractionally charged), the energy states after the transportation is exactly the same as before, and no extra cost of on-site Coulomb repulsion occurs. Thus the conductivity is expected to be the highest in this case. Most of the obtained conductive organic crystals are the type of (3) and possessing a fractional charge for each molecule [11].

Unlike neutral radicals, ion radicals of π-conjugated molecules can construct π-π networks, and then allow the system to be stabilized easily. In planar π-electron conjugated molecules, face-to-face stack is feasible, forming the conduction path. Tetrathiafulvalene (TTF) and 7,7,8,8-tetracyanoquinodimethane (TCNQ) are a representative planar donor and acceptor, respectively.

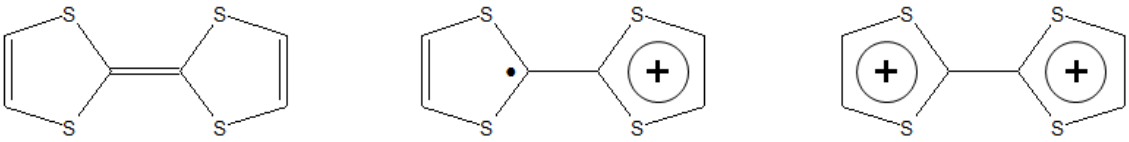

Figure 1.2.4. The structure of TTF. (a) The neutral charge state of TTF, (b) the TTF cation radical, (c) the dicationic state of TTF.

TTF does not have the stability derived from the aromaticity in the neutral state (Figure 1.2.4 (a)). When the one-electron oxidation occurs, the electron system turns the combination of 6π and 7π, which can keep the aromatic stability with replacing each other (Figure 1.2.4 (b)). Even when two-electron oxidation occurs, the stability can be maintained because of the 6π-6π electron system (Figure 1.2.4 (c)). In this way, TTF has two different stably oxidized states.

Figure 1.2.5. The structure of TCNQ; (a) the neutral state of TCNQ, (b) the TCNQ anion radical..

On the other hand, TCNQ has the quinoid ring centered on the molecule which turns benzenoid by one-electron reduction. Thus, TCNQ anion radical is also stable. Four cyano groups in the TCNQ molecule attract the negative charge, which contributes to the stabilization of the anionic state of TCNQ.

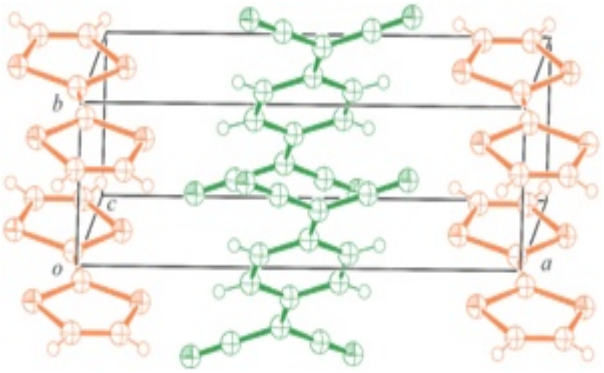

Figure 1.2.6. The crystal structure of TTF-TCNQ.

TTF-TCNQ, a CT complex consists of these donor and acceptor, is well known as the first metallic organic crystal [12]. The crystal structure is shown in Figure 1.2.4. In this crystal, TTF and TCNQ individually form face-to-face stacked columns. Since the degree of charge transfer is 0.59, in both columns radicals and neutral molecules co-exist. In this manner, both of the points (i) and (ii) were overcome. Thus, by adopting charge transfer complexes as the objects, the guideline for designing the

conductive organic crystals has been greatly progressed.

1.3. Background of the study

As stated in 1.2, “fractional charge in each molecule”, which is an important requirement for constructing conductive organic crystals, can be attained by using charge transfer complexes. In addition, planar component molecules can stack in a face-to-face manner, resulting in a large overlap of the molecular orbitals. However, not all the charge transfer complexes which consist of fractionally-charged molecules have a metallic behavior. This is because donor components and acceptor components can form mixed-stack structures. For mixed-stack structures, different energy levels of the adjacent molecules (HOMO of a donor and LUMO of an acceptor) contribute to the CT interaction, leading to a completely filled energy band as described in Figure 1.3.1.

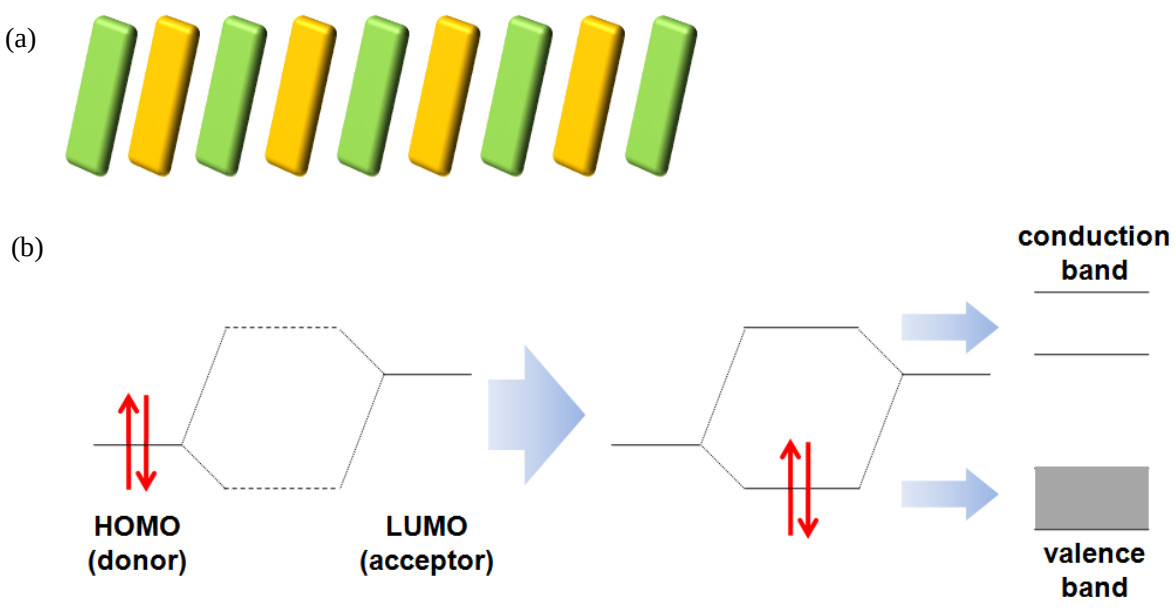

Figure 1.3.1. (a) The model of the mixed-stack structure. Different colors describe different kinds of molecules (donors or acceptors). (b) The energy state of the mixed-stack structure. The left side is before the complex formation, the right side is after the complex formation.

On the other hand, providing donor components or acceptor components form columns separately, the energy levels of the adjacent molecules or radicals will be equal to each other, forming incompletely occupied bands, as described in Figure 1.3.2. Therefore, “forming segregated columns” is another important condition for organic crystals to become a conductor.

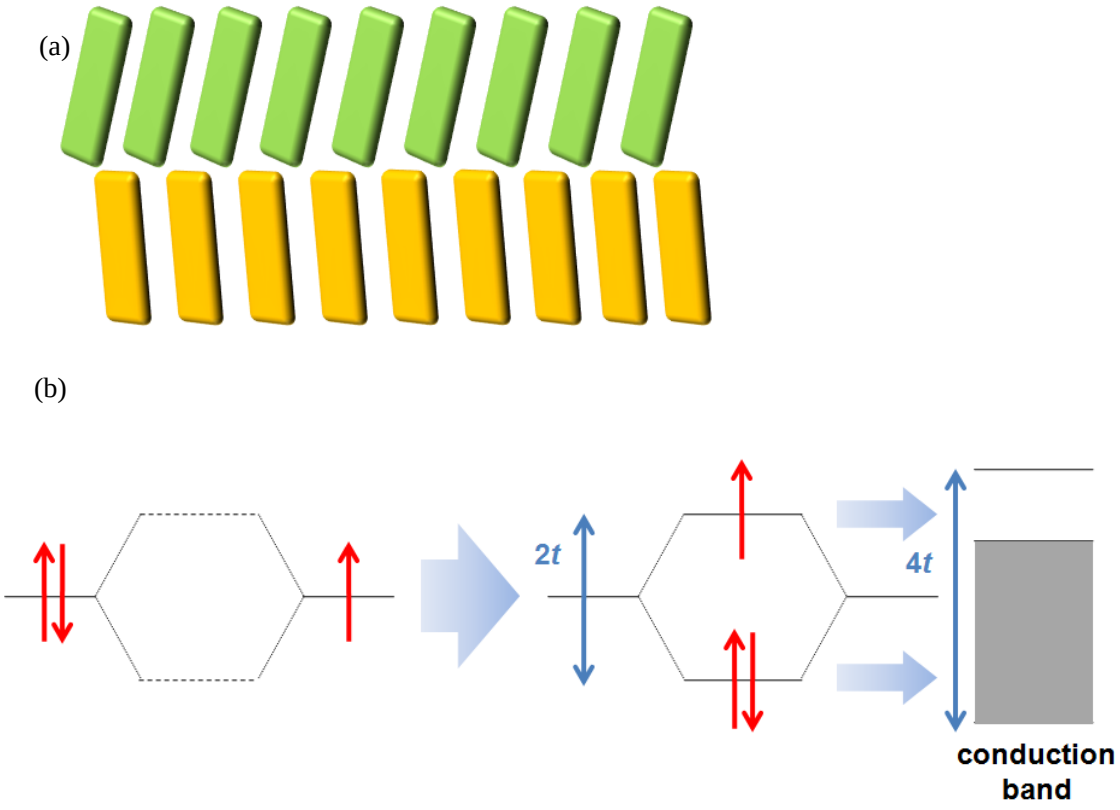

Figure 1.3.2. (a) The model of the segregated-stack structure. Different colors describe different kinds of molecules (donors or acceptors). (b) describes the energy state of the segregated-stack structure with the degree of charge transfer being 1/2. The left side is before the complex formation, the right side is after the complex formation.

For the CT complexes, the stacking patterns and the amount of the formal charge depend on various parameters; e. g., relative strength of the donor and acceptor,

molecular shape, relative size, and the stoichiometry of the two components.

1.4. The motivation and the aim of the study, and the advantage of anion radical salts

Considering above, in this study, what is emphasized on is not making new conductive organic crystals, but what condition can affect the formal charge, and how the stacking state and then the physical properties can be tuned under the given stoichiometry. This type of study is significant for the fundamental study of the design of the electronic function. For such investigation, the number of parameters which influence the degree of charge transfer should be reduced, and the crystal structure must be systematically modified, maintaining fractionally charged states. Radical ion salts are considered to be desirable for the requirements above [13, 14].

In a broad sense, radical ion salts can be regarded as a kind of charge transfer complex, and the fundamental properties are almost the same. The only difference is that one of the two components is a closed-shell ion. This difference is quite important in this study. Providing that the stoichiometry is other than 1:1, the fractionally charged state can certainly be obtained. In addition, in general, the closed-shell ionic component cannot interact with the counter donor or acceptor component by the overlap of the orbitals. Namely, there is only a little possibility to form a mixed-stack structure. Nevertheless, there exist radical salts with mixed-stack structure. These can be classified into the following types. (In the following discussion, the term “mixed-stack structure” will be used in a broad sense. In other word, it will describe the non-segregated stack. Providing that the donor component and the acceptor component (either one of which is a closed-shell ion) are indicated by D and A respectively, not only DADA type but also DAAD and DAA are included in mixed-stack structure.)

(1) The size of the closed-shell ionic component is much larger than that of the radical component, thus the crystal packing is dominated by the former component. In particular, if the closed-shell ionic component has bulky substituents or is a polymer, the stack of the radical component is often separated, leading to mixed-stack structure [15-18], as shown in Figures 1.3.3 and 1.3.4.

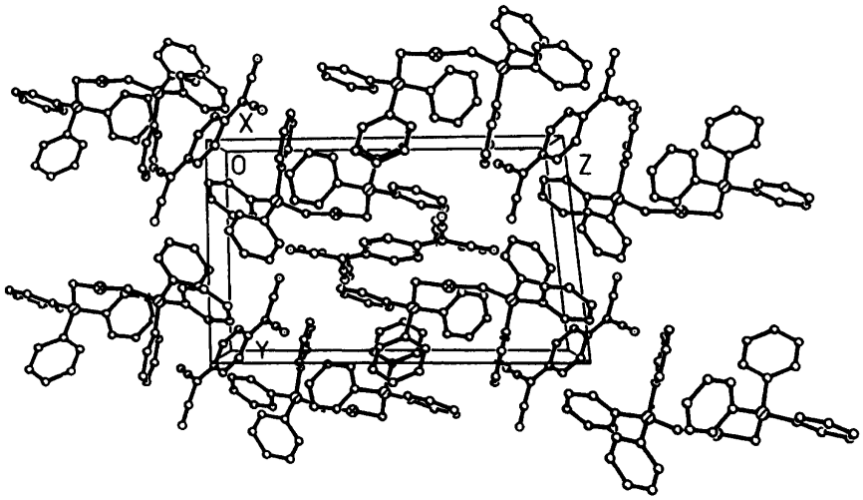

Figure 1.3.3. Packing diagram for $[Au(CH_2PPh_3)_2](TCNQ)$ [15]. The cation component has bis(triphenylphosphine) structure, and is much larger than TCNQ, leading to the mixed-stack (DADA) structure.

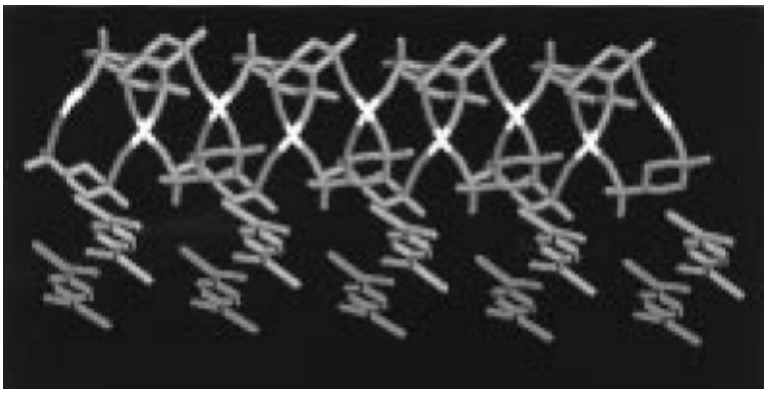

Figure 1.3.4. The structural model of the TCNQ salt of a cation polymer {[M(dmb)$_2$]$^+$}$_n$, M = Ag and dmb = 1,8-diisocyano-*p*-menthane [17]. The cation component is 1-D chain polymer. The crystal structure seems to be dominated by the arrangement of the cation polymer. As a result, TCNQ anion cannot form segregated columns, but dimerized instead. Each TCNQ dimer is completely independent of others.

(2) π–π interaction between the closed-shell ionic component and the radical component is possible. If both of the two components have aromatic rings, they can interact each other by having their ring part face-to-face (with the aid of electrostatic interactions) in some cases. Especially, both components are planar, mixed-stack structure such as DADA can occur [19-23], as shown in Figures 1.3.5 and 1.3.6.

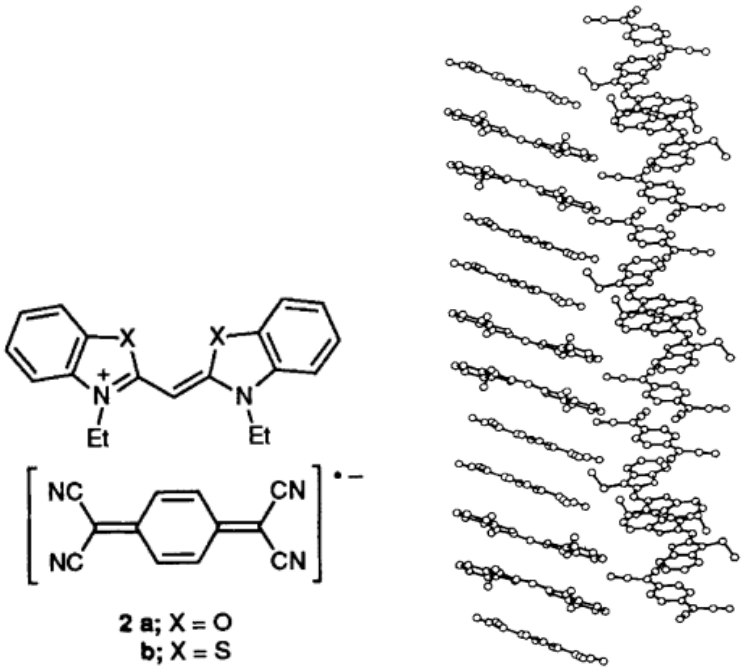

Figure1.3.5. The structural model of the 4,5,4',5'-Dibenzo-3,3'-diethyloxacyanine-TCNQ [19]. The cation component is π-conjugated and planar. Thus it can interact with another cation on one side and can also interact with TCNQ anion on the other side, leading to the formation of TCNQ anion dimer and DDAA type stack.

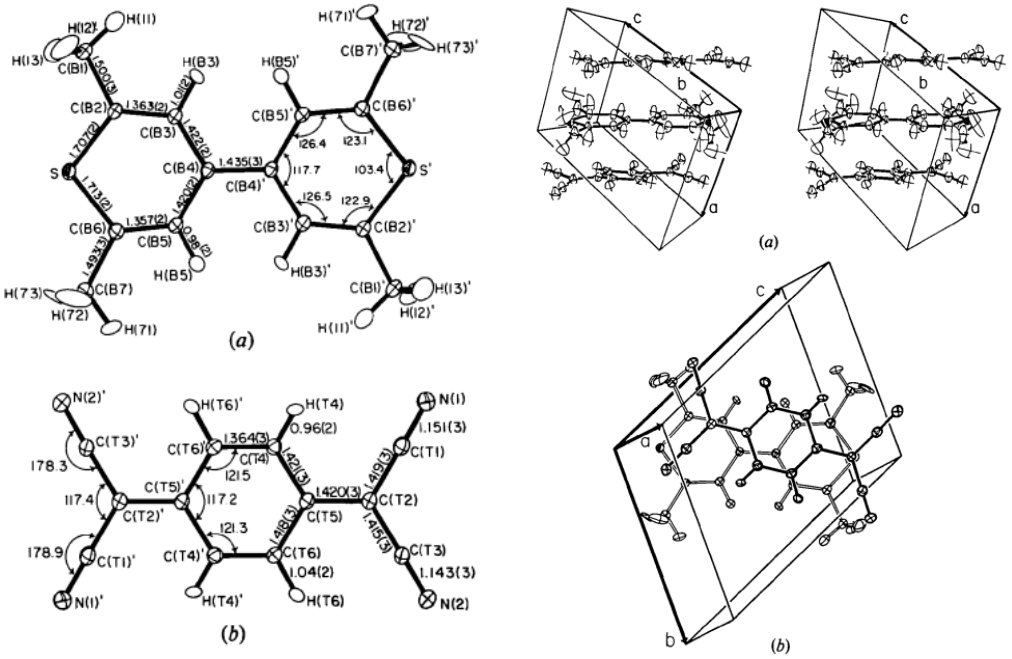

Figure 1.3.6. The structural model of TMBTP-TCNQ (TMBTP = 2,2',6,6'-tetramethyl-$\Delta^{4,4'}$-bithiopyran) [20]. The cation component is highly planar, and the positive charge is considered to be delocalized. The mixed-stack structure may be the result of the stability derived from the electrostatic interaction.

(3) There exists hydrogen-bond network(s). Since hydrogen bond is much stronger than π–π interaction, it is more dominant for crystal packing [24], as shown in Figure 1.3.7.

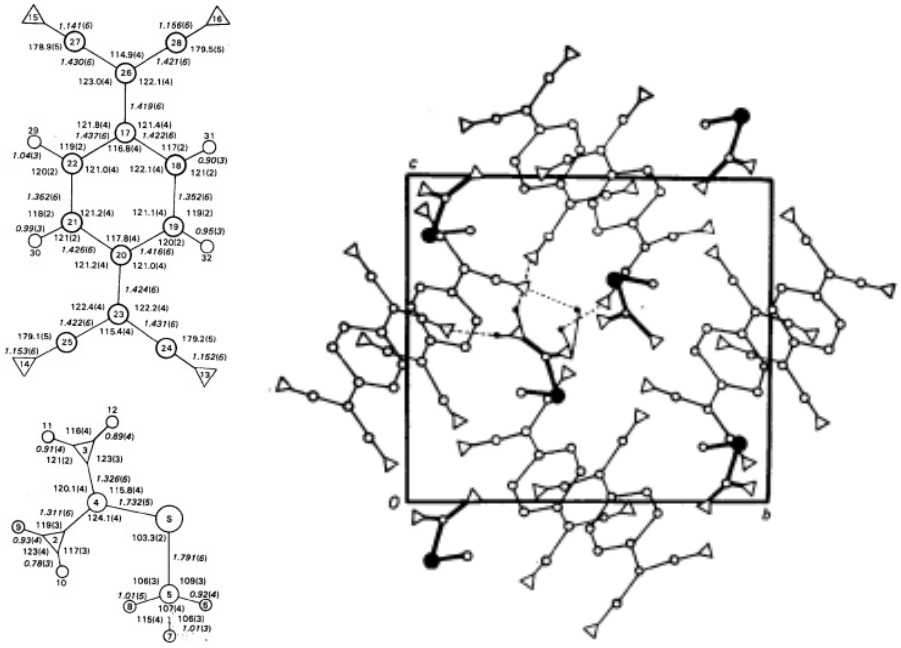

Figure 1.3.7. The structural model of S-Methylthiouronium-TCNQ [24]. The N atom in the TCNQ anion is connected with the H atom in the NH_2 group included in the cation component. Probably this hydrogen bond network is prior to the π–π interaction between the TCNQ anions, resulting in the independently located TCNQ anion dimer.

These examples are rather exceptional, and the main possible interaction is generally between donors or between acceptors, which are the counterpart of the closed-shell ionic component. Therefore, if we properly select the closed-shell ionic component, the segregated stack structure can be obtained automatically. Under an ideal condition, the stoichiometry of the crystal can only be influenced by the relative size of the closed-shell ionic component compared with the donor or acceptor.

The relationship between the size of the closed-shell ionic component and the stoichiometry was focused on in several studies. One is BEDO-TTF cation radical salts with tetracyanoallyl derivatives as the counter anions as shown in Figure 1.3.8 [26].

BEDO-TTF has a strong tendency to form 2-D π–π network systems. In this study, the variation of the effect of the interaction between BEDO-TTF and the anion component for the dimensionality was investigated by changing the anion size. The stoichiometry of the crystals varied 9:4, 2:1, 5:2, depending on the anion size. However, the crystal structures were analyzed only one of the four compounds, and the correlation between the anion size and the crystal structure and the stoichiometry has not been disclosed.

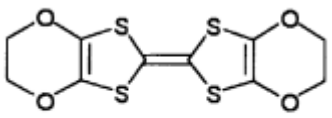

BEDO-TTF (BO)

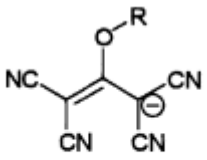

RO-TCA$^-$
(R=Me, Et, Pr, Bu)

Figure 1.3.8. The structure of BEDO-TTF (BO) and different size of tetracyanoallyl derivative anions.

Another is BTDA-TCNQ anion radical salts with various sizes of alkylammonium cations (Figure 1.3.9 (a)) [27]. For BTDA-TCNQ, the S atom in the heteroring can interact with the N atoms in adjacent BTDA-TCNQ, leading to the 2-D network formation as shown in Figure 1.3.9 (b). The stoichiometry showed some tendency to varying from 1:1 to 2:5 depending on the size of the alkylammonium cation, but only the part of the crystal structures were analyzed. This may be because the cation size

varies in three-dimensional, and in some cases it made very difficult to crystallize owing to the spatial requirement.

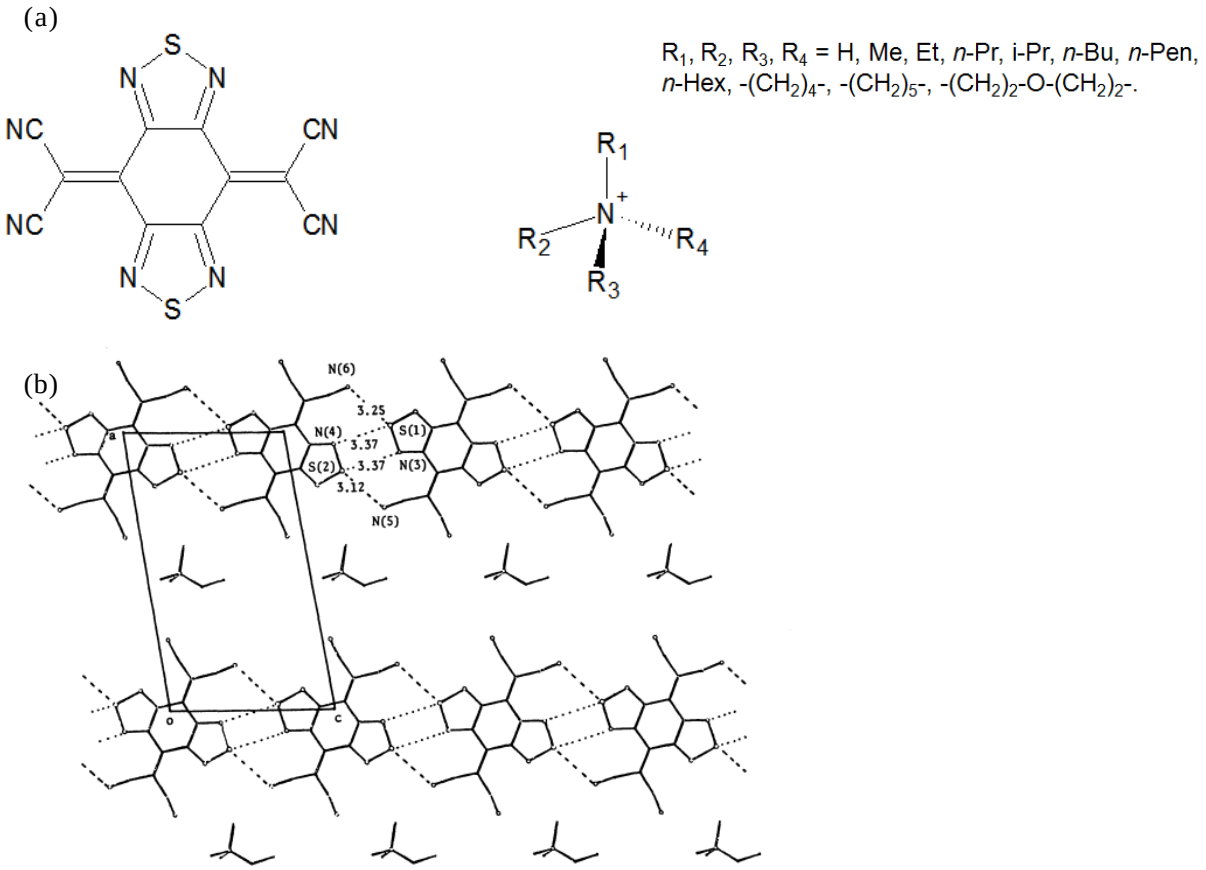

Figure 1.3.9. (a) The structure of BTDA-TCNQ and the ammonium cations. (b) The structural model of the BTDA-TCNQ salt with ethyltrimethylammonium cation [27]. The stoichiometry (cation : BTDA-TCNQ) is 1:1. Each S atom in the thiadiazole ring interacts with two N atoms of the adjacent BTDA anion, resulting in the formation of 2-D network (described as “ribbon-network” in the article).

In the above studies, radical salts with systematically varying the size of closed-shell ionic components were successfully prepared. The reason why the radical components form fractionally charged salts with closed-shell ionic components with various size may result from that they have ability to form two-dimensionally extended

networks. This property provides a capacity for accommodating various size closed-shell ionic components. Nevertheless, the structure analyses were possible only for a part of the radical salts. For the systematic size change of the closed-shell ionic component of the radical salts composed of donors or acceptors without ability to form two-dimensional networks, it is considered to be better to design the closed-shell ionic component with varying the length only along the one-dimensional direction. With such closed-shell ionic component design, the systematical investigation of the correlation between the crystal structure and the physical properties is expected to become possible.

For the counter donor or acceptor components, TTF or TCNQ is a good candidate for the study of the effects of relative size of closed-shell ionic components on the structure, stoichiometry, and properties of their radical salts, since they are excellent components that give partially charged radical salts. Many charge transfer complexes and cation radical salts using TTF analogues, especially ET (=BEDT, bis-ethylenedithiotetrathiafulvalene) are known [28-32]. Similarly, charge transfer complexes or anion radical salts of TCNQ are known [33, 34]. Considering the easiness of the design of the closed-shell ionic component, a series of TCNQ anion radical salts with the counter cation of which size is systematically modified are subjected to this study. The crystal structure and the relationship between the cation size and the crystal structure, the stoichiometry, and the physical properties are discussed in Chapter 2.

Even though the segregated stack structure and the fractional charge can successfully be achieved, the charge transport behavior of the crystal becomes often semiconducting instead of metallic. The main reason of this is as follows.

(1) There exists some lattice distortion in the segregated column, inducing the

multimerization such as dimerization or trimerization.

(2) The strong electron correlation operates, because the band width of the conduction band is narrow. In a broad sense, the case of $\gamma = 1$ is also involved in the category.

In such a semiconductor, there exists no carrier because of well-defined band gap in (1) and Coulomb repulsion energy in (2). Thus, they are an intrinsic semiconductor (only the charge transportation induced from the thermal activation is possible). The carrier transporting ability of the semiconductor can be improved if holes or electrons are doped. This feature is quite important because it can be applied for the fabrication of organic field effect transistors [35, 36].

For organic field effect transistors, the carriers (holes or electrons) are generally injected through the electrodes. In such cases, however, the injection barrier is generated between the electrodes and the semiconductors. In other words, the resistance is generated at the carrier injection. This resistance is 10^5-10^8 times larger than that of the carrier doping for inorganic semiconductors [37]. As a result, quite high applying voltage is required for driving, leading to the noise and the instability of the conduction.

On the other hand, in recent years, a metallic interface derived from the charge transfer by contacting TTF and TCNQ single crystals was reported by the research group of A. F. Morpurgo [38]. This method (contact doping) makes it possible to achieve an effective carrier doping in the semiconductor interface, and can be expected to overcome the problem generated at the carrier injection. However, the necessary conditions for the carrier doping of this method has not yet been fully disclosed. Thus,

more broad application of the contact doping is required. There are many semiconductors and insulators in the TCNQ anion radical salts due to the reasons (1) and (2), thus they are considered to be good objects for the study of contact doping.

On the basis of the viewpoints above, the carrier doping for the TCNQ anion radical salts is set as the second subject, and is described in Chapter 3.

1.5. Outline of this study

Chapter 1 gives the general introduction related to this study. Section 1.1 is devoted to the historical background and the significance of organic electronics. Section 1.2 describes the guidelines for designing conducting organic crystals by introducing ion radicals and then charge transfer complexes. Section 1.3 is about the background of the study. In Section 1.4 the motivation and the aim of this study and the advantage of the TCNQ anion radical salts for the investigation are described. Section 1.5 gives a general outline of this study.

Chapter 2 is focused on a series of the TCNQ anion radical salts with size-tunable dications. Section 2.1 is devoted to a general background of crystal design for obtaining organic conductors and the structural features of the dications. Section 2.2 is the experimental section, which includes synthesis and crystal growth of (C1BPy)$(TCNQ)_4CH_3CN$,(C2BPy)$(TCNQ)_3$, α-(C3BPy)$(TCNQ)_4$, β-(C3BPy)$(TCNQ)_4$, (C3BPy)$(TCNQ)_4$, (C5BPy)$(TCNQ)_4$, (C6BPy)$(TCNQ)_4$, (C6BPy)$(TCNQ)_3$ (the structure of C*n*BPy is described in Figure 1.5), and crystal structure analyses of the eight crystals, electrical conductivity measurements, magnetic susceptibility measurements, and calculations of the overlap integrals. Section 2.3 talks about the

results and discussion. Section 2.4 summarizes Chapter 2.

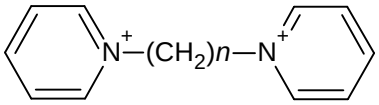

Figure 1.5. The structure of the dication, C*n*BPy.

In Chapter 3, carrier doping to the anion radical salt of K-TCNQ by the contact method is discussed. Section 3.1 is devoted to the background of the contact method and the original characteristics of K-TCNQ. Section 3.2 is the experimental sections which includes synthesis, crystal growth of as-grown K-TCNQ, electrical conductivity measurements, IR spectra measurements, the surface observation by SEM and AFM, current-voltage characteristics measurements. Section 3.3 describes the results and discussion, and Section 3.4 is the summary.

Chapter 4 describes the overall conclusion of the study as well as the future prospect.

References

[1] Akamatsu, H.; Inokuchi, H.; Matsunaga, Y. *Nature*, **1954**, 173, 168-169.

[2] Wickman, H. H.; Trozzolo, A. M.; Williams, H. J.; Hull, G. W.; Merritt, F. R. *Phys. Rev*, **1967**, 155, 563-566.

[3] Bray, J. W.; Hart, Jr, H. R.; Interrante, L. V.; Jacobs, I. S.; Kasper, J. S.; Watkins, G. D.; Wee, S. H., Bonner, J. C. *Phys. Rev. Lett*, **1975**, 35, 744-747.

[4] Jerome, D.; Mazaud, A.; Ribault, M.; Bechgaard, K. *J. Physique Lett*, **1980**, 41, 95-98.

[5] Clark, W. G.; Hammann, J.; Sanny, J.; Tippie, L.C. *Lecture Notes in Physics*, **1979**, 96, 255-264.

[6] Tang, C.W.; VanSlyke, S.A. *Appl. Phys. Lett.*, **1987**, 51, 913-915.

[7] Sze, S.M. *Semiconductor Devices, Physics and Technology*, 2nd ed., John Wiley & Sons, Inc., New York, **2002**; 33-34.

[8] Cordes, A. W.; Haddon, R. C.; Hicks, R. G.; Oakley, R. T.; Palstra, T. T. M.; Schneemeyer, L. F.; Waszczak, J. V. *J. Am. Chem. Soc*, **1992**, 114, 5000-5004.

[9] Itoh, K.; Itoh, H.; Naka, M.; Saito, S.; Hosako, I.; Yoneyama, N.; Ishihara, S.; Sasaki, T.; Iwai, S. *Phys. Rev. Lett*, **2013**, 110, 106401 (1-5).

[10] Mulliken, R. S. *J. Am. Chem. Soc*. **1952**, 74, 811-824.

[11] Metzger, R. M.; Day, P. R.; Papavassiliou, G. C. *Lower-Dimentional Systems and Molecular Electronics, Springer Science & Business Media*, **1990**,10-14.

[12] Ferraris, J.; Cowan, D. O.; Walatka, V, Jr.; Peristein, J. H. *J. Am. Chem. Soc*. **1973**, 95, 948-949.

[13] Inayoshi, T.; Komatsu, H.; Ono, I.; Matsumoto, S. *Synthetic Metals*, **2002**, 128, 333-342.

[14] Bryan, C. D.; Cordes, A. W.; Haddon,R. C.; Hicks,R. G.; Kennepohl, D. K.; MacKinnon, C. D.; Oakley, R. T.; Palstra, T. T. M.;Perel, A. S.; Scott, S. R.; Schneemeyer, L. F.; Waszczaklb, J. V. *J. Am. Chem. Soc*. **1994**, 116, 1205-1210.

[15] Cerrada, E.; Gimeno, M. C.; Laguna, A.; Laguna, M.; Orera, V.; Jones, P. G. *J. Organomet. Chem*, **1996**, 506, 203-210.

[16] Munoz, M. C.; Cano, J.; Ruiz, R.; Lloret, F.; Faus, J. *Acta Crystallogr*, **1995**, C51, 873-876.

[17] Fortin, D.; Drouin, M.; Harvey, P. D.*J. Am. Chem. Soc*. **1998**, 120, 5351-5352.

[18] Baird, P.; Bandy, J. A.; Green, M. L. H.; Hammett, A.; Marseglia, E.; Obertelli, S.D.; Prout, K.; Qin, J. *J. Chem. Soc. Dalton. Trans*, **1991**, 2377-2393.

[19] Grossel, M. C.; Evans, F. A.; Hriljac, J. A.; Prout, K.; Weston, S. C. *Chemical Communications*, **1990**, 1494-1495.

[20] Darocha, B. F.; Titus, D. D.; Sandman, D. J. *Acta Crystallogr*, **1979**, B35, 2445-2448.

[21] Büchner, R .; Field, J. S.; Haines, R. J. *J. Chem. Soc. Dalton Trans*, **1997**, 2403-2408.

[22] Ward, M. D.; Fagan, P. J.; Calabrese, J. C.; Johnson, D. C.; *J. Am. Chem. Soc*, **1989**, 111, 1719-1732.

[23] Miller, J. S.; Zhang, J. H.; Reiff, W. M.; Dixon, D. A.; Preston, L. D.; Reis, Jr, A. H.; Gebert, E.; Extine, M.; Troup, J.; Epstein, A. J.; Ward, M. D. *J. Phys. Chem*, **1987**, 91, 4344-4360.

[24] Murphy, V. J.; O'Hare, D. *Inorg. Chem*, **1994**, 33, 1833-1841.

[25] Abashev, G. G.; Vlasova, R. M.; Kartenko, N. F.; Kuzmin, A. M.; Rozhdestvenskaya, I. V.; Senkin, V. N.; Usov, O. A.; Russkikh, V. S. *Acta Crystallogr*, **1987**, C43, 1108-1112.

[26] Sekizaki, S.; Konsha, A.; Yamochi, H.; Saito, G. *Mol. Cryst. Liq. Cryst*, **2002**, 376, 207-212.

[27] Suzuki, T.; Kabuto, C.; Yamashita, Y.; Mukai, T.; Miyashi, T.; Saito, G. *Bull. Chem. Soc. Jpn*, **1988**, 61, 483-493.

[28] Saito, G.; Enoki, T.; Toriumi, K.; Inokuchi, H, *Solid State Commun*, **1982**, 42, 557-560.

[29] Yagubskii, E. B.; Shchegolev, I. F.; Laukhin, V. N.; Kononovich, P. A.; Kartsovnik, M. V.; Zvarykina, A. V.; Buravov, L. I. *JETP Lett*,**1984**, 39, 12-16.

[30] Kobayashi, A.; Kato, R.; Kobayashi, H.; Moriyama, S.; Nishio, Y.; Kajita, K.; Sasaki, W. *Chem. Lett*, **1986**, 15, 2017-2020.

[31] Kobayashi, A.; Kato, R.; Kobayashi, H.; Moriyama, S.; Nishio, Y.; Kajita, K.; Sasaki, W. *Chem. Lett*, **1987**, 16, 459-462.

[32] Urayama, H.; Yamochi, H.; Saito, G.; Nozawa, K.; Sugano, T.; Kinoshita, M.; Sato, S.; Oshima, K.; Kawamoto, A.; Tanaka, J. *Chem. Lett*, **1988**, 17, 55-58.

[33] Bechgaard, K.; Kistenmacher, T. J.; Bloch, A. N.; Cowan, D. O. *ActaCrystallogr*,**1977**, B33, 417-422.

[34] Zuppiroli, L.; Ardonceau, J.; Weger, M.; Bechgaard, K.; Weyl. C. *J. Physique Lett*, **1978**, 39, 170-173.

[35] Horowitz, G. *Adv. Mater*, **1998**, 10, 365-377.

[36] Koezuka, H.; Tsumura, A.; Ando, T. *Synthetic Metals*, **1987**, 18, 699-704.

[37] Shibata, K.; Wada, H.; Ishikawa, K.; Takezoe, H.; Mori, T. *Appl. Phys. Lett*, **2007**, 90, 193509 (1-4).

[38] Alves, H.; Molinari, A. S.; Xie. H.; Morpurgo. A. F. *Nature Mater*, **2008**, 7, 574-580.

Chapter 2.A series of TCNQ salts with size tunable dications

2.1. Introduction

The guidelines for designing conducting organic crystals have been considerably established. Structurally, molecules of the same type form π-π interaction networks in the crystal, and electronically every molecule that forms a π-π network carries a uniform fractional charge [1].To attain this electronic structure, not mixed stack structures but segregated stack structures are required for the two-component system. There are two candidates for the segregated stack structure; charge transfer complexes and charge transfer salts (anion or cation radical salts). As mentioned in Chapter 1, TTF-TCNQ is one of the most famous charge transfer complexes, in which both TTF and TCNQ form segregated stacks with the amount of charge transfer 0.59, making its physical property a metallic one. For charge transfer complexes, however, the mixed stack structure would be possible. Compared with charge transfer complexes that consist of donors and acceptors, anion or cation radical salts with closed-shell counter ions are advantageous for constructing conducting organic crystals since there is much less possibility to form mixed-stack structures when proper design of the counter ions is performed as discussed in Chapter 1 [2]. Another important requirement to achieve fractional charges is tuning the stoichiometry. However, controlling the stoichiometry is still difficult at the present stage, though some information about the variation of the stoichiometry can be obtained from several previous studies [3, 4].

The π radical anion or cation assemblies gain stabilization energy when the open-shell π orbitals overlap effectively, resulting in self assembled π-π networks [5, 6].For the self-assemblies, planar molecules are favorable. This is because planar

molecules can easily attain parallel stack structures, leading to large overlaps of the π-orbitals (i. e. large transfer integrals). TCNQ is one of the most favorable acceptor molecules to gain a good organic conductor, since TCNQ has not only a planar structure but also relatively high symmetry (the symmetrical shape also will contribute to the good conducting behavior because it can provide a well-ordered molecular stack). The magnitude of the overlap of the π-orbitals depends on the intermolecular distances or the shift of molecules from the regular stack. These parameters are strongly affected by the size and the conformation of the counter ions for the TCNQ-type anion radical salts. In particular, the relative size of the counter ion plays an important role in achieving the appropriate fractional charge [7]. In addition, the size of the counter ions regulates the assembling morphology of the π-radical molecules, resulting in a critical effect on the electronic states. To study how the size of the counter ions influences the stoichiometry and the structure of the radical salts, systematic modification of the size of the counter ions and investigations on both the crystal structures and physical properties of the salts obtained is expected to be an effective method. In addition, considering that the modification is applied to along one direction, the counter ions must be designed to attain one-directional size modification (If the size variation of the closed-shell ions were two-dimensional or three-dimensional, the arrangement of the radical component could be greatly changed, and it could be difficult to perform a systematic study). In this study, the TCNQ anion radical component is selected, and the size of the counter organic close-shelled cations is systematically tuned. There are organic closed-shell cations derived from heterocyclic aromatic compounds including N atoms, such as pyridinium, quinolinium, acridinium. Additionally, cations with a linear substituent bonded with N atoms, such as alkyl chain, can easily be synthesized by S_N2 reaction.

When pyridinium derivatives with alkyl chains were utilized as closed-shell ions, any mixed-stack type TCNQ anion radical salts have not been obtained as mentioned in Chapter 1. Therefore such organic closed-shell cations are especially favorable for the size-tuning study. For this study, 1,1'-(1,*n*-alkyl)bis-pyridinium (abbreviated by C*n*BPy) was chosen as the target cations, as described in Scheme 2.1(a). The size of the cations can be systematically tuned by changing the number of carbons in the intervening alkyl chain. The following three points are important in crystal design:

i) Interdigitation of the alkyl chains rarely occurs. Tuning the size of an ion by the carbon number of alkyl chains is also possible for the *N*-alkyl-pyridinium monocation [8]. However, in this case the terminal chains of two of the cations can interact with each other, leading to a decrease in the effective size (Scheme 2.1(b)).

ii) It is difficult for two adjacent pyridinium rings to overlap with each other. Since pyridinium rings carry positive charges, having two pyridinium rings close together is energetically unfavorable because of the Coulomb repulsions (Scheme 2.1(c)).

iii) Both ends of the dication were unified in pyridinium rings. If the terminal groups were different, especially in the case of a NH^+ terminal group, the packing of the components was significantly altered by the hydrogen bonding. Thus, this was not suitable for studying the correlation between the dication size and the crystal structures or the electronic states. With regard to this point, the series of dications in this study may minimize such extrinsic effects.

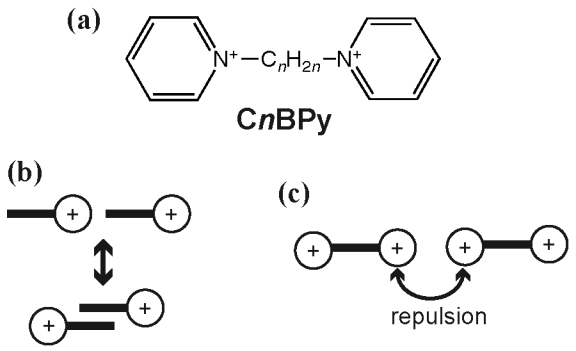

Scheme 2.1. (a) The structure of the target dication(s). (b) The possible model of an interdigitation by using the *N*-alkyl-pyridinium monocation. (c) The model of coulomb repulsion caused by having the two pyridinium rings close together.

Many TCNQ anion radical salts with various counter organic cations have been reported [9-15]. In the 1970s and 1980s Ashwell investigated similar (dication)$(TCNQ)_x$ series using dipyridinium salts, as indicated in Scheme 2.2 [16–25]. The most remarkable salt among those studied is $(DEPE)(TCNQ)_4$ (DEPE = 1,2-di(*N*-ethyl-4-pyridinium) ethylene). The conductivity of $(DEPE)(TCNQ)_4$ is 150 – 2200 S cm^{-1} at room temperature and it shows metallic behavior down to 30 mK [14]. Unfortunately, its crystal structure was not disclosed. All of the other salts had semiconducting behavior and their TCNQ columns were subjected to multimeric distortion, corresponding to their stoichiometries. However, the influence of the dication size on the systematical change of the crystal structure or the electronic states was not mentioned. Some dications in our study (n = 3 and 4) were also investigated by Ashwell from a structural point of view [26, 27], but they were not systematically compared with other series of dications.

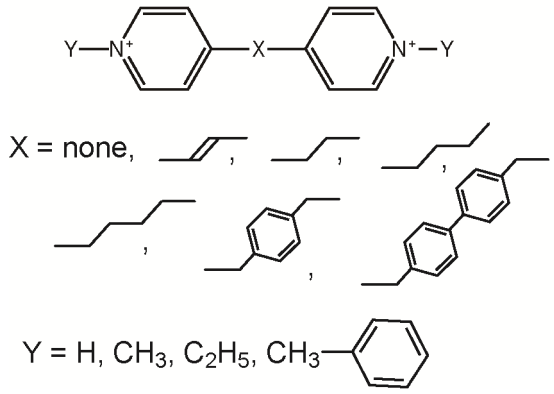

Scheme 2.2 Dications used in the Ashwell's studies.

In 1971 Hadek, et al. investigated the TCNQ salts of ionene $\{[-N^+(CH_3)_2-(CH_2)_x-N^+(CH_3)_2-(CH_2)_y-]_n\}$ polymers [28], in which the size of the polymeric dications could be systematically altered by changing the number of CH_2 groups between positively charged nitrogens. However, the crystal structure of each salt was not disclosed, thus the correlation between the structure of the polymeric dications and the physical properties of the TCNQ salts has not been elucidated.

The systematic change in the crystal structures and physical properties of the TCNQ salts are studied where the alkyl chain lengths (*n*) in C*n*BPy are varied from 1 to 6. The size of the cations of the optimized structure in the isolated state is indicated in Scheme 2.3.The length is calculated as the distance between the edges of the van der Waals radii of the two hydrogen atoms located farthest in the dication. The length of the cation changes from 11.184 Å to 18.344 Å. Although the alkyl chain length is a simple parameter, there exist some polymorphs or different stoichiometries, in spite of the molecule having the same *n* value, making the total system complicated. Nevertheless, the size of the dication ranged from being smaller than to larger than that of the TCNQ

molecule. Especially, I succeeded to determine the crystal structures for a full series of the TCNQ anion radical salts in this study. This is a significant feature for this series of salts and may make it possible to examine the continuously varying crystal structures and spin structures by tuning the dication size.

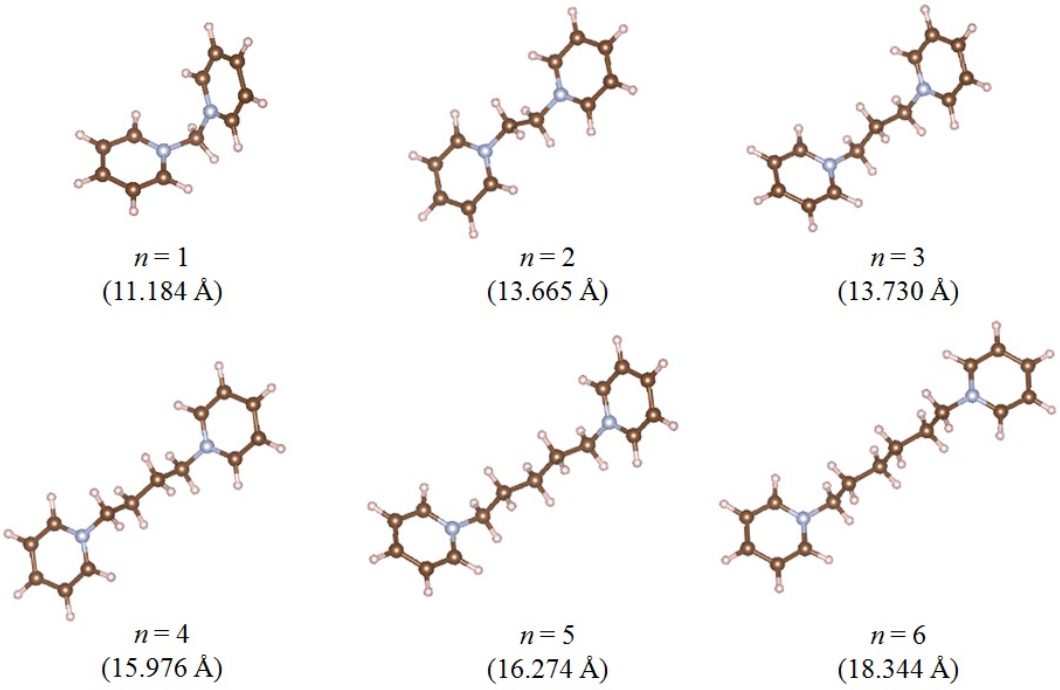

Scheme 2.3. The size of the cations of the optimized structure based on the Gaussian Revision C. 01 MP2/6-31G calculation in the isolated state.

2.2. Experimental

2.2.1. Synthesis and crystal growth of (C*n*BPy)(TCNQ)$_x$ salts

1,1'-(1,*n*-alkyl)bis-pyridiniumdiiodide [(C*n*BPy)I_2] salts were prepared for the synthesis of TCNQ anion radical salts for *n* = 1, 2, 3, 4, 5, 6. For each diiodide salts, the

synthesis was a simple S_N2 reaction, and pyridine plays not only the reactant but also the solvent. Then the product was mixed with TCNQ in a solvent to obtain TCNQ anion radical salts by the reduction reaction by I^-. The details are described as follows.

(C1BPy)(TCNQ)$_4$CH$_3$CN

1 mL (3.32 g, 12.4mmol) of diiodomethane (Tokyo Kasei Kogyo Co. Ltd.) and 10 mL (9.8 g, 0.124 mol) of pyridine (Wako chemical Co. Ltd.) were mixed in the 50 mL egg-plant shaped flask, and then refluxed at 80˚C for 3 days. The chemicals were used without further purification. Yellow powder 1,1'-(1,1-methyl) bis-pyridiniumdiiodide [(C1BPy)I_2] was obtained in a yield of 4.68 g, and the response rate was 88.7%. Then 19.9 mg (0.0467 mmol) of (C1BPy)I_2 and 45.5 mg (0.223 mmol) of TCNQ(Wako chemical Co. Ltd.) were dissolved in 15 mL and 25 mL of hot acetonitrile respectively, and then the solutions were mixed. (C1BPy)I_2 was used without further purification, and TCNQ was used after the purification by recrystallization. Black, block single crystals of (C1BPy)(TCNQ)$_4$CH$_3$CN were obtained by allowing the solution to stand for 3 days.

(C2BPy)(TCNQ)$_3$

1.06g (3.76 mmol) of 1,2-diiodoethane (Wako chemical Co. Ltd.) and 5 mL (4.9 g, 0.062 mol) of pyridine (Wako chemical Co. Ltd.) and 45 mL of acetonitrile (Wako chemical Co. Ltd.) were mixed in the 100 mL egg-plant shaped flask, and then refluxed at 80˚C for 4 days. The chemicals were used without further purification. In this case, E2 reaction preferentially occurs without acetonitrile. Therefore, acetonitrile was added as the solvent to promote the S_N2 reaction and get a higher yield. After the reflux, the product was washed by ethanol and acetone to remove the impurities. Orange powder 1,1'-(1,2-ethyl)bis-pyridiniumdiiodide [(C2BPy)I_2] was obtained in a yield of 46.4 mg, and the response rate was 1.05 %. Then 11.2 mg (0.0254 mmol) of (C2BPy)I_2 and 25.0

mg (0.122 mmol) of TCNQ (Wako chemical Co. Ltd.) were dissolved in 25 mL, 15 ml of hot acetonitrile respectively, and then the solutions were mixed. $(C2BPy)I_2$ was used without further purification, and TCNQ was used after the purification by recrystallization. Black, platelet single crystals of $(C2BPy)(TCNQ)_3$ were obtained by allowing the solution to stand for 3 days.

α-(C3BPy)(TCNQ)$_4$

1 mL (2.52 g, 8.52 mmol) of 1,3-diiodopropane (Wako chemical Co. Ltd.) and 10 mL (9.8 g, 0.124 mol) of pyridine (Wako chemical Co. Ltd.) were mixed in the 50 mL egg-plant shaped flask, and then refluxed at 85˚C for 6days. The chemicals were used without further purification. Pale yellow powder 1,1'-(1,3-propyl)bis-pyridiniumdiiodide[$(C3BPy)I_2$] was obtained in a yield of 2.88 g, and the response rate was 88.1%. Then 20.2 mg (0.0444mmol) of $(C3BPy)I_2$ and 40.5 mg (0.198 mmol) of TCNQ (Wako chemical Co. Ltd.) were dissolved in 15 mL, 25 mL of hot acetonitrile respectively, and then the solutions were mixed. $(C3BPy)I_2$ was used without further purification, and TCNQ was used after the purification by recrystallization. Black, block single crystals of α-$(C3BPy)(TCNQ)_4$ were obtained by allowing the solution to stand for 3 days.

β-(C3BPy)(TCNQ)$_4$

25.8 mg (0.0568 mmol) of $(C3BPy)I_2$ and 62.5 mg(0.306 mmol) of TCNQ (Wako chemical Co. Ltd.) were dissolved in 15 mL, 25 mL of hot acetonitrile respectively, and then the solutions were mixed. $(C3BPy)I_2$ was used without further purification, and TCNQ was used after the purification by recrystallization. Black, block single crystals of β-$(C3BPy)(TCNQ)_4$ were obtained by allowing the solution to stand for 1 day.

(C4BPy)(TCNQ)$_4$

1 mL (2.37 g, 7.65mmol) of 1,4-diiodobuthane (Wako chemical Co. Ltd.) and 10 mL (9.8 g, 0.124 mol) of pyridine (Wako chemical Co. Ltd.) were mixed in the 50 mL egg-plant shaped flask, and then refluxed at 85˚C for 7 days. The chemicals were used without further purification. Pale yellow powder 1,1'-(1,4-buthyl)bis-pyridiniumdiiodide [(C4BPy)I_2] was obtained in a yield of 3.23 g, and the response rate was 90.2%. Then 28.3 mg (0.0605 mmol) of (C4BPy)I_2 and 55.2 mg (0.270 mmol) of TCNQ (Wako chemical Co. Ltd.) were dissolved in 15 mL of hot acetonitrile respectively, and then the solutions were mixed. (C4BPy)I_2 was used without further purification, and TCNQ was used after the purification by recrystallization. Black, block single crystals of (C4BPy)$(TCNQ)_4$ were obtained by allowing the solution to stand for 1 day.

(C5BPy)$(TCNQ)_4$

1 mL (2.20 g, 6.79 mmol) of 1,5-diiodopentane (Alfa Aesar, Shore Road, Lancs., imported by Wako Chemical Co. Ltd.) and 10 mL (9.8 g, 0.124 mol) of pyridine (Wako chemical Co. Ltd.) were mixed in the 50 mL egg-plant shaped flask, and then refluxed at 85˚C for 5 days. The chemicals were used without further purification. Pale yellow powder 1,1'-(1,5-pentyl)bis-pyridiniumdiiodide[(C5BPy)I_2] was obtained in a yield of 2.88 g, and the response rate was 88.1%. Then 30.0 mg (0.0622 mmol) of (C5BPy)I_2 and 64.2 mg (0.314 mmol) of TCNQ (Wako chemical Co. Ltd.) were dissolved in 14 mL and 15 mL of hot acetonitrile respectively, and then the solutions were mixed. (C5BPy)I_2 was used without further purification, and TCNQ was used after the purification by recrystallization. Black, block single crystals of (C5BPy)$(TCNQ)_4$ were obtained by allowing the solution to stand for 3 days.

(C6BPy)$(TCNQ)_4$

1 mL (2.05 g, 6.06 mmol) of 1,6-diiodohexane (Lancaster, Eastgate, White Lund,

Morecambe, England.) and 10 mL (9.8 g, 0.124 mol) of pyridine (Wako chemical Co. Ltd.) were mixed in the 50 mL egg-plant shaped flask, and then refluxed at 85˚C for 6 days. The chemicals were used without further purification. Pale yellow powder 1,1'-(1,6-hexyl)bis-pyridiniumdiiodide[$(C6BPy)I_2$] was obtained in a yield of 2.83 g, and the response rate was 94.0%. Then 20.0 mg (0.0402 mmol) of $(C6BPy)I_2$ and 40.5 mg (0.198 mmol) of TCNQ (Wako chemical Co. Ltd.) were dissolved in 7 mL and 18 mL of hot acetonitrile respectively, and then the solutions were mixed. $(C6BPy)I_2$ was used without further purification, and TCNQ was used after the purification by recrystallization. Black, block single crystals of $(C6BPy)(TCNQ)_4$ were obtained by allowing the solution to stand for 2 days.

$(C6BPy)(TCNQ)_3$

25.2 mg (0.0507 mmol) of $(C6BPy)I_2$ and 40.5 mg (0.198 mmol) of TCNQ (Wako chemical Co. Ltd.) were dissolved in 20 mL of hot acetonitrile respectively, and then the solutions were mixed. $(C6BPy)I_2$ was used without further purification, and TCNQ was used after the purification by recrystallization. Black, block single crystals of $(C6BPy)(TCNQ)_3$ were obtained by allowing the solution to stand for 2 days.

Two polymorphs were obtained for C3BPy. One of them, α-$(C3BPy)(TCNQ)_4$, was the same as that previously reported [26]. These two polymorphs could selectively be grown by slightly changing the conditions (concentration and cooling rate) and they could be distinguished from the appearance. $(C4BPy)(TCNQ)_4$ was also the same as a previously reported crystal [27]. For C6BPy, two different stoichiometries were obtained under the same conditions, and they also could be distinguished from the appearance. The majority of these two stoichiometries could be controlled by the cooling rate. After careful examination of the presence of other polymorphs, a trace

amount of polymorphic byproducts were found to form for n = 2 and n = 5. However, the byproducts were produced very rarely, and the bulk samples for the magnetic measurements were confirmed not to contain any byproducts.

2.2.2. Crystal structure analyses

The X-ray diffraction intensity data for single crystals of the TCNQ salts were obtained using an automated Rigaku R-Axis rapid X-ray diffractometer with graphite monochromated Mo*K*α radiation. The crystal structures were solved by employing the direct methods of SIR2004 [29] and SHELX-97 [30] in the CrystalStructure4.0 [31] crystallographic software package. The crystal data for the salts are summarized in Table 1. Refinement of the structures was carried out using a full-matrix least squares refinement on F^2. All of the non-hydrogen atoms were refined anisotropically. The hydrogen atoms were placed at the theoretically calculated ideal positions, related to their respective parent atoms, with a riding model for the structure refinement.

Table2.1. Crystallographic data for the TCNQ salts

	(C1BPy)-$(TCNQ)_4CH_3CN$	(C2BPy)-$(TCNQ)_3$	α-(C3BPy)-$(TCNQ)_4$[a]	β-(C3BPy)-$(TCNQ)_4$
Formula	$C_{61}H_{31}N_{19}$	$C_{48}H_{26}N_{14}$	$C_{61}H_{32}N_{18}$	$C_{61}H_{32}N_{18}$
Formula Weight	1030.04	798.83	1017.04	1017.04
Crystal System	triclinic	triclinic	monoclinic	triclinic
Space Group	$P\bar{1}$	$P\bar{1}$	$P2_1$	$P1$
a /Å	13.1547(9)	8.0675(9)	7.7599(4)	7.792(3)

b /Å	13.6652(9)	8.0934(9)	25.3409(12)	12.715(4)
c /Å	15.5920(10)	15.5631(18)	13.0885(6)	13.100(4)
α / degree	105.4713(19)	83.1512(14)		86.007(14)
β / degree	100.898(2)	76.1582(14)	92.7802(13)	87.137(12)
γ / degree	103.6797(18)	76.0042(14)		82.964(18)
V / Å^3	2527.7(3)	955.34(19)	2570.7(2)	1283.9(7)
Z	2	1	2	1
D_{calc} / g cm^{-3}	1.353	1.389	1.314	1.315
μ(Mo Ka) / cm^{-1}	0.87	0.88	0.84	0.84
Temperature / K	293	153	296	273
No. of Unique Reflections	11285	4395	11570	9209
R_{int}	0.0405	0.0468	0.0303	0.0343
$R1$ [I> 2.0σ(I)]	0.0534	0.0433	0.0365	0.0568
R_w (all reflections)	0.1783	0.1239	0.1053	0.1696
Goodness of fit indicator	1.095	1.030	0.951	1.022

[a]The crystal is the same as that reported in ref. 26.

Table2.1(continued). Crystallographic data for the TCNQ salts

	(C4BPy)-(TCNQ)$_4$[b]	(C5BPy)-(TCNQ)$_4$	(C6BPy)-(TCNQ)$_4$	(C6BPy)-(TCNQ)$_3$
Formula	$C_{62}H_{34}N_{18}$	$C_{63}H_{36}N_{18}$	$C_{64}H_{38}N_{18}$	$C_{52}H_{34}N_{14}$
Formula Weight	1031.07	1045.10	1059.12	854.93

Crystal System	triclinic	triclinic	triclinic	triclinic
Space Group	$P\bar{1}$	$P\bar{1}$	$P\bar{1}$	$P\bar{1}$
a /Å	7.7633 (17)	7.7658(17)	7.6612(2)	7.8494(17)
b /Å	13.078(4)	13.274(4)	13.068(4)	9.803(3)
c /Å	13.081(4)	25.224(5)	14.039(4)	14.557(4)
α / degree	76.175(13)	93.634(13)	76.243(11)	76.285(10)
β / degree	88.07(2)	95.231(10)	76.680(16)	82.750(7)
γ / degree	87.743(13)	90.757(10)	80.966(12)	81.523(11)
V / Å^3	1288.2(7)	2583.6(11)	1320.6(6)	1071.5(5)
Z	1	2	1	1
D_{calc} / g cm^{-3}	1.329	1.343	1.332	1.325
μ(Mo Ka) / cm^{-1}	0.84	0.85	0.84	0.83
Temperature / K	123	153	153	153
No. of Unique Reflections	5707	11590	5921	4874
R_{int}	0.0311	0.0579	0.037	0.0363
$R1$ [$I > 2.0\sigma(I)$]	0.0480	0.0707	0.0499	0.0445
R_w (all reflections)	0.1226	0.2250	0.1475	0.1314
Goodness of fit indicator	1.017	1.066	1.050	1.034

[b]The crystal is the same as that reported in ref. 27.

2.2.3. Electrical conductivity measurements

The electrical resistivity was measured along the TCNQ stacking direction in a

single crystalline sample using a four-probe method. Gold paste (Tokuriki Chemical Research Co. Ltd.) was used to connect two gold wires (ϕ = 20 μm) at opposite ends of a plate crystal such that the cross section of the crystal was covered with paste. The temperature dependence was measured using a closed cycle cryostat system in the temperature range of 100–300 K.

2.2.4. Magnetic susceptibility measurements

Magnetic susceptibility measurements were performed on a Quantum Design MPMS superconducting quantum interference device (SQUID) susceptometerwith a static field of 1 T in the temperature range of 2–300 K for the randomly oriented polycrystalline sample. For each crystal, the sample was set in the straw. The edge of the straw was closed by cotton to prevent the sample from scattering outside. The diamagnetic core contribution was estimated based on Pascal's constants described in the Table 2.2 [32]. In some cases, the paramagnetic contribution was quantified by the ESR signal intensity. The molar susceptibility was defined as susceptibility for the (C*n*BPy)$(TCNQ)_4$ or(C*n*BPy)$(TCNQ)_3$ unit.

Table 2.2. Pascal's diamagnetic susceptibilities (10^{-6} emu/mol)

H	-2.93
C	-6.00
N (aromatic)	-4.61
N (aliphatic)	-5.57

2.2.5. Calculation of the overlap integrals

Orbital overlap integrals between two adjacent TCNQ molecules on each crystal in the extended Hückel approximation [33, 34] were calculated using the CAESAR program package [35].

2.3. Results and discussion

2.3.1. Crystal structures

As a result of the crystal structure analyses, there were two different stoichiometries (dication : TCNQ), 1:3 and 1:4. Crystals with 1:3 stoichiometry were obtained only for n = 2 and 6, while crystals with 1:4 stoichiometry were obtained n = 1, 3, 4, 5, 6. Of the five 1:4 crystals, solvent molecules were involved only for n = 1. To obtain detailed information about the size effect of the dications for the stoichiometry and crystal packing, crystal structures of the 1:4 salts (for n = 3, 4, 5, 6) will be initially discussed. Then, the n = 1 salt will be compared with the other 1:4 salts from the structural point of view. Finally, crystal structure of 1:3 salts (for n = 2, 6) will be focused on, and then the reason why they take this stoichiometry will be considered.

Crystal structures of the 1:4 salts

The crystal structures for *n* = 3, 4, 5 and 6 are shown in Figure 2.3.1.

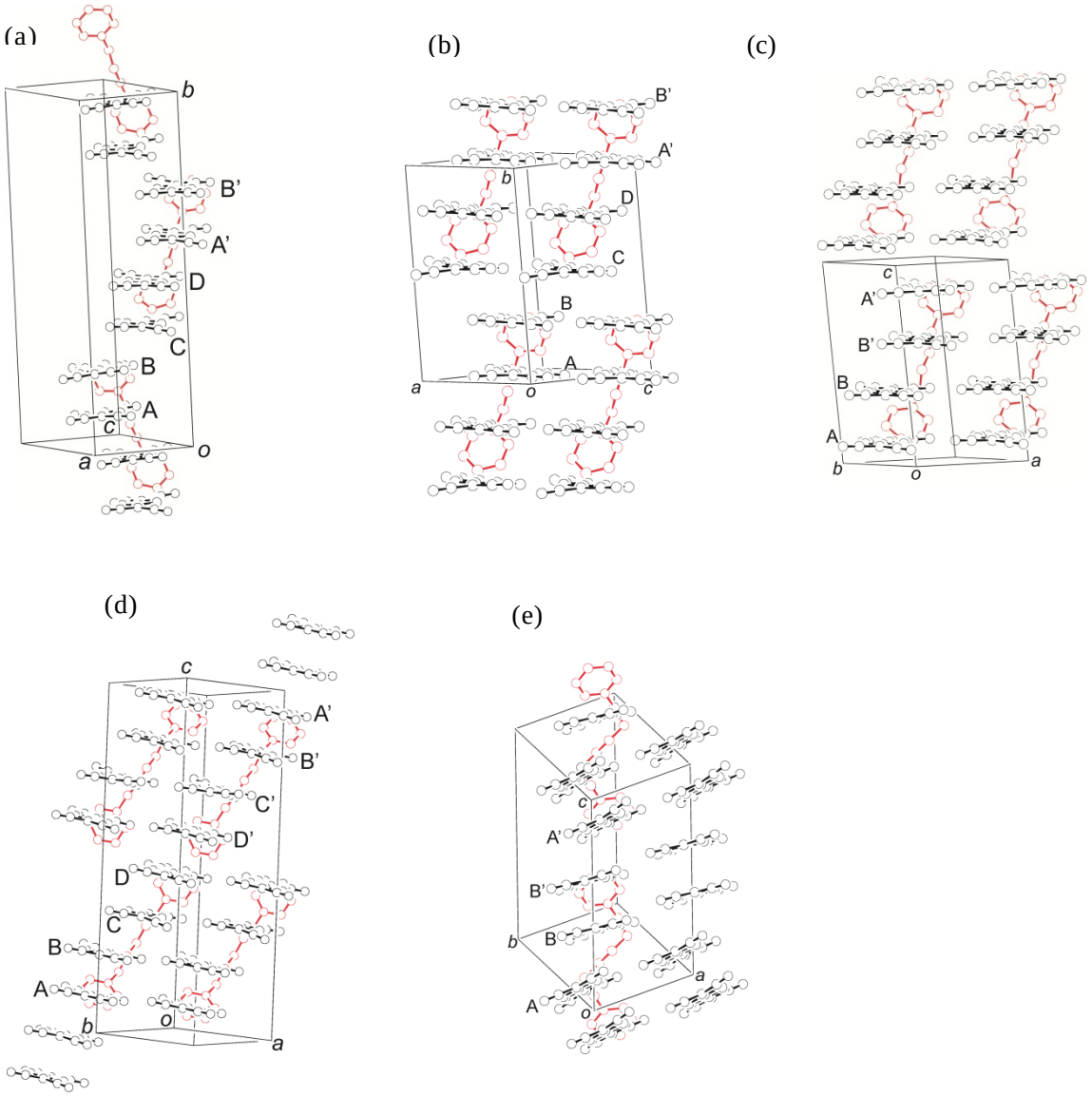

Figure 2.3.1. Perspective view of the unit cell for (a) α-(C3BPy)(TCNQ)$_4$ (the structure is the same as that reported in ref. [26]), (b) β-(C3BPy)(TCNQ)$_4$, (c) (C4BPy)(TCNQ)$_4$ (the structure is the same as that reported in ref. [27]), (d) (C5BPy)(TCNQ)$_4$, and (e) (C6BPy)(TCNQ)$_4$.

For *n* = 3, two polymorphs were obtained. One of them (α-form) was identical to that previously reported [26]. Interestingly, neither of the two polymorphs had a center

of symmetry. This is because *n* was an odd number and packing occurs when there is no center of symmetry between two adjacent dications. For the α-form, the two adjacent dications were related by the 2_1 axis (Figure 2.3.1(a)), while the dications were related by a simple translation in the β-form (Figure2.3.1(b)). This difference in the dication arrangements led to a difference in TCNQ column formation, as shown in Figures 2.3.1(a) and 2.3.1(b). On the other hand, the overlap integrals (Table 2.3), which indicates the overlap of the lowest unoccupied molecular orbitals between two adjacent TCNQ molecules and is a measure of the intermolecular interactions, did not differ from each other with both showing strong dimerization. In addition, the formal charge of TCNQ, which was calculated from the TCNQ geometry [36] (Table 2.4.) did not display any charge disproportionation and every TCNQ molecule had a charge of approximately −1/2 for both polymorphs. For $n = 4$ (Figure 2.3.1(c)), only crystal obtained was the same as one that has been previously reported [27]. For the dications with a center of symmetry, it was located on the inversion center in the crystal, and TCNQ formed a 1-D column with dimerized distortion. For $n = 5$ (Figure 2.3.1(d)), the dications had no center of symmetry, but two adjacent dications were related to each other by the center of symmetry in the crystals. A center of symmetry also existed in the TCNQ column. Two types of tetramers were formed because of the periodicity of the overlap integral (see Table 2.3). The formal charge in TCNQ was partly localized; in the CDD'C' tetramer D and D' were almost −1, and C and C' were neutral, while in the BAA'B' tetramer A and B had a charge of approximately −1/2 (Table 2.3). This charge disproportionation was quite different from the other dication-TCNQ salts, resulting in peculiar magnetic properties (vide infra).

Table 2.3. Formal charge of the TCNQ molecules and the overlap integral between the lowest unoccupied molecular orbitals of the neighboring TCNQ molecules

Compound	Overlap integral		Formal charge (γ)	
$(C1BPy)(TCNQ)_4$	AB	0.0172	A	0.40
	BC	0.0121	B	0.76
	CD	0.0176	C	0.29
	DA	0.0148	D	0.58
$(C2BPy)(TCNQ)_3$	AB	0.0215	A	0.58
	BA’	0.0215	B	0.58
	A’A	0.0044		
α-$(C3BPy)(TCNQ)_4$	AB	0.0200	A	0.58
	BC	0.0039	B	0.54
	CD	0.0193	C	0.46
	DA	0.0067	D	0.58
β-$(C3BPy)(TCNQ)_4$	AB	0.0213	A	0.58
	BC	0.0042	B	0.54
	CD	0.0199	C	0.51
	DA	0.0053	D	0.58
$(C4BPy)(TCNQ)_4$	AB	0.0208	A	0.42
	BB’	0.0038	B	0.51
	B’A’	0.0208		
	A’A	0.0041		

$(C5BPy)(TCNQ)_4$	AA’	0.0191	A	0.67
	AB	0.0220	B	0.46
	BC	0.0019	C	0.21
	CD	0.0193	D	0.96
	DD’	0.0176		
$(C6BPy)(TCNQ)_4$	AB	0.0008	A	0.54
	BB’	0.0212	B	0.54
	B’A’	0.0008		
	A’A	0.0204		
$(C6BPy)(TCNQ)_3$	AB	0.0229	A	0.88
	BA’	0.0229	B	0.58
	A’A	0.0038		

Table 2.4. Geometry of TCNQ and derived formal charges (γ)

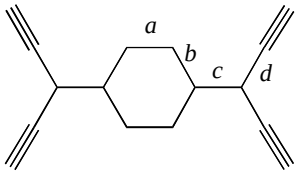

		a[a]	b[a]	c[a]	d[a]	δ[b]	γ
(C1BPy)(TCNQ)$_4$	A	1.349(4)	1.435(4)	1.389(4)	1.426(5)	0.485	0.40
	B	1.358(5)	1.427(4)	1.405(4)	1.416(5)	0.494	0.76
	C	1.346(4)	1.439(4)	1.385(4)	1.429(5)	0.483	0.29
	D	1.357(4)	1.430(4)	1.399(4)	1.425(5)	0.490	0.58
(C2BPy)(TCNQ)$_3$	A	1.359(2)	1.432(3)	1.400(2)	1.425(3)	0.490	0.58
	B	1.356(2)	1.430(5)	1.398(2)	1.422(5)	0.490	0.58
α-(C3BPy)(TCNQ)$_4$	A	1.353(3)	1.432(3)	1.401(3)	1.425(3)	0.490	0.58
	B	1.352(3)	1.435(3)	1.398(3)	1.424(3)	0.489	0.54
	C	1.354(3)	1.435(3)	1.393(3)	1.427(3)	0.487	0.46
	D	1.351(3)	1.432(3)	1.399(3)	1.423(3)	0.490	0.58
β-(C3BPy)(TCNQ)$_4$	A	1.351(4)	1.435(4)	1.403(4)	1.430(7)	0.490	0.58
	B	1.354(4)	1.437(7)	1.400(4)	1.428(7)	0.489	0.54
	C	1.358(4)	1.434(17)	1.398(4)	1.429(22)	0.488	0.51
	D	1.350(7)	1.433(6)	1.400(4)	1.427(7)	0.490	0.58
(C4BPy)(TCNQ)$_4$	A	1.352(2)	1.440(5)	1.394(3)	1.431(7)	0.486	0.42
	B	1.351(2)	1.437(8)	1.400(2)	1.432(4)	0.488	0.51
(C5BPy)(TCNQ)$_4$	A	1.362(8)	1.426(6)	1.404(4)	1.425(20)	0.492	0.67
	B	1.349(12)	1.434(10)	1.393(5)	1.425(18)	0.487	0.46
	C	1.351(4)	1.439(16)	1.381(4)	1.435(26)	0.481	0.21
	D	1.359(6)	1.425(4)	1.418(6)	1.419(9)	0.499	0.96
(C6BPy)(TCNQ)$_4$	A	1.353(2)	1.432(5)	1.398(2)	1.429(5)	0.489	0.54
	B	1.355(2)	1.433(7)	1.400(2)	1.428(8)	0.489	0.54
(C6BPy)(TCNQ)$_3$	A	1.358(2)	1.423(2)	1.411(2)	1.416(2)	0.497	0.88
	B	1.350(2)	1.427(6)	1.394(2)	1.420(6)	0.490	0.58

[a]Averaged bond lengths under D_{2h} symmetry. Values in parentheses are maximum standard deviation or maximum difference from the averaged value. [b]$\delta = c / (b + d)$.

For n = 6 (Figure 2.3.1(e)), the dication maintained its center of symmetry in the crystal. However, the alkyl chain did not take on the trans configuration and was strongly distorted. TCNQ formed 1-D columns with a dimeric distortion and the center of symmetry was located at the midpoint of the TCNQ dimer. As a result, the interactions between two adjacent dimers were uniform. The charge of the TCNQ molecule was almost uniform, but the molecular planes between two adjacent dimers greatly slide and the planes were not parallel, leading to a small overlap integral between the dimers. This slide of the dimers was induced by the strongly distorted alkyl chain of the dication.

The five crystals mentioned above had similar TCNQ column structures, even though the size of their dications varied. The crystal structures can be summarized with the concept of the ‘effective dication length’. This corresponds to the distance between the centers of two adjacent dications. These results are presented in Figure 2.3.2, which shows that the effective dication length had no correlation with the value of n, falling within a narrow range from 13.2 to 15.4 Å.

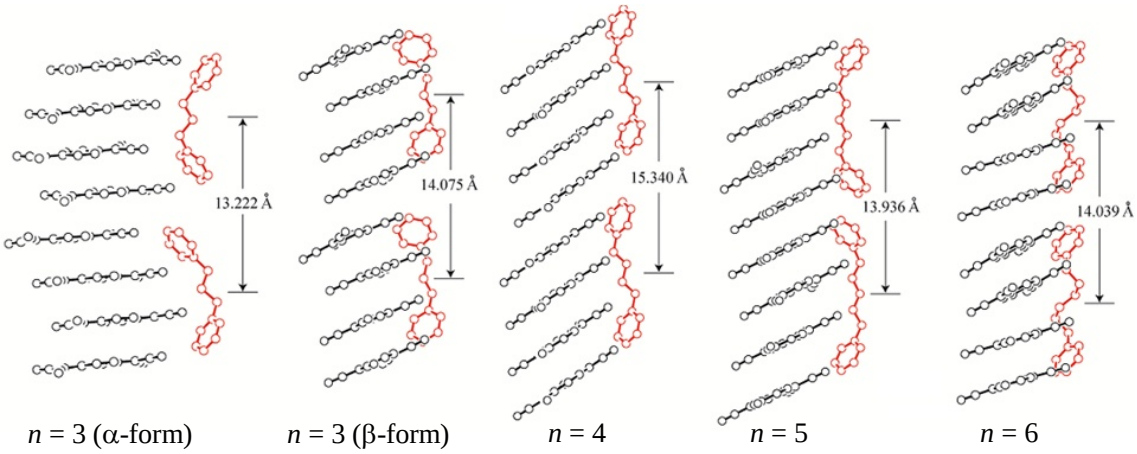

Figure 2.3.2. Effective dication lengths in the 1:4 salts for n = 3, 4, 5, and 6.

The length of the individual dications in the crystal represented following the style

adopted for Scheme 2.3 is shown in Scheme 2.4. The length is not so much different from that in the calculated isolated state except n = 6. The length is somewhat different from the “effective dication length”, indicating molecular packing is important for the “effective dication length”.

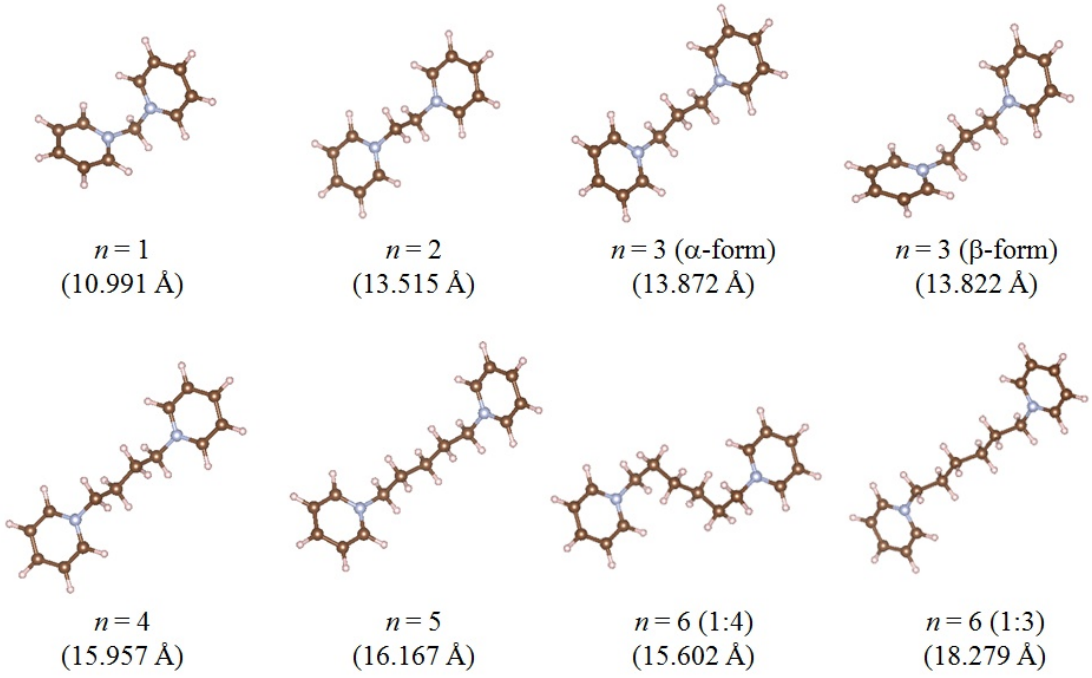

Scheme 2.4. The size of the cations in the TCNQ anion radical crystals.

Taking the above into consideration, the n = 1 salt will now be discussed. The crystal structure is shown in Figure 2.3.3(a). Since n was an odd number, the dication occupied a general position. CH_3CN was involved as the crystal solvent and it aligned alternately with the dication in one dimension. TCNQ formed 1-D columns with a tetrameric period, where the overlap integrals were fairly uniform. Every TCNQ molecule had a formal charge of approximately −1/2 (Table 2.3). The effective dication length is shown in Figure 2.3.3(b) and was in the range that was found for the five

crystals mentioned above. Therefore, for n = 1, the CH_3CN molecules occupied the space that was formed between two adjacent and relatively small dications. The synthesis of the n = 1 salt was attempted by using other solvents than CH_3CN (ethanol, propionitrile, benzonitrile), but no single crystal was obtained. Thus, only the acetonitrile is considered to fit the space to form the stable single crystal.

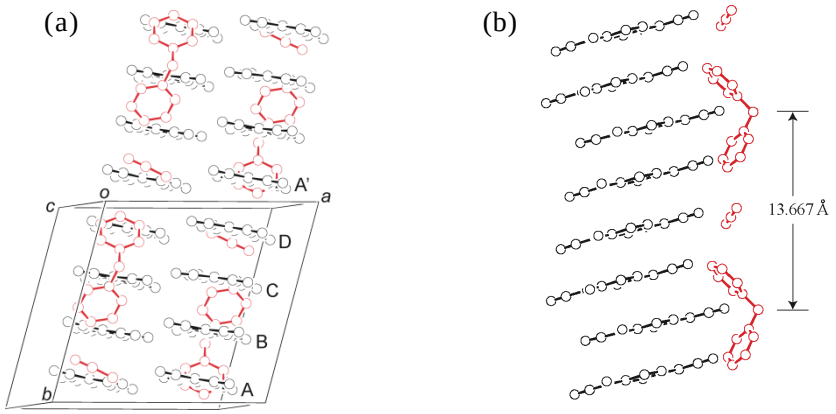

Figure 2.3.3. (a) Perspective view of the unit cell for $(C1BPy)(TCNQ)_4 \cdot CH_3CN$. (b) Effective dication length in $(C1BPy)(TCNQ)_4 \cdot CH_3CN$.

Crystal structures of the 1:3 salts

The crystal structure of an n = 2 salt is shown in Figure 2.3.4. Dication was located at the center of symmetry and one of the two independent TCNQ molecules was located on the center of symmetry. The TCNQ molecules formed discrete trimers with their centers of symmetry at the midpoints. In this case, the appropriate effective dication length for the 1:4 stoichiometry could not be attained because the dication size was too small. The reason for this may be because the dication size was smaller than the thickness of four TCNQ molecules, making the trimerization of TCNQ preferential. However, to form ideal 1-D columns of the trimerized TCNQ units, neighboring

pyridinium rings must be touching. This is why the TCNQ stack was largely distorted.

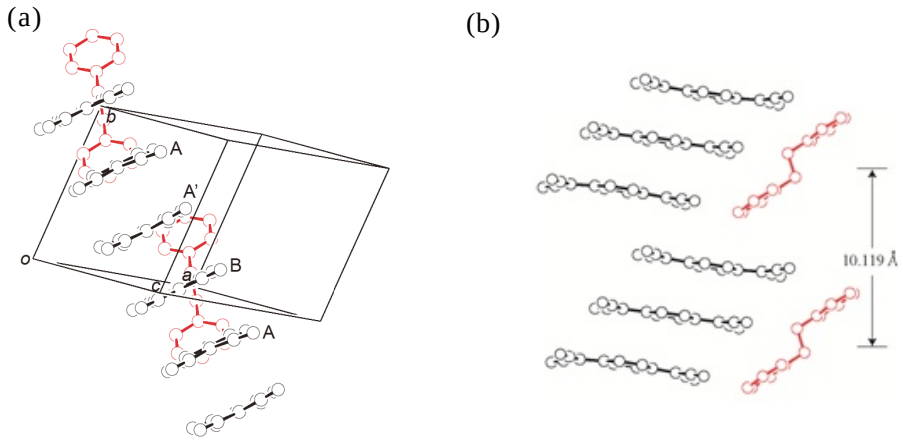

Figure 2.3.4. (a) Perspective view of the unit cell for (C2BPy)$(TCNQ)_3$ and (b) its side view.

The crystal structure for an n = 6 salt is shown in Figure 2.3.5. Dication was located on the center of symmetry and one of the two independent TCNQ molecules was also located on the center of symmetry. The TCNQ molecules formed discrete trimers with the center of symmetry at the midpoint. These characteristics were the same as those for the n = 2 salt. The 1:4 salt was also given by the n = 6 dication, but the configurations of the dications were quite different from each other (the 1:3 and 1:4 salts). Namely, all-trans configuration was maintained and the dications were not further shortened in the 1:3 salt. The reason for this is as follows: if the n = 6 dication aligned along one direction with a completely trans configuration, the dication length was too long for the appropriate effective dication length for the 1:4 stoichiometry. Accordingly, the effective dication length had to be shortened to form the 1:4 salt, which is energetically unfavorable. As a compromise, there were two choices; one was to break the all-trans configuration, decreasing the effective dication length to form the 1:4 salt, and the other

was to shift the dication alignment from a simple 1-D arrangement while keeping an all-trans configuration accompanied by a large distortion of the TCNQ stack, leading to the formation of the 1:3 salt. This level of flexibility in the composition resulted from the configurational flexibility, owing to the long alkyl chain for the n = 6 dication.

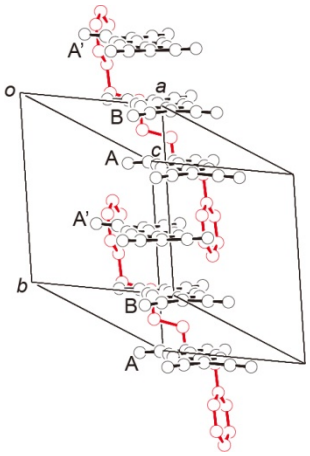

Figure 2.3.5. Perspective view of the unit cell for (C6BPy)$(TCNQ)_3$.

The sum of the formal charges in the (CnBPy)$(TCNQ)_x$ (x = 3 or 4) unit was found to be in a range between -1.74 and -2.34 (Table 2.5), which was rather close to the ideal value of -2. Considering the accuracy of the formal charge determined from the molecular geometry, the results were rather good. Therefore, it is safe to discuss the charge uniformity based on these data.

Table 2.5. Sum of the formal charges of TCNQ in the (C*n*BPy)$(TCNQ)_x$ (x = 3 or 4) unit.

	The sum of the formal charges
(C1BPy)$(TCNQ)_4$	2.03
(C2BPy)$(TCNQ)_3$	1.74
α-(C3BPy)$(TCNQ)_4$	2.16
β-(C3BPy)$(TCNQ)_4$	2.21
(C4BPy)$(TCNQ)_4$	1.86
(C5BPy)$(TCNQ)_4$	2.30
(C6BPy)$(TCNQ)_4$	2.16
(C6BPy)$(TCNQ)_3$	2.34

From the information above, the range of the variation of the stoichiometry in the present system will be discussed. At first the stoichiometry (dication:TCNQ) was expected to vary widely depending on the dication size. However, the obtained stoichiometries were only 1:4 and 1:3. In particular, the salts with 1:4 stoichiometry were obtained for every n value except for n = 2, and their conformations resemble each other. Thus, the 1:4 stoichiometry is considered to be prior to any other conditions for the crystal growth. In this stoichiometry, an averaged charge of each TCNQ is -1/2, and the stabilization by the delocalized electrons is considered to be most effectively attained. This stabilization will still be effectively attained in case of 1:3 stoichiometry, in which the averaged charge of each TCNQ is -2/3, close to -1/2. It is considered that the periodicity of two or three molecules in which one or two electrons are accommodated is relatively easily attained. If the periodicity becomes larger than four molecules, the lattice strain may exceed the electron delocalization energy. Therefore, it was difficult to form salts of (dication)$(TCNQ)_x$ with $x > 5$.

On the other hand, if the relationship between the effective dication lengths and the state of the TCNQ columns are focused on, the TCNQ molecular plane tilts more

significantly in the crystal with a longer effective dication length. Assuming the angle between the stacking direction and the TCNQ molecular plane to be ϕ, ϕ= 90° for α-(C3BPy)$(TCNQ)_4$, in which the effective dication length is relatively short (13.222Å). On the contrary, ϕ = 51.5° for (C4BPy)$(TCNQ)_4$, in which the effective dication length is the longest of the series (15.340Å). For a longer effective dication length, the tilted TCNQ molecular plane allows the dication to be the all-trans conformation, resulting in the formation of the favorable 1:4 stoichiometry. For too much tilted molecular plane, the overlap of the π-orbital between the adjacent TCNQ molecules cannot be assured, thus the all-trans conformation was not able to attained for (C6BPy)$(TCNQ)_4$. Nevertheless, the tilting ability makes it possible for the crystals to have some range of the effective dication length required for the 1:4 stoichiometry.

2.3.2. Electrical properties

The temperature dependence of the single-crystal resistivity for the C*n*BPy TCNQ salts is shown in Figure 2.3.6.

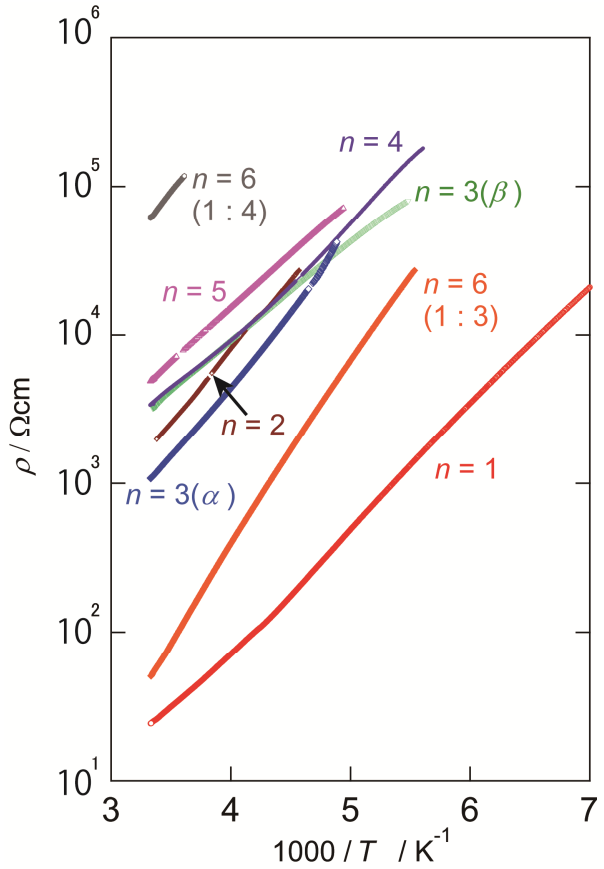

Figure 2.3.6. Temperature dependence of the single-crystal resistivity for the C*n*BPy TCNQ salts.

The n = 1 salt had the lowest resistivity (22 Ω cm) among all the salts studied. For all of these crystals, the temperature dependence of the resistivity was thermally activated. This was considered as follows: Even though the formal charges were nearly uniform, the overlap integrals were not uniform. Thus, the behavior of the resistivity reflected the multimeric structural characteristics to some extent. The n = 6 salt (1:4 stoichiometry) had the smallest overlap integral between two adjacent dimers, which reflected the significant slide between the dimers, leading to the lowest conductivity among this series of TCNQ salts. For the n = 1 salt, the relatively uniform overlap integrals in the TCNQ column resulted in the highest conductivity. In this manner, a

correlation was observed between the conductivity and the overlap integrals between the TCNQ molecules, to some extent. The room temperature resistivities and the activation energies of these salts are summarized in Table 2.6. The activation energy was nearly 0.2 eV in all the salts. Compared to the variation of the conductivity, the variation of the activation energy is not so obvious. Therefore, it is very difficult to find the correlation between the conductivity and the activation energy. Nevertheless, taking the overlap integrals (Table 2.3) into account, the correlation between them can be discussed to some extent. From the band structural point of view, the energy of the band gap is twice the amount of the activation energy, and corresponds to the difference between transfer energies in the dimer (t) and between the dimers (t') (Scheme 2.5). The band bap is dominated by the overlap of the π-orbitals in the TCNQ dimer. For almost all the salts, the overlap integrals in the multimer are around 0.02. Probably this is the reason why the resistivity and the activation energy is not so much different among all the TCNQ salts. Another factor which affects the activation energy is the lattice defects. The lattice defects may act both the source of carriers and a trap for charge transport. In addition, the effects of the lattice defects will stronger if the TCNQ stack is closer to an ideal 1-D column. This can be affected by the degree of the slip between the TCNQ multimer and the difference of the stoichiometry. Therefore, the activation energy of the n = 6 salt (1:4 stoichiometry) is not so much high in spite of the high resistivity, while the activation energy of the n = 6 salt (1:3 stoichiometry) is relatively larger in spite of the low resistivity. The optical absorption band with the lowest energy in these salts occurred in the infrared region with a broad peak at 0.4-0.5eV (Figure 2.3.7). This indicates that they are band insulators with a band gap between the valence and conduction bands. Considering that the segregated column structures and the fractional

charge of the TCNQ molecules were attained principally in all the crystals, these semiconducting behaviors are considered to be derived from the uneven stack in the TCNQ columns (dimerized, trimerized or tetramerized) and the strong electron correlations

Table 2.6. Resistivity at room temperature (RT) and the activation energy for conduction in the C*n*BPy TCNQ salts.

	Resistivity at RT [Ω cm]	Activation energy [eV]
$n = 1$	22	0.16
$n = 2$	2.0×10^{3}	0.20
$n = 3(\alpha)$	1.1×10^{3}	0.19
$n = 3(\beta)$	3.3×10^{3}	0.13
$n = 4$	3.4×10^{3}	0.16
$n = 5$	4.9×10^{3}	0.14
$n = 6(1:4)$	6.2×10^{4}	0.20
$n = 6(1:3)$	50	0.25

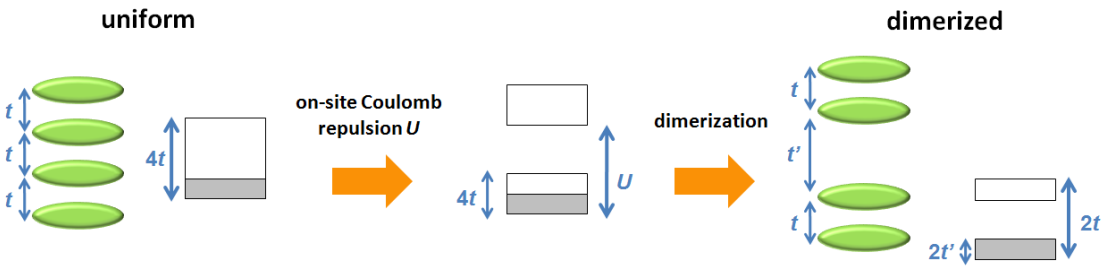

Scheme 2.5. The band structural model of the 1/4-filled TCNQ column.

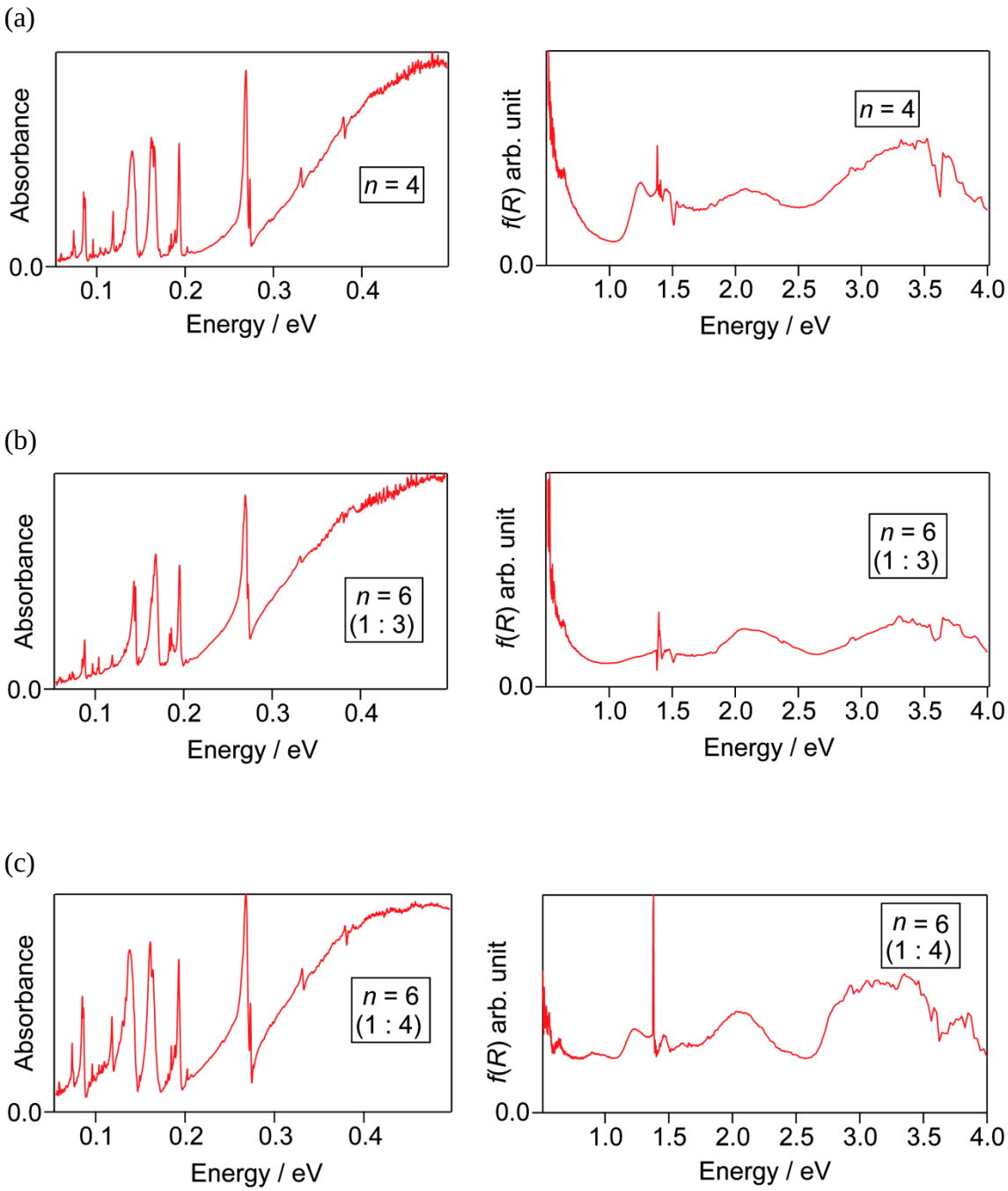

Figure 2.3.7. Optical spectra of (a) $(C4BPy)(TCNQ)_4$, (b) $(C6BPy)(TCNQ)_3$, and (c) $(C6BPy)(TCNQ)_4$. For each compound, the left-side panel indicates the IR spectrum, and the right-side panel indicates the diffuse reflectance spectrum (nearIR-vis-UV region) converted to the Kubelka-Munk function, $f(R)$, corresponding to the absorption. Optical spectra of other $(CnBPy)(TCNQ)_x$ salts are practically the same as those shown above.

The conductivity of this series will be evaluated referring to the guideline for designing the conductive organic crystals. If the condition described in 2.1.1 are applied for the dication-TCNQ salts, segregated TCNQ columns and fractionally charged TCNQ molecules are required to obtain good conductivities. The former was attained for all salts, and the latter was also attained for almost all salts except for n = 5. Nevertheless, the electric behavior of them was not metallic but semiconducting. This is because the TCNQ columns take multimeric structures in the crystals. Namely, the overlap of the LUMO decreases periodically, and then the electronic transportation is hampered. This means that the band widths were not successfully spread. This multimerization are obvious except for n = 1. It is because the packing of the dications are prior to TCNQ stack. This effect will be greater as the size of the dications gets larger. On the other hand, alkyl chains do not have strong chemical interaction with TCNQ, which is favorable for obtaining uniform TCNQ columns. However, even if an alkyl chain takes the all-trans conformation, it cannot be a complete linear chain, leading to obstruction of a uniform stack of TCNQ column from the spatial point of view. The effect of the steric hindrance derived from the alkyl chain will be greater as the size of the dication become larger, and more it will be if the dication cannot take the an all-trans conformation. These effects are reflected in the multimerization of the TCNQ column for n = 3, 4, 5, 6, where the size of the dication is relatively larger than that of TCNQ. Therefore a smaller size of dication is required to improve the conductivity of the crystal. For n = 2, another problem occurred; an appropriate dication length cannot be obtained to achieve 1:4 stoichiometry, which forces the stoichiometry to be 1:3. For n = 1, most of the obstacles mentioned above were alleviated. An extremely short alkyl chain contributes the decrease of the steric hindrance for the

uniform TCNQ stack. The steric hindrance is reduced also by the insertion of the solvent acetonitrile. Moreover, due to the small size of the dication itself, the self-assembly of the TCNQ can be prior to the conformation of the dication, leading to the relatively uniform TCNQ stack. As a result, a wide band width was successfully obtained, and the highest conductivity was achieved in this series of the TCNQ salts.

2.3.3. Magnetic properties

Although the series of the TCNQ salts exhibited a variety of structures, the charge transport did not show dramatic change by the difference in the π–π stacking patterns. Since the charge transport exhibited rather localized charge features in all the salts, their magnetic properties were expected to be a sensitive probe of the electronic structure in these TCNQ anion radical salts. Magnetic susceptibility derived from the unpaired electron has a variety of temperature-dependence owing to the difference in the interaction between the adjacent spins. These magnetic behaviors have been studied for inorganic materials, and they have been succeedingly applied for organic materials. In most cases, inorganic materials consist of metal atoms or their oxides, and the magnetic properties reflect the overall three-dimensional crystal structures. On the other hand, organic compounds consist of anisotropic shaped molecules. Thus, spin-spin interaction will become also anisotropic, resulting in the limited directional magnetic networks. These organic magnets are useful as models of low-dimensional magnets, and for the verification of the theory. If the magnetic properties of organic crystals can be controlled by modifying the crystal structures, it will be possible to generate desired magnetic properties by crystal design. Therefore systematic control of the magnetic property can lead to multiple applications such as the development of new switching

devices, manifestation of photomagnetic effects, and for controlling spin cross over.

However, it has been very difficult to precisely control the magnetic properties by modifying the crystal structures. This is because the intermolecular interactions are very weak for organic magnets, and the crystal packing can greatly vary by only a slight change of structural parameters. For all of the TCNQ anion radical salts obtained in this study, segregated 1-D TCNQ columns were attained. Thus, the problem described above is overcome, and with these crystals it is possible to investigate systematically the variation of the magnetic properties by changing the intermolecular interactions. The magnetic susceptibility of each crystal was examined not only for confirming the multimerization but also for understanding the electronic structures through the magnetic interaction in the multimeric 1-D chain.

Magnetic susceptibility of (C1BPy)(TCNQ)$_4$CH$_3$CN

The result of the magnetic susceptibility measurement for (C1BPy)(TCNQ)$_4$CH$_3$CN is shown in Figure. 2.3.8.

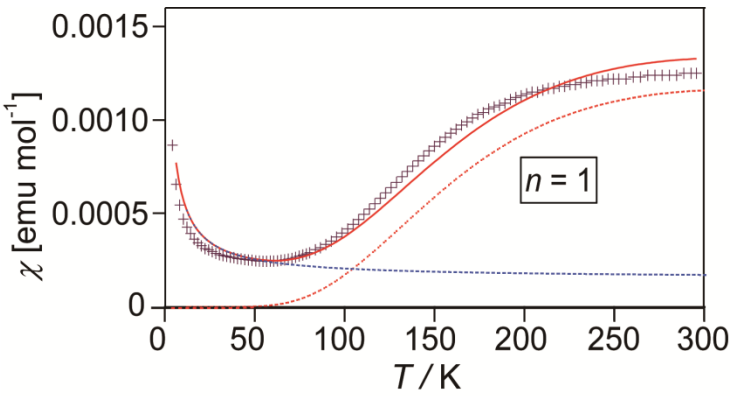

Figure 2.3.8. Magnetic susceptibility of (C1BPy)(TCNQ)$_4$CH$_3$CN. The crosses are the observed values, and the solid lines are the best results of fitting.

For the n = 1 salt, singlet-triplet magnetic behavior was observed from room

temperature to around 50 K and the contribution from the Curie component became visible below 50 K, as shown in Figure 2.3.8. The magnetic susceptibility was fitted to the summation of the thermally activated component and the Curie component [37-40]. Fitting function is as follows:

$$\chi = \frac{2Ng^2\beta^2}{kT\left[3+\exp\left(|J|/kT\right)\right]}x + \frac{C}{T-\theta}(1-x)$$

where N stands for the number of the spins, which corresponds to twice of the Avogadro's number (one spin per TCNQ dimer), and C is the Curie constant, 0.375 emu K mol^{-1}, g is the g-factor, β is the Bohr magneton, J is the exchange magnetic interaction between two adjacent spins, k is the Boltzmann constant, x is a fraction of the thermally activated component, and θ is the Weiss temperature. As a result of fitting, $|J|/k$ = 510 K, x = 0.986 (θ = -2.5 K).

According to the values of the overlap integrals, it was suggested that TCNQ columns were not significantly dimerized. Because of this, the n = 1 salt had the highest conductivity among this series of TCNQ salts studied. The reproduction of the magnetic behavior with the singlet-triplet model meant that a spin dimer was formed in the ground state. Furthermore, the value of $|J|$ was considerably high for this salt. The activation energy of the conduction (0.16 eV) suggested that there was a large charge gap. This was consistent with the large $|J|$ and the semiconducting behavior. The spin model for the n = 1 salt is described in Scheme 2.6.

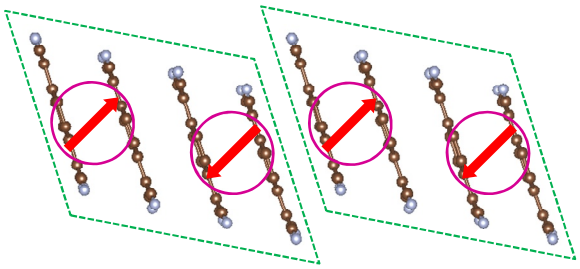

Scheme 2.6. Singlet-triplet type spin model for *n* = 1. Each green parallelogram surrounds the configurational repeating unit of the TCNQ column, in which the spins form a singlet pair.

Magnetic susceptibility of (C2BPy)(TCNQ)$_3$

For the *n* = 2 salt, the magnetic susceptibility was almost equal to zero in the whole temperature region (2-300 K). As described in structural discussion, the TCNQ column was trimerized, and each TCNQ molecule had -2/3 charge. Thus it is considered that two spins are shared by three TCNQ molecules, and the two spins are cancelled their magnetic moments with each other, leading to the extinction of the magnetic moment and non-magnetic behavior.

Magnetic susceptibility of α-(C3BPy)(TCNQ)$_4$

The result of the magnetic susceptibility measurement for α-(C3BPy)(TCNQ)$_4$ is shown in Figure. 2.3.9.

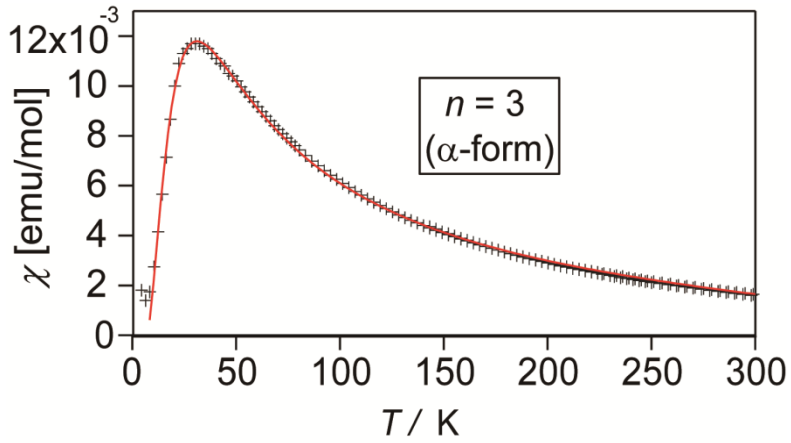

Figure 2.3.9. Magnetic susceptibility of α-(C3BPy)(TCNQ)$_4$. The crosses are the observed values, and the solid lines are the best results of fitting.

In this salt, the TCNQ column is dimerized and the formal charge is almost -1/2 for each TCNQ molecule. Thus, it is considered that one spin is shared by two TCNQ molecules. According to the crystal structure, there is no center of symmetry between two adjacent TCNQ dimers. Therefore the interactions between two adjacent dimers were alternatingly different, so were the exchange interactions between the spins. The spin model could be described using Scheme 2.7. The magnetic susceptibility was fitted to the function of an alternating chains model with the alternating parameter $\alpha \leq 0.4$for antiferromagnetically coupled S= 1/2 spins [37, 41].

$$\chi = \frac{Ng^2\beta^2}{kT}\frac{A + Bx + Cx^2}{1 + Dx + Ex^2 + Fx^3}$$

where $x = \frac{|J|}{k}$.

J is the exchange magnetic interaction between two adjacent spins, k is the Boltzmann constant, β is the Bohr magneton, N stands for the number of the spins, which corresponds to twice of the Avogadro's number (one spin per TCNQ dimer),and

A = 0.25,

$B = -0.062935 + 0.11376\alpha$

$C = 0.0047778 - 0.033268\alpha + 0.12742\alpha^2 - 0.32918\alpha^3 + 0.25203\alpha^4$

$D = 0.053860 + 0.70960\alpha$

$E = -0.00071302 - 0.1058\alpha + 0.54883\alpha^2 - 0.20603\alpha^3$

$F = 0.047193 - 0.0083778\alpha + 0.87256\alpha^2 - 2.7098\alpha^3 + 1.9798\alpha^4$.

As a result from fitting, $\alpha = 0.17$ and $|J|/k = 47.8$ K.

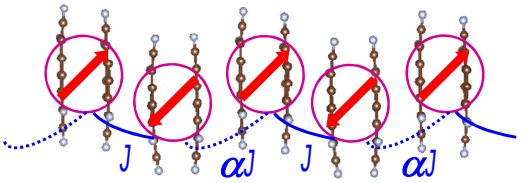

Scheme 2.7. Alternating chain type spin model. The red arrows are $S = 1/2$ spin in the dimeric unit, the blue solid curves are the one kind of exchange interactions (J), and the dashed curves are the other kind of exchange interactions (αJ).

Magnetic susceptibility of β-(C3BPy)(TCNQ)$_4$

The result of the magnetic susceptibility measurement for β-(C3BPy)(TCNQ)$_4$ is shown in Figure 2.3.10.

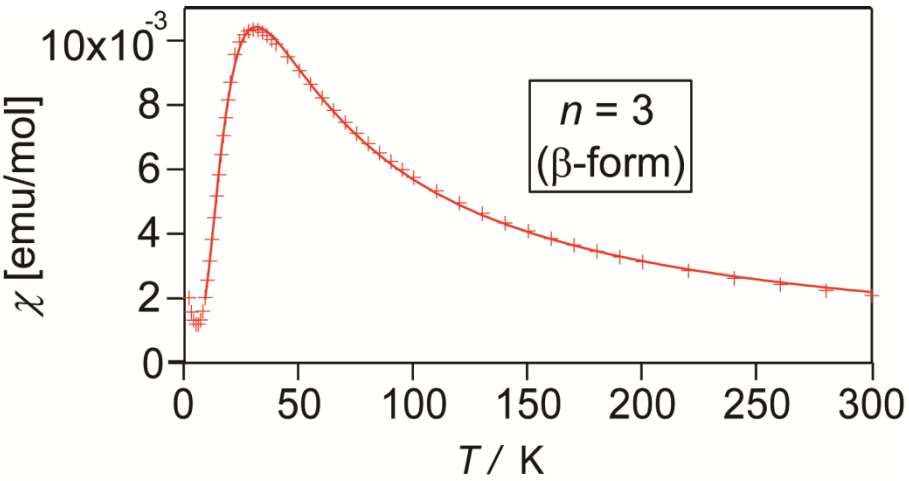

Figure 2.3.10. Magnetic susceptibility of β-(C3BPy)(TCNQ)$_4$. The crosses are the observed values, and the solid lines are the best results of fitting.

In this salt, the TCNQ column is dimerized and the formal charge is almost -1/2 for each TCNQ molecule. Thus, it is considered that one spin is shared by two TCNQ molecules. According to the crystal structure, there is no center of symmetry between two adjacent TCNQ dimers. Therefore the interactions between two adjacent dimers were alternatingly different, so were the exchange interactions between the spins. The spin model could be described just the same as α-(C3BPy)$(TCNQ)_4$, using Scheme 3. The magnetic susceptibility was fitted to the function of an alternating chains model with the alternating parameter $\alpha \leq 0.4$for antiferromagnetically coupled S= 1/2 spins described for α-(C3BPy)$(TCNQ)_4$. As a result from fitting (Figure 2.3.10), $\alpha = 0.12$ and $|J|/k = 51.6$ K.

Magnetic susceptibility of (C4BPy)$(TCNQ)_4$

The result of the magnetic susceptibility measurement for (C4BPy)$(TCNQ)_4$ is shown in Figure 2.3.11.

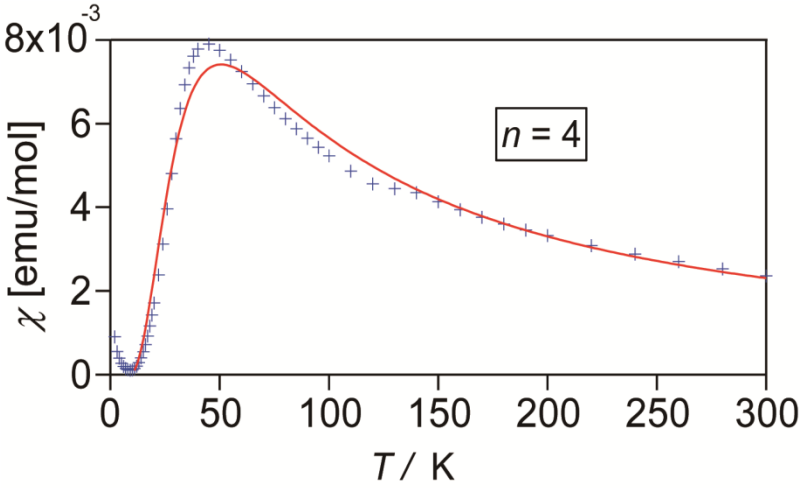

Figure 2.3.11. Magnetic susceptibility of (C4BPy)$(TCNQ)_4$. The crosses are the observed values, and the solid lines are the best results of fitting.

In this salt, the TCNQ column is dimerized and the formal charge is almost -1/2 for each TCNQ molecule. Thus, it is considered that one spin is shared by two TCNQ molecules. According to the crystal structure, there is no center of symmetry between two adjacent TCNQ dimers. Therefore the interactions between two adjacent dimers were alternatingly different, so were the exchange interactions between the spins. The spin model could be described just the same as α-(C3BPy)$(TCNQ)_4$ and β-(C3BPy)$(TCNQ)_4$using Scheme 6. The magnetic susceptibility was fitted to the function of an alternating chains model with the alternating parameter $\alpha \leq 0.4$for antiferromagnetically coupled S= 1/2 spins described previously. As a result from fitting (Figure 2.3.11), $\alpha = 0.03$ and $|J|/k = 80.6$ K.

Magnetic susceptibility of (C5BPy)$(TCNQ)_4$

The result of the magnetic susceptibility measurement for (C5BPy)$(TCNQ)_4$ is shown in Figure 2.3.12.

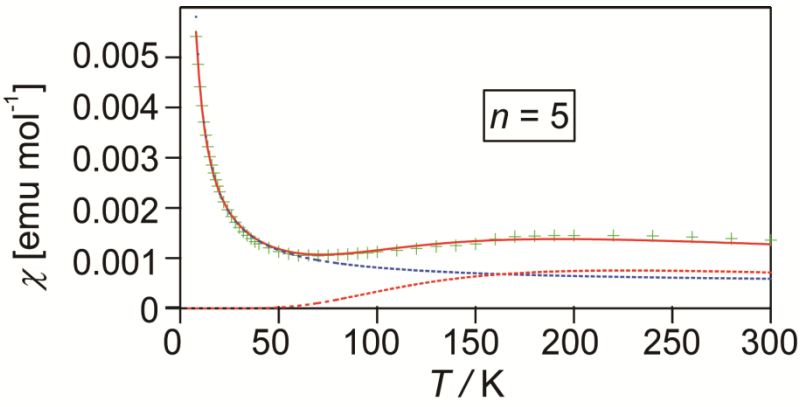

Figure 2.3.12. Magnetic susceptibility of (C5BPy)$(TCNQ)_4$. The crosses are the observed values, and the solid lines are the best results of fitting.

As described in the structural discussion, two types of tetramers were arranged

alternately. In one of the tetramers (CDD'C'), the charges were localized on the two middle molecules (D, D') and the two spins are cancelled each other, leading to the extinction of the magnetic moment resulting in a spin singlet in this part. From this future, the two spins that were accommodated in the other tetramer (BAA'B') were isolated, leading to singlet-triplet type magnetic behavior (Scheme 2.8) in which one-half of the formal TCNQ dimers contributed to the paramagnetism (*N* becomes just the Avogadro's number). The fitting was performed using the equation used for (C1BPy)$(TCNQ)_4CH_3CN$. As a result of fitting in Figure 2.3.12, $|J|/k$ = 353 K, x = 0.905 (θ = 1.0 K).

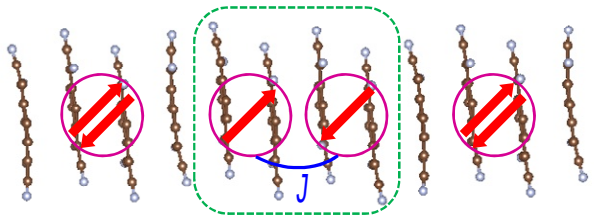

Scheme 2.8. Singlet-triplet type spin model for n = 5.The green dashed line surrounds a pair of the TCNQ dimers that contribute to the singlet-triplet type paramagnetism.

Magnetic susceptibility of (C6BPy)$(TCNQ)_4$

The result of the magnetic susceptibility measurement for (C6BPy)$(TCNQ)_4$ is shown in Figure 2.3.13.

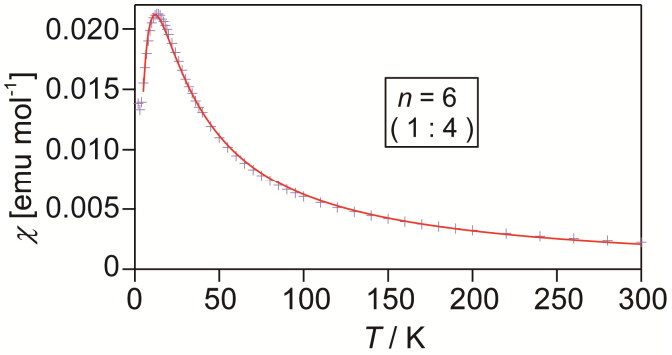

Figure 2.3.13. Magnetic susceptibility of (C6BPy)(TCNQ)$_4$. The crosses are the observed values, and the solid lines are the best results of fitting.

In this salt, the TCNQ column is dimerized and the formal charge is almost -1/2 for each TCNQ molecule. Thus, it is considered that one spin is shared by two TCNQ molecules. According to the crystal structure, there is a center of symmetry between two adjacent TCNQ dimers, leading to a uniform exchange interactions between them. The spin model for antiferromagnetically coupled S= 1/2 spins could be described using Scheme 2.9 and the susceptibility was fitted to:

$$\chi = \frac{Ng^2\beta^2}{kT}\frac{0.25 + 0.074975\ x + 0.075235\ x^2}{1.0 + 0.9931\ x + 0.172135\ x^2 + 0.757825\ x^3}$$

where $x = \frac{|J|}{k}$, and N stands for the number of the spins, which corresponds to twice of the Avogadro's number [35, 40-42].

As a result of fitting (Figure 2.3.13), $|J|/k$ = 7.2 K.

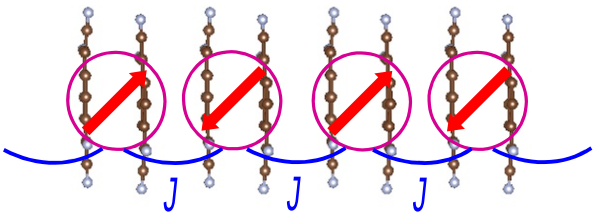

Scheme 2.9. Antiferromagnetic 1-D chain (Bonner-Fisher type) spin model. The red arrows are S = 1/2 spin in the dimeric unit, and all the blue solid curves represent the same scale of exchange interaction (J).

Magnetic susceptibility of (C6BPy)(TCNQ)$_3$

For the (C6BPy)(TCNQ)$_3$, the magnetic susceptibility was almost equal to zero in the whole temperature region (2-300 K). As described in structural discussion, the TCNQ column was trimerized, and each TCNQ molecule had -2/3 charge. Thus it is considered that two spins are shared by three TCNQ molecules, and the two spins are cancelled each other, leading to the extinction of the magnetic moment and non-magnetic behavior.

The temperature dependence of the susceptibility is classified into four types; namely, alternating chain, Bonner-Fisher, singlet-triplet, and spin singlet ones.

Alternating chain type salts. The n = 3 (α-form), n = 3 (β-form) and n = 4 salts are classified as alternating chain type salts. In these salts, the TCNQ column is composed of TCNQ dimer units. Since the interactions between two adjacent dimers were alternatingly different, so were the exchange interactions between the spins, each of which were accommodated in the dimer.

Antiferromagnetic 1-D chain (Bonner-Fisher type) salts. The n = 6 (1:4) salt is a Bonner-Fisher type salt. The 1-D chain was composed of TCNQ dimer units and the center of symmetry was located on the midpoint of each dimer unit (AA' and BB'). Consequently, the exchange interactions between two adjacent dimers were uniform.

Singlet-triplet type salts. The n = 1 and n = 5 salts are singlet-triplet type salts. For

both of them, the magnetic susceptibilities of the two salts were fitted to the summation of the thermally activated component and the Curie component [37, 42–45]. However, the spin model is different between these two salts. For the n = 1 salt, the spin dimer was formed in the ground state, but the dimerization was not significant from the structural point of view. In the case of an antiferromagnet, the magnetic susceptibility does not become zero at the lowest temperature. For the n = 1 salt, the ground state is singlet, which means that the dimerization between the TCNQ dimers (each accommodates one spin) is rather strong (at least, the dimerization of the spins should become strong at the lower temperature). This behavior is inconsistent with the good conductivity, but the details have not been clarified. However, this feature of the spin structure in the n = 1 salt was reflected on the electric behavior (high conductivity but semiconducting with large activation energy).

On the other hand, for the n = 5 salt, singlet-triplet type magnetic behavior was derived from the long distance between the two-spin dimers owing to the absence of the magnetic moment because of the spin cancellation. For the n = 5 salt, the distribution of the Curie component is much larger (Figure 2.3.14). This is probably because of the lattice defect or the not-fully dimerized spin (D, D’ described in Figure 2.3.1 (d)) due to the poorer crystallinnity than other crystals of this series.

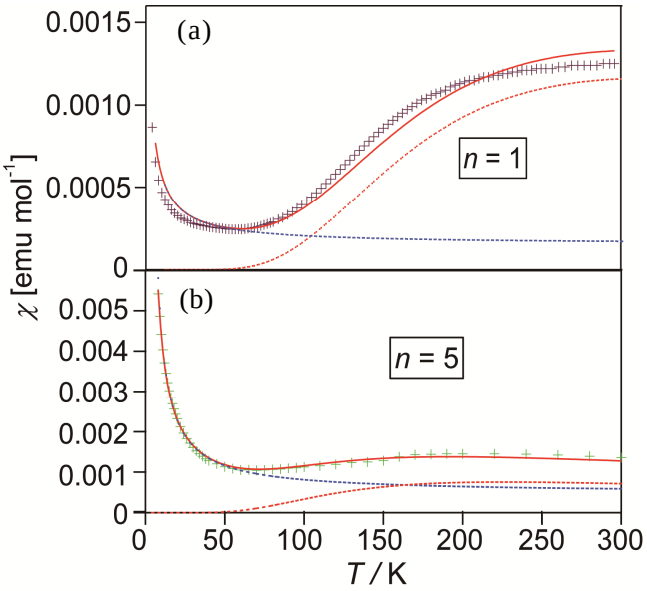

Figure 2.3.14. Magnetic susceptibility of (a) $(C1BPy)(TCNQ)_4$ and (b) $(C5BPy)(TCNQ)_4$. The crosses are the observed values, the red dotted lines are the thermally activated components, the blue dotted lines are the Curie components, and the solid red lines are the best fit of the summation of the thermally activated and Curie components.

Spin singlet type salts. The n = 2 and n = 6 salts (1:3 stoichiometry) are spin singlet type salts. The two spins were accommodated in the TCNQ trimer and the antiferromagnetic interactions between the two spins in the trimer were considerably strong, leading to non-magnetic behavior (Scheme 2.10).

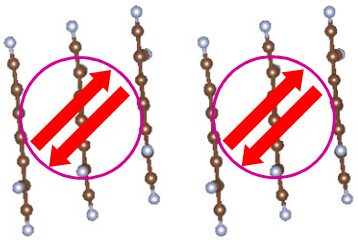

Scheme 2.10. Spin singlet type spin model

As mentioned above, the magnetic behavior of this series of TCNQ salts depended on the value of *n*. These magnetic behaviors can be explained by the spin models where the spins were accommodated in the TCNQ and were classified into several types. If these spin models were arranged according to the change of *n* and stoichiometry, there was an interesting relationship between the size change of the dications and the variations in the spin structures, as summarized in Figure 2.3.15.

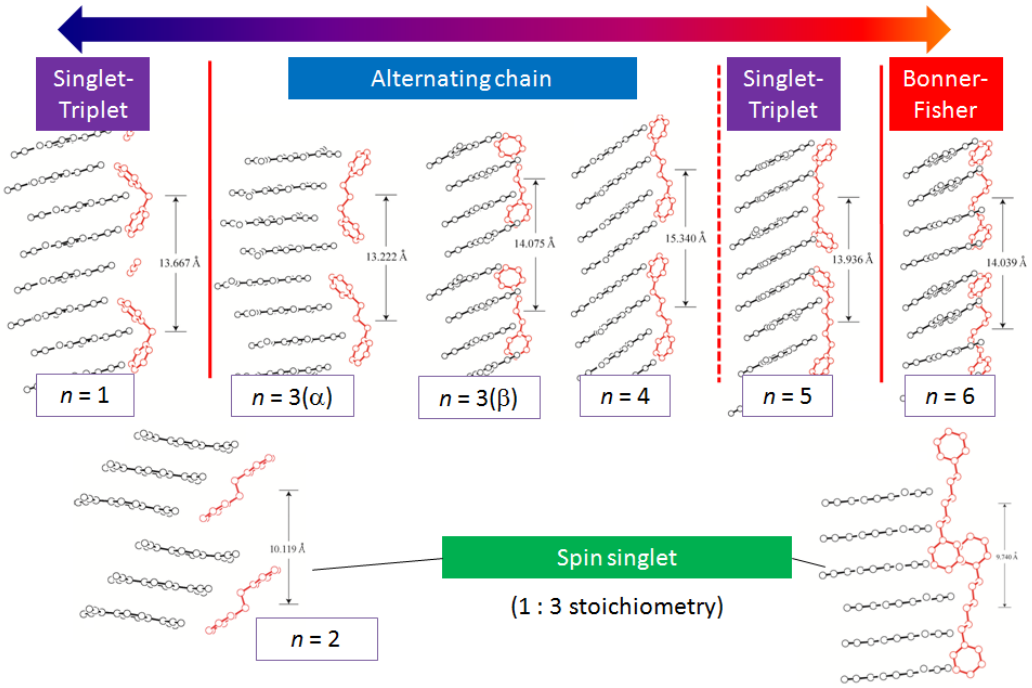

Figure 2.3.15. Correlations between the variations in the magnetic behavior and the size of the dication.

Taking the concept of the effective dication length into account, it can be presumed that the appropriate dication sizes for forming 1:4 TCNQ salts were achieved when *n* = 3 and 4. In this case, significant dimerization of the TCNQ column appeared, corresponding to alternating chain-type magnetic behavior. If the *n* value was further increased, the dication size became too big. Therefore, the TCNQ molecules were

required to arrange in an energetically disadvantageous manner, resulting in different spin structures from that of n = 3 and 4 salts. Now the n = 5 and n = 6 (1:4) salts will be compared with the n = 3 and 4 salts. In the n = 6 case, the $|J|$ value between the TCNQ dimers greatly decreased, reflecting the decline in the molecular planes in the two adjacent TCNQ dimers, accompanied with the dication transformation. The dimerized TCNQ column was similar to that in the n = 3 and 4 salts, therefore the magnetic behavior of the n = 6 (1:4) salt was rather similar to those of the n = 3 and 4 salts. On the contrary, for the n = 5 salts, the magnetic behavior was quite different from that of the n = 3, 4 and 6 salts, reflecting the charge localization. This large change in the magnetic behavior was likely derived from the parity of n for the crystal packing.

For the n = 1 or 2 cation, it was difficult to take the 1:4 stoichiometry because of the small size of the dication. For n = 2, the stoichiometry changed into 1:3, leading to spin singlet type magnetic behavior. For n = 1, there was a relatively uniform TCNQ stack, owing to the introduction of solvent molecules, which may have resulted in different magnetic behavior from that of the n = 3 and 4 salts. As stated above, variations in the spin structures with different dication sizes can be rationalized by introducing the concept of the effective dication length.

2.4. Summary and conclusion

By using size tunable dications a series of TCNQ salts, (CnBPy)$(TCNQ)_x$ were fabricated. For all of these crystals, the TCNQ molecules stacked in a face-to-face manner, thus the segregated conducting columns were attained. The stoichiometry did not vary much with a change in the dication size, taking only two stoichiometries, either 1:3 or 1:4. This meant that the stoichiometries of the TCNQ salts in this study were

dominated by the preferential charge in TCNQ and the dications flexibly adjusted their lengths over a certain range to achieve the desired stoichiometry. For either of the two stoichiometries, each TCNQ molecule had fractional charge in principle. Therefore, this series of TCNQ salts met both the structural and electronic requirements for conducting organic crystals. However, all of the salts demonstrated semiconducting behavior. This was because the non-uniform overlap of the LUMO between the TCNQ molecules prevented the column TCNQ from obtaining sufficient band widths to have the valence bands and conduction bands overlap. There was a correlation between the conductivity and the overlap integrals in the TCNQ columns. The smallest overlap integral was found for n = 6 salt (1:4 stoichiometry), resulting in the lowest conductivity of this series. On the contrary, there was not a significant alternation of the overlap integrals for n = 1 salt owing to the relatively small dication and inserted solvent molecules, leading to the highest conductivity of this series. Therefore one effective attitude to improve the conductivity was able to be proposed. Another proposal about crystal design for the improvement of the conductivity could be carried out. Now the disarray of the TCNQ stack proved to be a hindrance to high conductivity and it derives from the flexibility of the alkyl chains of the dication. Thus the hindrance would be reinforced by using a rigid alkene or alkyne as the organic spacer instead of alkyl chains. If such TCNQ salts are successfully designed, the conductivity can be higher than that of n = 1 salt, giving further information about the design of conductors with size tunable counter ions.

Of the possible two stoichiometries, the dominant one was 1:4, but it could shift to 1:3 depending on the dication size. Considering the effective dication length, the TCNQ stacking state and the formal charge, the 1:4 stoichiometry was preferred when n = 3 or

4. When *n* was increased above these values, some load was applied to form a 1:4 salt. This effect appeared as a charge localization for the $n = 5$ salt and as a severe distortion of the dication molecules or a stoichiometry change for the $n = 6$ salt. On the contrary, the 1:3 stoichiometry occurred when $n = 2$. Insertion of solvent molecules occurred when $n = 1$, caused by their short lengths.

The different assembling states resulted in variations in the spin states, and their magnetic properties were investigated by classifying the temperature dependence of the susceptibility and by modeling the spin structure based on the crystal structure. Since this study is the first example in which single crystals of a full series of TCNQ anion radical salts with a size-tunable cation were successfully prepared and the details of their charge transport and magnetic properties were determined, the results described in the chapter is quite valuable. From the knowledge about structure-property correlation obtained from this study of the series of TCNQ salts, one can estimate the magnetic properties to some extent if only the crystal structure is known. This estimation may be applied for the other charge transfer salts or charge transfer complexes with π-stacks. Therefore, this series of TCNQ salts can be one good prototype for designing the organic crystals with desired magnetic properties.

References

[1] Saito, G.; Ferraris, J. P. *Bull. Chem. Soc. Jpn.*, **1980**, 53, 2141-2145.

[2] Torrance, J. B. *Acc. Chem. Res*., **1979**, 12, 79-86.

[3] Sekizaki, S.; Konsha, A.; Yamochi, H.; Saito, G. *Mol. Cryst. Liq. Cryst*, **2002**, 376, 207-212.

[4] Suzuki, T.; Kabuto, C.; Yamashita, Y.; Mukai, T.; Miyashi, T.; Saito, G. *Bull. Chem. Soc. Jpn*, **1988**, 61, 483-493.

[5] Ferraris, J.; Cowan, D. O.; Walatka, V.; Perlstein, J. H. *J. Am. Chem. Soc.*, **1973**, 95, 948-949.

[6] Fahrenbach, A. C.; Sampath, S.; Late, D. J.; Barnes, J. C.; Kleinman, S. L.; Valley, N.; Hartlieb, K. J.; Liu, Z.; Dravid, V. P.; Schatz, G. C.; Duyne, R. P. V.; Stoddart, J. F. *ACS NANO*, **2012**, 6, 9964-9971.

[7] Berr, S.; Jones, R. R. M.; Johnson, J. S. *J. Phys. Chem.*, **1992**, *96*, 5611-5614.

[8] Konno, M.; Saito, Y. *Acta Crystallogr. B*, **1981**, *37*, 2034-2043.

[9] Rizkallah, P. J.; Wallwork, S. C.; Graja, A. *Acta Crystallogr. C*, **1983**, *39*, 128-131.

[10] Malatesta, V.; Millini, R.; Montanari, L. *J. Am. Chem. Soc.*, **1995**, *117*, 6258-6264.

[11] Takagi, S.; Nakao, K.; Nakatsu, K. *J. Phys. Soc. Jpn.*, **1994**, *63*, 271-282.

[12] Takagi, S.; Nakatsu, K.; Date, M. *J. Phys. Soc. Jpn.*, **1988**, *57*, 2154-2161.

[13] Mathieu, F. *Acta Crystallogr. C*, **1986**, *42*, 1169-1172.

[14] Ashwell, G. J.; Allen, D. W.; Kennedy, D. A.; Nowell, I. W. *Acta Crystallogr. B*, **1982**, *38*, 2525-2528.

[15] Filhol, A.; Zeyen, C. M. E.; Chenavas, P.; Gaultier, J.; Delhaes, P. *Acta Crystallogr. B*, **1980**, *36*, 2719-2726.

[16] Ashwell, G. J.; Eley, D. D.; Wallwork, S. C.; Willis, M. R. *Nature*, **1976**, *259*, 201-202.

[17] Ashwell, G. J.; Eley, D. D.; Fleming, R. J.; Wallwork, S. C.; Willis, M. R. *Acta Crystallogr. B*, **1976**, *32*, 2948-2952.

[18] Ashwell, G. J. *Phys. Stat. Sol. A*, **1984**, *83*, 669-673.

[19] Ashwell, G. J.; Eley, D. D.; Harper, A.; Torrance, A. C.; Wallwork, S. C.; Willis, M. R. *Acta Crystallogr. B*, **1977**, *33*, 2258-2263.

[20] Ashwell, G. J.; Allen, J. G.; Goodings, E. P.; Kennedy, D. A.; Nowell, I. W. *Phys. Stat. Sol. A*, **1983**, *75*, 663-667.

[21] Ashwell, G. J.; Nowell, I. W. *Phys. Stat. Sol. A*, **1984**, *83*, 39-45.

[22] Ashwell, G. J.; Eley, D. D.; Wallwork, S. C.; Willis, M. R.; Welch, G. D.; Woodward, J. *Acta Crystallogr. B*, **1977**, *33*, 2252-2257.

[23] Ashwell, G. J.; Eley, D. D.; Drew, N. J.; Wallwork, S. C.; Willis, M. R. *Acta Crystallogr. B*, **1977**, *33*, 2598-2602.

[24] Ashwell, G. J.; Eley, D. D.; Drew, N. J.; Wallwork, S. C.; Willis, M. R. *Acta Crystallogr. B*, **1978**, *34*, 3608-3612.

[25] Ashwell, G. J. *Phys. Stat. Sol. B*, **1978**, *86*, 705-715.

[26] Ashwell, G. J.; Bartlett, V. E.; Davies, J. K.; Eley, D. D.; Wallwork, S. C.; Willis, M. R.; Harper, A.; Torrance, A. C. *Acta Crystallogr. B*, **1977**, *33*, 2602-2607.

[27] Waclawek, W.; Wallwork, S. C.; Ashwell, G. J.; Chaplain, E. J. *Acta Crystallogr. C*, **1983**, *39*, 131-134.

[28] Hadek, V.; Noguchi, H.; Rembaum, A. *Macromolecules*, **1971**, *4(4)*, 494-499.

[29] SIR 2004. Burla, M. C.; Caliandro, R.; Camalli, M.; Carrozzini, B.; Cascarano, G. L.; De Caro,L.; Giacovazzo, C.; Polidori, G.; Spagna, R. *J. Appl. Crystallogr*., **2005**, *38*, 381-388.

[30] SHELX97. Sheldrick, G. M. **1997.**

[31] CrystalStructure4.0™: Crystal Structure Analysis Package, Rigaku Corporation (2000-2010). Tokyo 196-8666, Japan.

[32] Bain, G. A.; Berry, J. F. *J. Chem. Educ.*, **2008**, *85*, 532-536.

[33] Hoffmann, R. *J. Chem. Phys*. 1963, *39*, 1397-1412.

[34] Whangbo, M. -H.; Hoffmann, R.; Woodward, R. B. *Proc. R. Soc. London, Ser.* A **1979**, *366*, 23-46.

[35] Ren, J.; Liang, W.; Whangbo, M.-H. *CAESAR*; Prime-Color Software, Inc.: Raleigh, NC, **1998**.

[36] Kistenmacher, T. J.; Emge, T. J.; Bloch A. N.; Cowan, D. O. *Acta Crystallogr. B*, **1982**, *38*, 1193-1199.

[37] Kahn, O. In *Molecular Magnetism*; VCH Publishers, Inc.: New York, 1993.

[38] Nomura, M.; Fourmigue, M. *New J. Chem.*, **2007**, *31*, 528-534.

[39] Iwase, K.; Yamaguchi, H.; Ono, T.; Shimokawa, T.; Nakano, H.; Matsuo, A.; Kindo, K.; Nojiri, H.; Hosokoshi, Y. *J. Phys. Soc. Jpn.*, **2013**, *82*, 074719.

[40] Bleaney, B.; Bowers, K. D. *Proc. R. Soc. London, Ser. A*, **1952**, *214*, 451-465.

[41] Hall, J. W.; Marsh, W. E.; Weller, R. R.; Hatfield, W. E. *Inorg. Chem.*, **1981**, *20*, 1033-1037.

[42] Mukherjee, P. S.; Dalai, S.; Mostafa, G.; Lu, T. H.; Rentschler, E.; Chaudhuri, N. R. *New J. Chem.*, **2001**, *25*, 1203-1207.

[43] Bonner, J. C.; Fisher, M. E. *Phys. Rev. A*, **1964**, *135*, 640-658.

[44] Estes, W. E.; Gavel, D. P.; Hatfield, W. E.; Hodgson, D. *Inorg. Chem.*, **1978**, *17*, 1415-1421.

Chapter 3. Carrier doping to the TCNQ anion radical salts by the contact method

3.1. Introduction

3.1.1. The background of the contact method

Thus far, the guideline to design new conductive organic crystals by synthesis has been introduced. Based on the guideline, the specific components have been selected, and the correlation between the crystal structure and their physical properties has been discussed. In this chapter, by the contact method introduced in Chapter1, carrier injection to organic crystals and the improvement of the conductivity induced by the modification of the electronic structure are described. In this section, previously performed studies are described. From these studies, the mechanism of the contact doping is speculated. Along the mechanism proposed, the perspective view and the objects of this study are described. Then, the effects of the carrier doping are evaluated and discussed by several physical measurements.

The carrier doping by the contact method was at first demonstrated by H. Alves et al. in 2008 [1]. In that study, TTF single crystal and TCNQ single crystal were contacted with each other (Figure 3.1.1(a)).

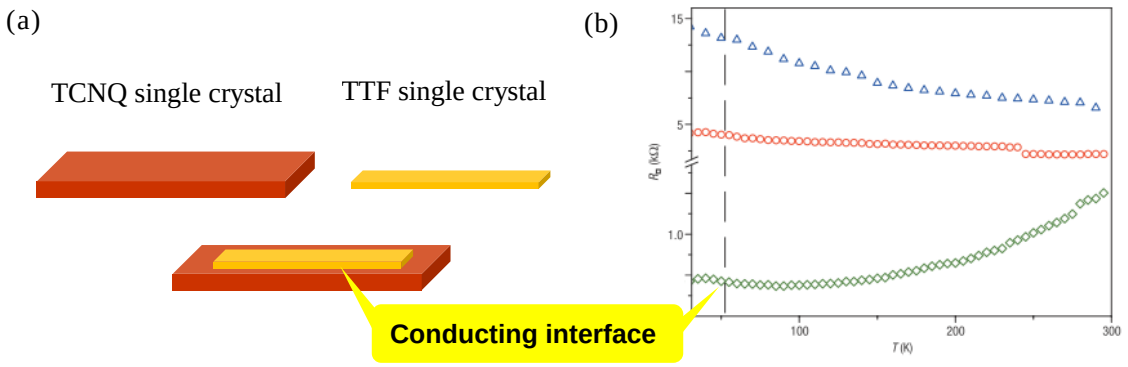

Figure 3.1.1. (a) The initial contact doping with TTF and TCNQ single crystal. (b) The result of the sheet resistance measurement at the interface of the two single crystals.

Originally both of the two are insulators. After the contact, the conductivity of the interface increased and showed a metallic behavior (Figure 3.1.1(b)). A detailed investigation of this interface was executed by Y. Takahashi et al. [2]. In the investigation, growth of new nano crystals was observed at the interface by AFM (Figure 3.1.2(a)). As a result of the Raman spectroscopic measurements of the interface, two peaks different from the original materials were observed (Figure 3.1.2(b)). One of the peak corresponded to that of TTF-TCNQ, and the other corresponded to that of K-TCNQ, namely -1 charged TCNQ. Accordingly, at the interface charge-transfer complex TTF-TCNQ and charge doped crystal surface are formed, and both of them were considered to contribute to the path of the current.

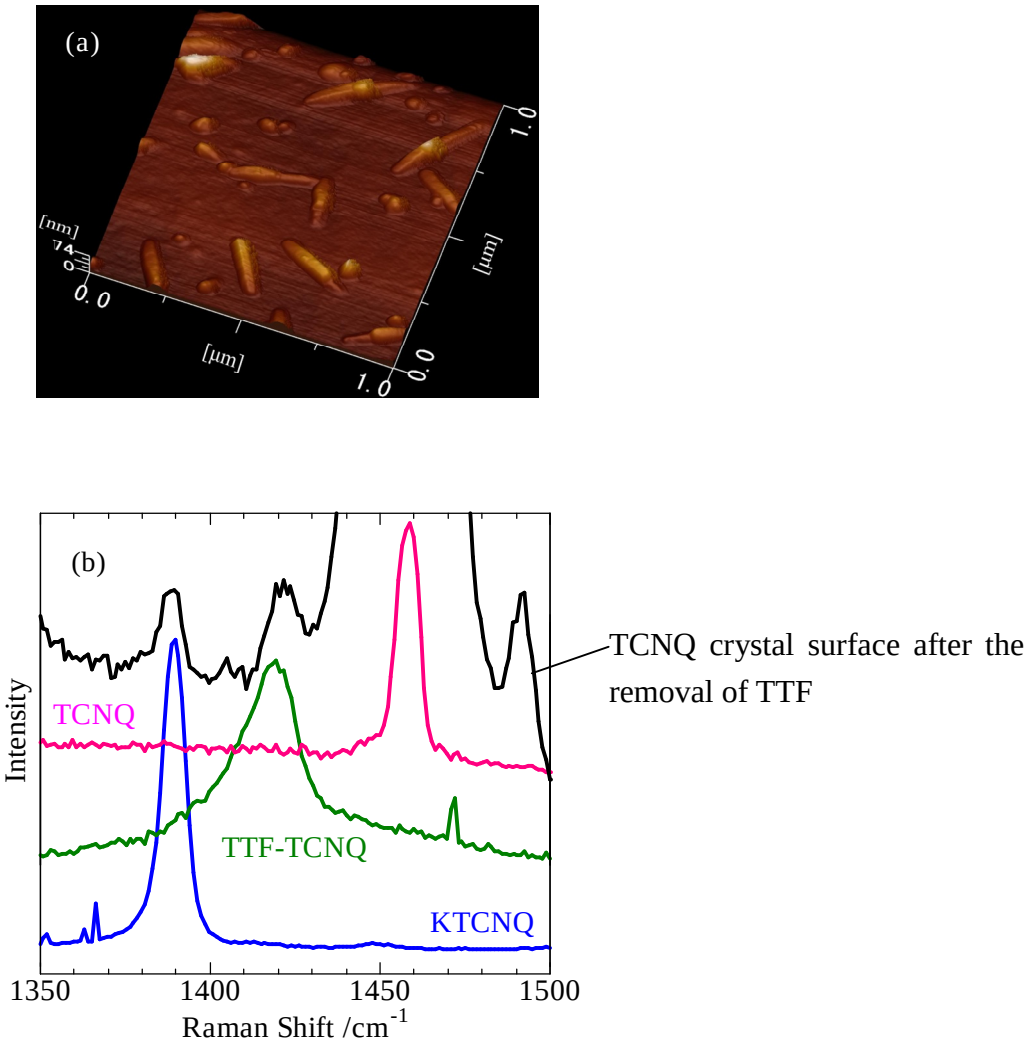

Figure 3.1.2. The AFM image (a) and the Raman scattering spectra (b) of the TCNQ crystal surface after the removal of the TTF powder.

In this manner, the contact method makes it possible to dope carrier to the object very easily, so that it is an effective way to improve the conductivity of semiconductors or insulators and to obtain metallic surfaces. There are two approaches to extend the application of the contact method.

(i) Either “complexes generated on the interface” or “carrier doped interface” can individually contribute to the increase of the conductivity. Only the latter would be

realized when the combination would not give any charge transfer complexes, leading to pure carrier doping to organic semiconductors.

(ii) In the first attempt demonstrated for a combination of TTF and TCNQ, both of them were single component crystals. It might be applicable to the two-component systems, in other words, charge transfer complexes. The doping variation of this method will be greatly increased.

As an example of (i), the combination of nickel-phthalocyanine (NiPc) and 2,5-difuluoro-tetracyanoquinodimethane (F_2TCNQ) was investigated as an object of the contact method (Figure 3.1.3(a)) [3]. It is already known that these two components do not form a charge transfer complex. Nevertheless, the conductivity of the interface was found to be increased after the contact (Figure 3.1.3(b)). Based on this observation, the carrier doping at the contact interface was proved to occur for the proper combination.

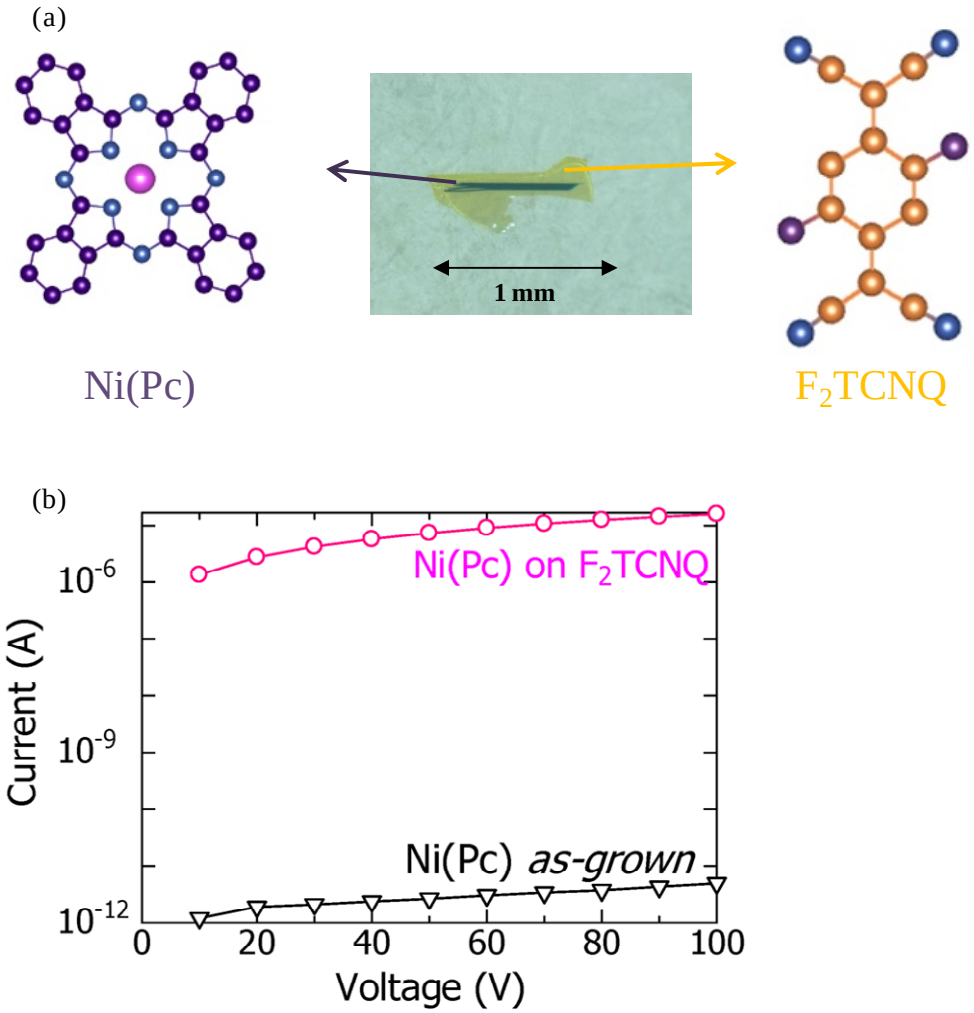

Figure 3.1.3. (a) The contact of NiPc and F_2TCNQ single crystal. (b) The current increase at the interface of the two crystals.

With regard to (ii), carrier doping to the ionic charge transfer complex of ET-F_2TCNQ was performed by contacting TTF on its surface (Figure 3.1.4(a)) [4]. In this experiment, electron doping occurs on the ET-F_2TCNQ crystal surface since TTF is a stronger donor molecule than ET, which is the donor component of the substrate. This is accompanied by the extraction of the F_2TCNQ, leading to the generation of charge transfer complex TTF-F_2TCNQ. Since TTF-F_2TCNQ is an insulator as well as

ET-F_2TCNQ, carrier doped interface is considered to contribute to the increase of the conductivity (Figure 3.1.4(b)).

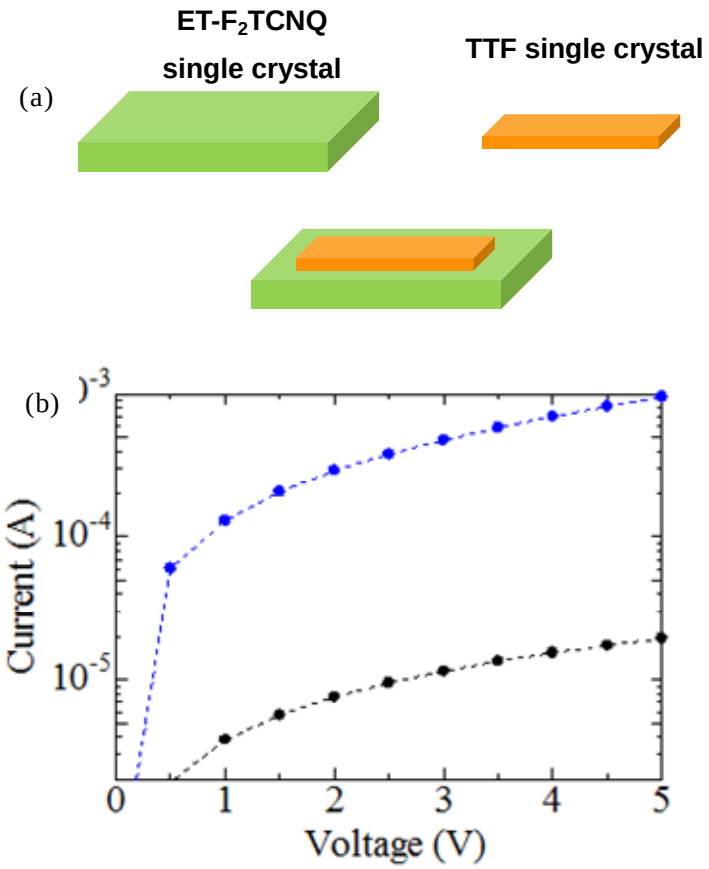

Figure 3.1.4. (a) The contact of ET-F_2TCNQ and TTF single crystal. (b) The current increase at the interface of the two crystals.

Based on these investigations, the mechanism of the carrier doping by the contact method for two-component system can be discussed as follows. Depending on the degree of charge transfer, charge transfer complexes are classified into neutral complexes and ionic complexes.

For neutral complexes, donor components (D) and acceptor components (A) are

regarded to be neutral (described as D^0, A^0, respectively, in this chapter). In such cases, only mixed-stack structures of D^0 and A^0 are obtained, since no cohesive force operates in the segregated-stack structures. For the purpose of the electron doping, the extrinsic donor molecule (D_{ex}) is required to be a stronger one ($D<D_{ex}$). When the electron doping occurs, no other component in the substrate can receive electron than A^0.Therefore, in this case, D_{ex} turns D_{ex}^+, and A^0 turns A^{-1}. In general, a new complex is formed at the interface; $A^{-1}$is extracted to the crystal surface to form an ionic complex of $D_{ex}A$ (Figure 3.1.5). On the other hand, carrier doping without forming ionic CT complexes may not occur, since no stabilization energy is gained by incorporating ionic A^- in the original mixed stack.

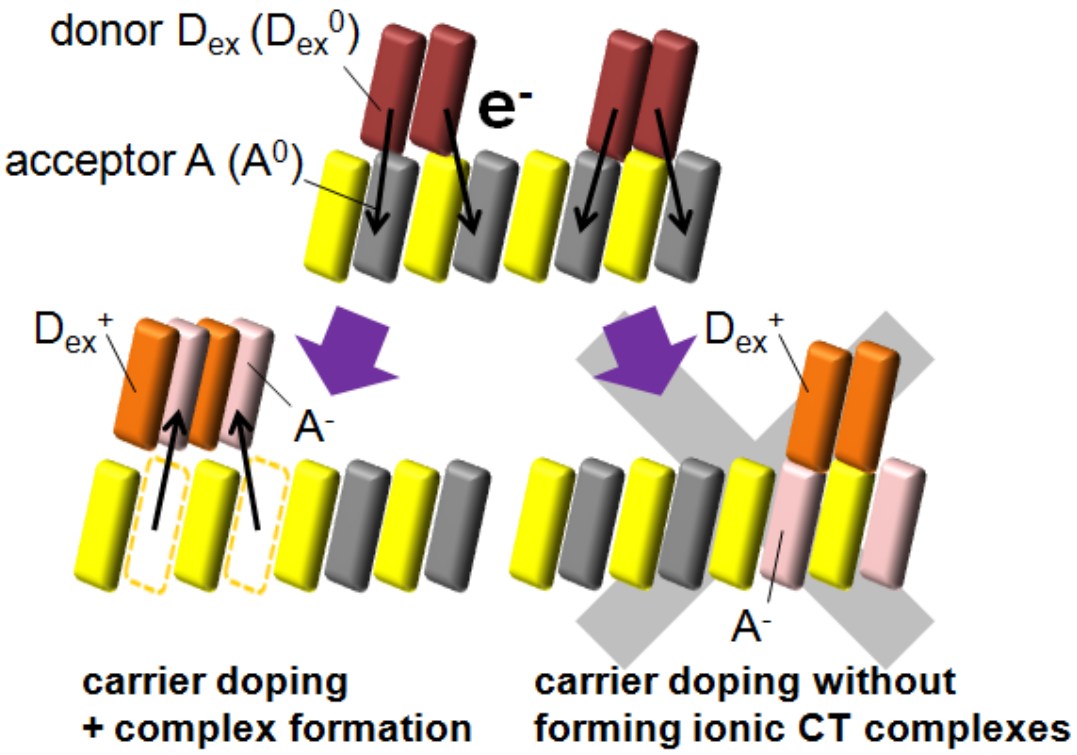

Figure 3.1.5. The electron-doping process for charge transfer complexes with a neutral ground state.

For ionic complexes, donor components and acceptor components are regarded to be ionic states (D^+ and A^-, respectively). In this case, the donor and acceptor components may take either mixed-stack or segregated-stack structures. The electron doping occurs when a stronger donor D_{ex} is contacted on the surface. Since the acceptor components are already ionized (A^{-1}) in the substrate, D^+ will receive the electron. Thus, D_{ex}^0 turns D_{ex}^+, and D^+ turns D^0 as a result of the carrier doping. If a new complex is formed, A^{-1} is extracted to the crystal surface to form $D_{ex}A$ (Figure 3.1.6). Carrier doping without forming $D_{ex}A$ complex might occur for the segregated-stack structure.

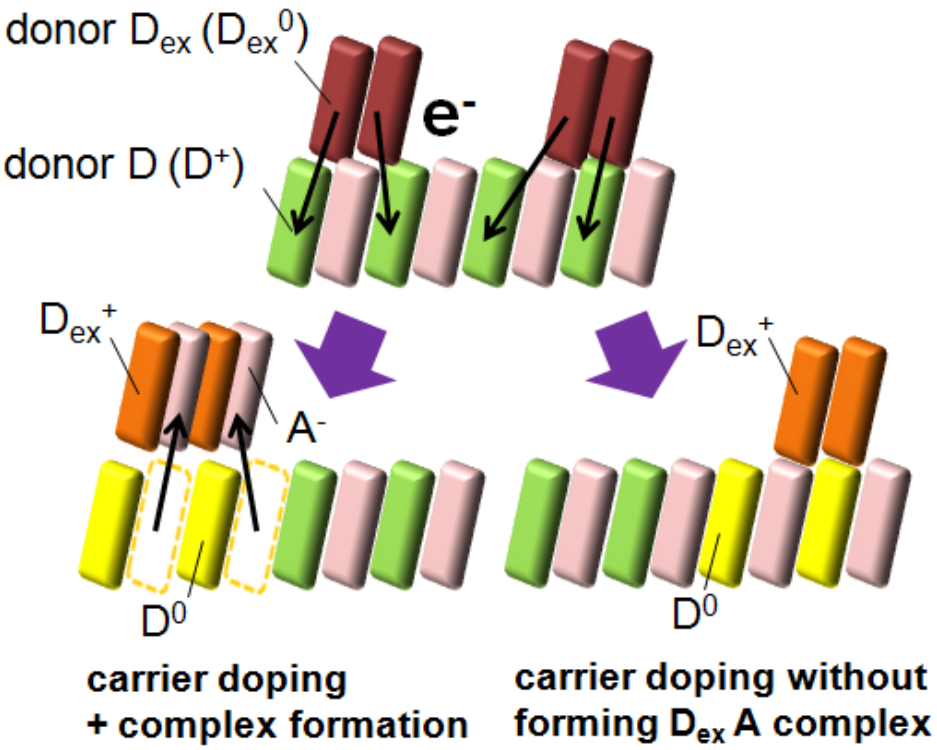

Figure 3.1.6. The electron-doping process for an ionic charge transfer complex.

According to the discussion above, the strength of the donor is important to attain the electron doping. However, it was found that in some cases the electron doping did

not occur even if this condition is fulfilled. Since the contact doping is a novel method for the carrier doping, there are many other parameters to be clarified. To establish systematical conditions for contact doping, it is important to expand its application.

In order to confirm the conditions, a new object for the contact doping was designed in this study. The following points were focused on.

(i) The electron doping to the two-component systems has been attained by contacting strong donor of TTF. However, the hole-doping to the two-component systems has not been attained. If it is shown that the hole-doping is feasible by contacting an extrinsic acceptor, the application of the contact method can widely be expanded.

(ii) The carrier doping for two-component system has been attained only for the complexes with mixed-stack structure so far. There is no example of the carrier doping for the complex with segregated-stack structure.

Based on (i) and (ii), both “the hole doping to the two-component system” and “the carrier doping to the crystal with segregated-stack structure” became the objective of this study. TCNQ anion radical salts are again suitable for this investigation. It is considered that the hole-doping is possible if a stronger acceptor than TCNQ, such as 2,3,5,6-tetrafuluoro-tetracyanoquinodimethane (F_4TCNQ), is conjugated on the surface of the TCNQ anion radical salts. In addition, anion radical salts have segregated-stack structure without any exception, thus they fit the point (ii). At first the TCNQ salts with dications described in Chapter 2 were considered as the candidates. This is because the crystal structures have been disclosed and the direction of TCNQ column can easily be distinguished owing to their clear crystal habit. Additionally, systematical modification of the change in the TCNQ stack was expected to be possible. However, the electrical properties of the dication-TCNQ salts did not changed at all when F_4TCNQ was

conjugated on their surface, therefore no effect of the hole-doping was obtained. As a result of searching appropriate TCNQ anion radical salts, the effect of the hole-doping was observed when K-TCNQ was used as the substrate crystal. In this chapter, the hole-doping for K-TCNQ by F_4TCNQ contact is described. In the next section, the original characteristics of K-TCNQ are explained. Then, the effects of the hole-doping by contacting F_4TCNQ in this study are described, in which the results of AFM, SEM, IR, and conductivity measurements are discussed.

3.1.2. The original characteristics of K-TCNQ

K-TCNQ is a completely-charge transferred anion radical salt, in which the stoichiometry of the potassium ion and TCNQ anion is 1:1. Thus, the initial charge state of TCNQ is fully ionized, which means that the conduction band is half-filled. The crystal structure and the structural phase transition around 395K of K-TCNQ were reported by M. Konno in 1977 [5]. The phase below 395K is called low temperature (LT) phase, where two independent TCNQ molecules individually form segregated columns, and both of the two columns are dimerized (Figure 3.1.7(a), space group: $P2_1/n$, $Z = 8$). This dimerization is verified by the alternating inter-planar distances and the overlap integrals. (In the reference [5], the dimerization is assessed only by the inter-planar distances. In this thesis the overlap integrals were calculated using the CIF crystal data reported.) Owing to this dimerization, a band gap is formed, and the electric behavior of K-TCNQ is insulating. Thus, the LT phase is a band insulator. On the other hand, the TCNQ column becomes uniform stack above 395 K (high temperature (HT) phase, Figure 3.1.7(b), space group: $P2_1/c$, $Z = 2$). This is confirmed by the symmetry of the crystal. In this phase, in spite of the uniform TCNQ stack the electric behavior is

insulating because of the on-site Coulomb repulsion. Thus, the HT phase is a Mott insulator. The inter-planar spacing and the overlap integrals of adjacent TCNQ for respective phases are shown in Table 3.1.1.

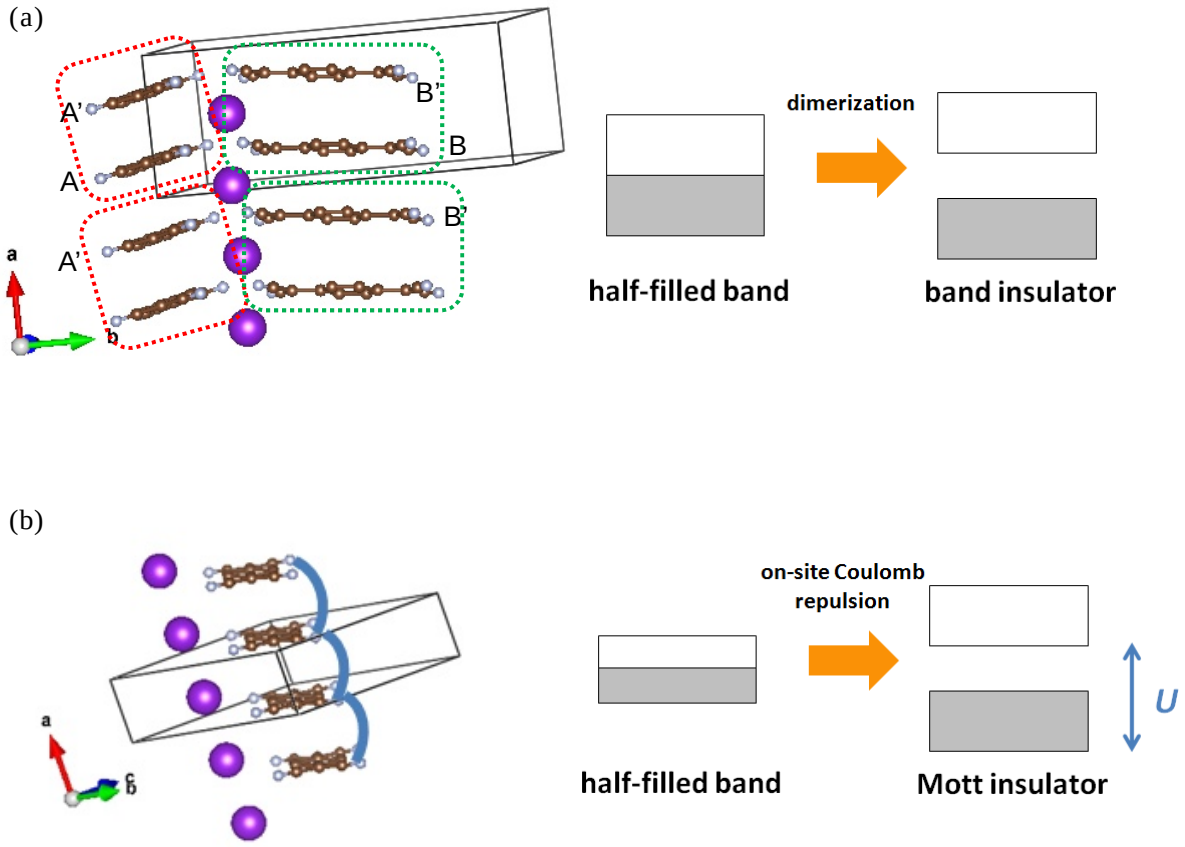

Figure 3.1.7. The crystal structure of K-TCNQ for (a) LT phase and (b) HT phase. For (a), the red and green dotted square describe two independent TCNQ columns. For (b), the blue wavy line means the TCNQ stack is uniform.

Table3.1.1. The interplanar spacing and the overlap integrals of K-TCNQ for LT phase and HT phase

		Inter-planar spacing (Å)	Overlap Integral
LT phase	AA’	3.240	0.0217
(Stack 1)	A’A	3.554	0.0085
LT phase	BB’	3.234	0.0222
(Stack 2)	B’B	3.580	0.0081
HT phase		3.479	0.0128

Another important property of K-TCNQ is the non-linear current-voltage (*I-V*) characteristics, i.e. negative differential resistance characteristics. This is a phenomenon that the resistance rapidly decreases above a certain applying voltage. The negative differential resistance characteristics of K-TCNQ were discovered by R. Kumai in 1999 (Figure 3.1.8) [6].

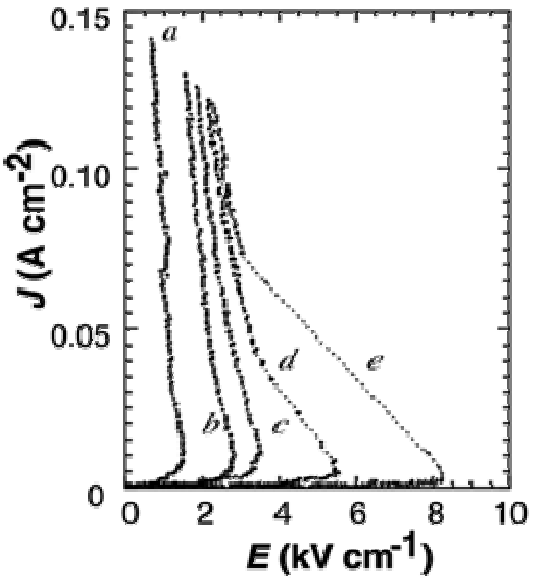

Figure 3.1.8. The negative differential resistance characteristics of K-TCNQ at different temperatures (curve a, 300 K; curve b, 280 K; curve c, 230 K; curve d, 180 K; curve e, 180 K).

If the hole-doping for K-TCNQ occurs, these characteristics will be changed. Thus, in this study, the modification of the electrical properties by the contact doping is investigated.

3.2. Experimental

3.2.1. Crystal growth of K-TCNQ

Potassium iodide was commercially obtained and used without further purification. TCNQ was also commercially obtained and used after the purification by recrystallization. 38 mg of potassium iodide (Wako chemical Co. Ltd.) and 30mg of TCNQ (Wako chemical Co. Ltd.) were each dissolved in 20 mL of hot acetonitrile and then the solutions were mixed. 2 or 3 days later, red purple block crystals of K-TCNQ were obtained. All the steps were performed in the ambient conditions.

3.2.2. Contact doping using F_4TCNQ powder

F_4TCNQ was commercially obtained and used without further purification. For the contact doping, powder F_4TCNQ was conjugated on the surface of the K-TCNQ single crystal. This state was kept for a couple of days in an incubator with setting the temperature at 313 K. After that the powder F_4TCNQ was removed by an air duster, and then the hole-doped crystal surface was obtained. The sheet resistance was measured along the TCNQ stacking direction in a hole-doped crystal surface using a two-probe method. Gold paste (Tokuriki Chemical Research Co. Ltd.) was used to connect two gold wires (ϕ = 20 μm) at opposite ends of a plate crystal surface. The resistance was measured by KEITHLEY 6487 PICOAMMETER/VOLTAGE SOURCE. The

temperature dependence was measured using a closed cycle cryostat system.

3.2.3. Time dependence of the electrical conductivity

The time dependence of the current was measured in an incubator keeping the F_4TCNQ conjugated on the surface of the K-TCNQ single crystal, setting the temperature at 313 K. The sheet resistance was measured along the TCNQ stacking direction using a two-probe method. Gold paste (Tokuriki Chemical Research Co. Ltd.) was used to connect two gold wires (ϕ = 20 μm) at opposite ends of a plate crystal surface. The resistance was measured by KEITHLEY 6487 PICOAMMETER/VOLTAGE SOURCE.

3.2.4. Optical measurements

Accompanied by the hole-doping, a new complex can be generated on the surface of the K-TCNQ crystal. According to 3.1.1, the complex could be K-F_4TCNQ. To confirm this, IR spectra were measured at room temperature using a Spectrum One FT-IR spectrometer (Perkin Elmer Instruments) for five samples; neutral TCNQ, neutral F_4TCNQ, K-TCNQ, the mixture of K-TCNQ and F_4TCNQ (this corresponds to the contacted states of the two components), and K-F_4TCNQ.

3.2.5. The surface images of the interface

The surface SEM images were scanned by a JSM-6700FT field emission microscope. The samples were mounted on a sample holder using adhesive carbon tape. An accelerating voltage 5.0 kV was applied during the observations. An as-grown K-TCNQ surface and a hole-doped surface were compared to each other. The

hole-doped surface was fabricated in the same way as described in section 3.2.2. Using AFM (Nanocute, SII Co. Ltd.) equipped with an ARTCAM-300MI-HHS-WOM unit (ARTRAY Co. Ltd.), the conductivity of the hole-doped surface was measured. The method for the measurement is described in Fig. 3.3.6. At first, a F_4TCNQ single crystal was contacted on the surface of a K-TCNQ crystal, and then it was removed after about 15 minutes. Since the F_4TCNQ single crystal is smaller than the K-TCNQ, both the as-grown surface and the hole-doped surface can be observed, and the boundary is easily distinguished. Crossing the boundary, the current was measured. The applied voltage was 0.01V.

3.2.6. Electrical conductivity measurement at high temperature

To investigate the effects of the hole-doping on the structural phase transition, the sheet resistance was measured in the high temperature region of 300-420 K using a home-made thermostat system along the TCNQ stacking direction in a hole-doped crystal surface using a two-probe method. Gold paste (Tokuriki Chemical Research Co. Ltd.) was used to connect two gold wires (ϕ = 20 μm) at opposite ends of a plate crystal surface.

3.2.7. Current-Voltage characteristics measurement at low temperature region

To investigate the effects of the hole-doping on the negative differential resistance characteristics, the current-voltage (*I*-*V*) characteristics were measured with a load resistor of 2 MΩ connected in series with KEITHLEY 6487 PICOAMMETER / VOLTAGE SOURCE as a voltage source and a current detector along the TCNQ stacking direction in a hole-doped crystal surface using a two-probe method at 300 K,

260 K, 240 K, respectively in a closed cycle cryostat system. Gold paste (Tokuriki Chemical Research Co. Ltd.) was used to connect two gold wires (ϕ = 20 μm) at opposite ends of a plate crystal surface.

3.3. Results and discussion

3.3.1. Phenomena observed by the contact doping

The results of the conductivity measurement performed as described in 3.2.2 are shown in Figure 3.3.1.

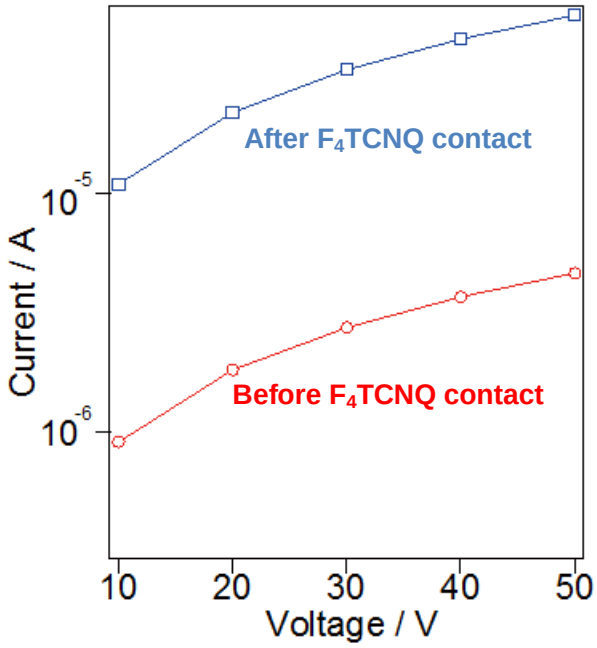

Figure 3.3.1. The current measurement of the K-TCNQ surface before and after the F_4TCNQ powder contact.

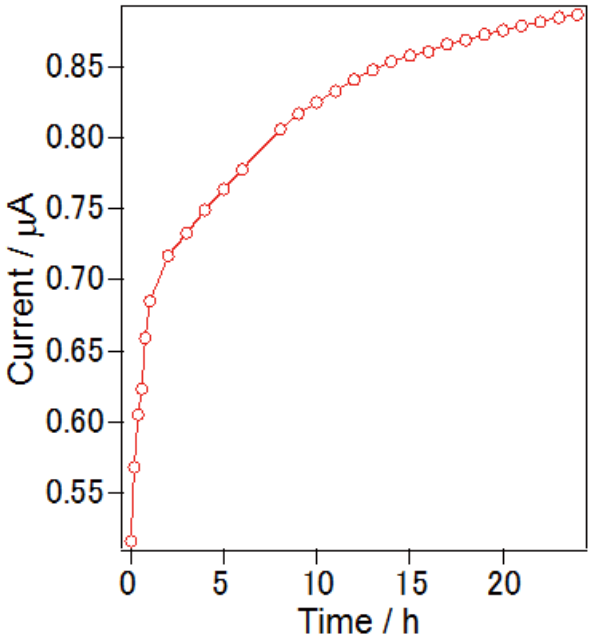

Figure 3.3.2. The time dependence of the current of the K-TCNQ surface after the F_4TCNQ contact.

After the F_4TCNQ powder contact, the sheet resistance of the K-TCNQ surface became one order of magnitude smaller than that of the as-grown K-TCNQ. Thus, the increase of the conductivity by the F_4TCNQ powder contact was confirmed. Keeping the powder of F_4TCNQ contacted on the surface of K-TCNQ, the time-dependence of the current was measured at 313 K, applying 1 V. The results are shown in Figure 3.3.2. Soon after the conjugation of the F_4TCNQ powder, the current of the interface got rapidly increased, and then gradually increased. As described in 3.1.1, when the acceptor is contacted, in some cases the complex with the contacted acceptor is formed at the interface, while in other cases is not. If the complex with the contacted acceptor was not formed, the current would increase instantly because it would not take any time for the carrier injection. Figure 3.3.2 indicates that the current increase requires a certain period of time, suggesting the complex formation. Therefore, in this case it is

considered that a new complex is generated on the K-TCNQ surface. In addition, the current was not decreased after the F_4TCNQ powder was removed. This also supports the complex formation.

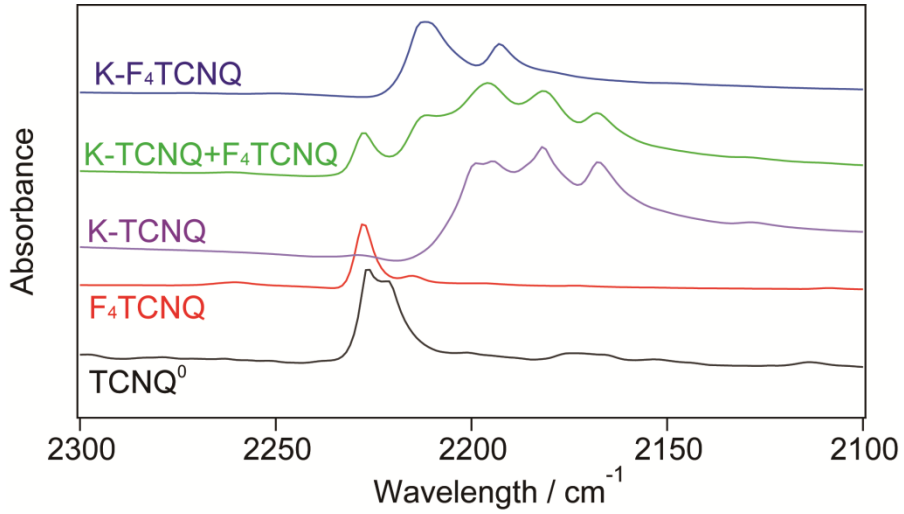

Figure 3.3.3. The IR spectra of $TCNQ^0$, F_4TCNQ^0, K-TCNQ, the mixture of the K-TCNQ and F_4TCNQ, and K-F_4TCNQ.

The complex formation was confirmed by measuring the IR spectra. Figure 3.3.3 shows five spectra of neutral TCNQ, neutral F_4TCNQ, K-TCNQ, the mixture of K-TCNQ and F_4TCNQ, which corresponds to F_4TCNQ-contacted K-TCNQ, and synthesized K-F_4TCNQ. For TCNQ and F_4TCNQ, the CN stretching vibrational peak is located around 2200 cm^{-1}, and the position shifts depending on the charge of molecule [7, 8]. Thus, the spectra around 2200 cm^{-1} were focused on. For the spectrum of the mixture of K-TCNQ and F_4TCNQ, a new peak appears at ca. 2215 cm^{-1}, which is different from either that of K-TCNQ or that of neutral F_4TCNQ. Since this peak was found to be identical with that of K-F_4TCNQ, it was confirmed that the hole-doping to K-TCNQ by contacting F_4TCNQ accompanied by the formation of K-F_4TCNQ.

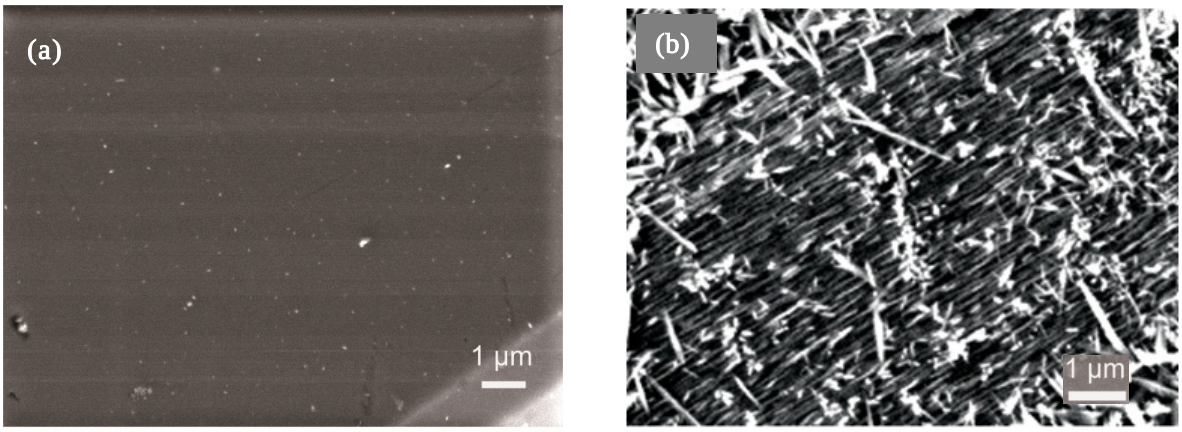

Figure 3.3.4. The SEM images of the K-TCNQ surface; (a) before the F_4TCNQ contact, (b) after the F_4TCNQ contact.

The SEM images of the surface state of the K-TCNQ were obtained before and after the F_4TCNQ powder contact, as shown in Figure 3.3.4. The left image is before F_4TCNQ contact, and the right one is after the F_4TCNQ powder contact. For the latter, fine crystals exist with random orientations. Among these crystals K-F_4TCNQ must be included, but the crystals of neutral F_4TCNQ may co-exist, which could not be completely removed by an air duster. Taking a closer look at the K-TCNQ crystal surface of the right image, lines along the specific direction can be seen. This direction corresponds to the TCNQ stacking direction. One possible explanation of the formation of the aligned needle crystals on the surface of K-TCNQ is that K-F_4TCNQ is formed along the TCNQ stacking direction.

Based on the above data, the mechanism of the hole-doping can be described as Figure. 3.3.5. The hole-doping occurs by means of the electron transport from $TCNQ^{-1}$ to neutral F_4TCNQ. As a result, hole doped TCNQ anion turns neutral. In this region K^+ lose their counterpart and then are pulled toward F_4TCNQ^- at the surface of the

K-TCNQ, leading to the formation of K-F_4TCNQ (Figure 3.3.5).

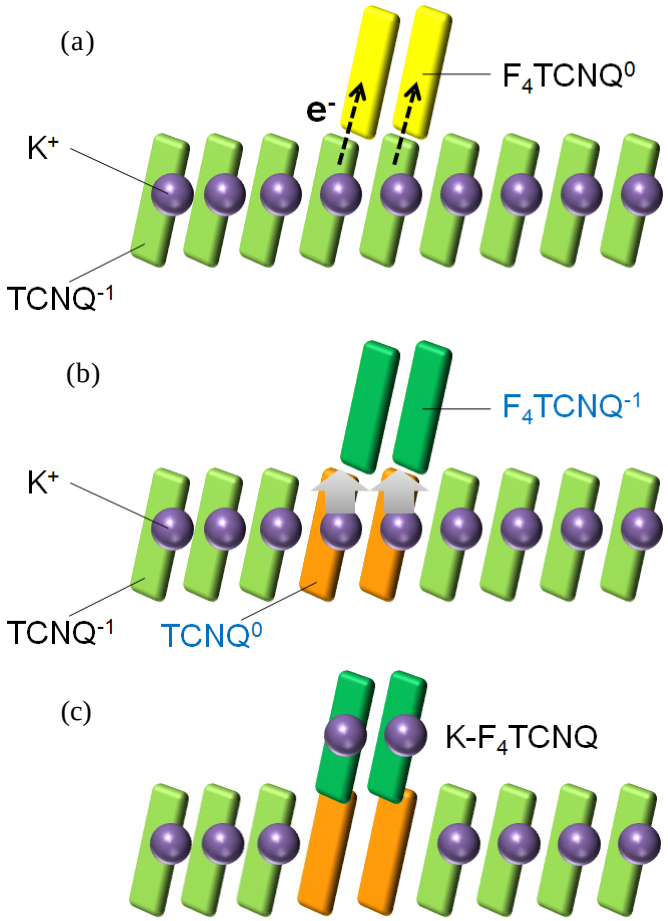

Figure 3.3.5. The mechanism of the hole-doping for K-TCNQ. (a) The hole-doping by F_4TCNQ for $TCNQ^{-1}$. (b) As a result of hole-doping, $TCNQ^0$ and F_4TCNQ^{-1} are generated. (c) K^+ is extracted to the surface, leading to the formation of K-F_4TCNQ.

3.3.2. The charge transport mechanism by the contact doping

Secondly, let us consider about the enhancement of the conductivity by F_4TCNQ contact. For F_4TCNQ contacted K-TCNQ surface, the path of the current can be "K-F_4TCNQ formed on the K-TCNQ surface" or "Charge-doped K-TCNQ surface". Since when K-F_4TCNQ was prepared individually the crystallinity of K-F_4TCNQ was

very poor, it was impossible to compare the electrical conductivity of K-F_4TCNQ with that of K-TCNQ in a single-crystal state. In a compressed-pellet state, K-F_4TCNQ and K-TCNQ were found to have almost the same resistivity, about 1500 Ω cm. Thus, the conductivity enhancement by F_4TCNQ contact is highly likely not due to "K-F_4TCNQ formed on the K-TCNQ surface" but "Charge-doped K-TCNQ surface". To confirm this, the conductivities of the two were measured using a conductive AFM.

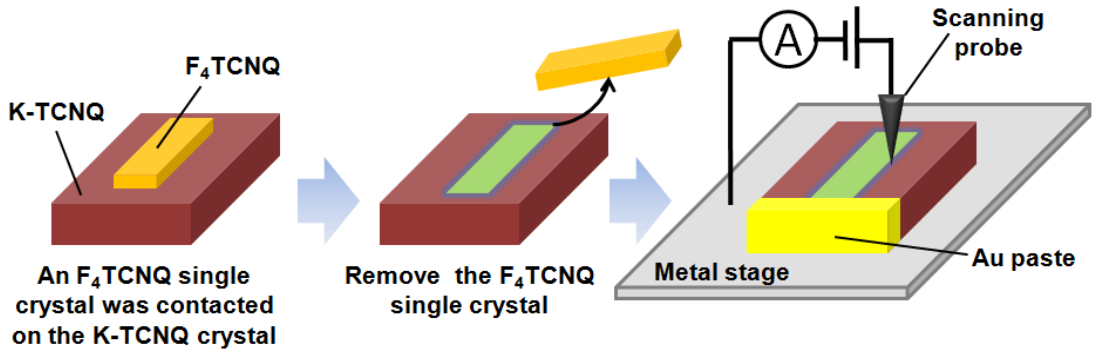

Figure 3.3.6. The fabrication of the boundary between K-TCNQ and K-F_4TCNQ, and the method to measure the current around the boundary.

For conductive AFM, the current passing through the sample is measured between the probe as one electrode and the metal stage as the other electrode (Figure 3.3.6). If the sample is organic compound or semiconducting material, the sample must electrically connect with the metal sample stage. In this measurement, an F_4TCNQ single crystal was contacted on a larger K-TCNQ single crystal, and then removed after around 15 minutes. After the removal of F_4TCNQ, K-F_4TCNQ was formed on the K-TCNQ surface, and a clear boundary between K-F_4TCNQ and K-TCNQ was obtained because of the single crystal to single crystal contact. The K-TCNQ surface including the boundary was held on the metal sample stage by gold paste. Then the

surface current was measured from the K-F_4TCNQ region to K-TCNQ region, across the boundary. The applied voltage was 0.01 V.

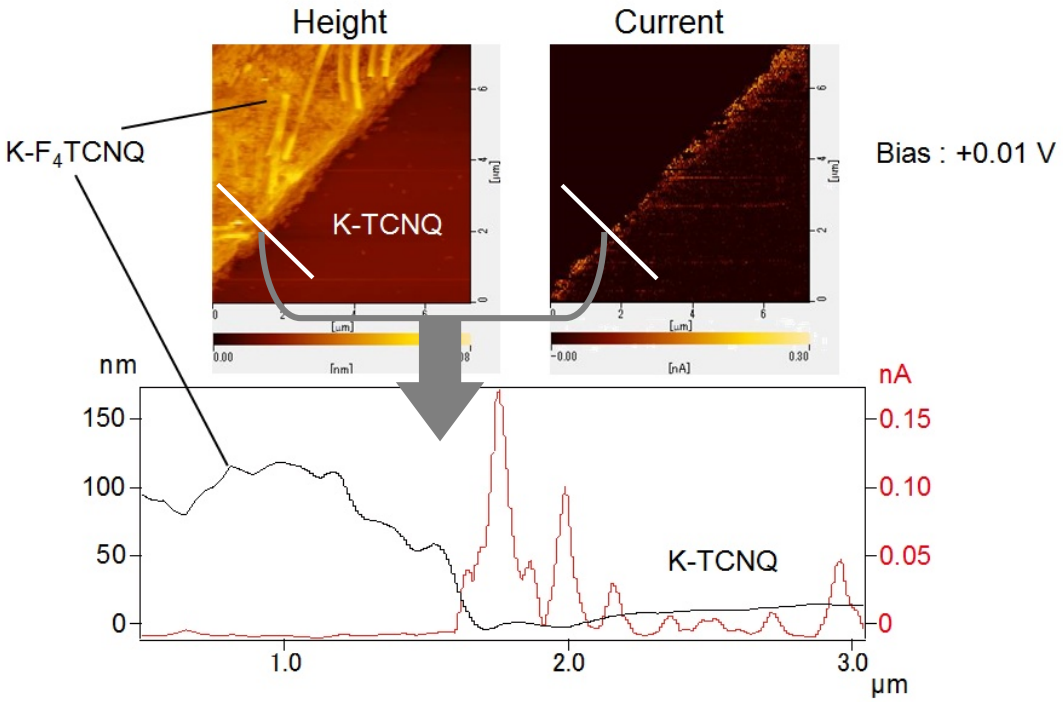

Figure 3.3.7. The AFM images of the height and the current across the boundary between K-F_4TCNQ and K-TCNQ (described as a white line in the current image).

The results of the measurements are shown in Fig. 3.3.7. The left image represents the height, in which brighter region is higher region. The higher region and the lower region are obviously separated by the boundary, thus the former is considered to correspond to the newly formed K-F_4TCNQ crystals and the latter corresponds to the flat as-grown K-TCNQ surface. The right image represents the amount of current passing between the probe and the Au paste through the surface of the sample, in which brighter region represents higher current region. According to this image, it is clear that the current did not flow in the K-F_4TCNQ region, but flow mainly at the boundary. The increased current at the boundary is also described in the graph below, in which the

height and the current along the white lines in the images are plotted across the boundary. From these data, “Charge-doped K-TCNQ surface” is proved to be the path of the current.

3.3.3. Effects on the phase transition by the contact doping

On the charge-doped K-TCNQ surface, not only the conductivity but also the original physical properties can be modified. As described in 3.1.2, K-TCNQ has structural phase transition at 395 K, and shows the negative differential resistance characteristics in the low temperature region. Therefore, the corresponding physical properties were investigated in this study.

First of all, the effect of the hole-doping for the structural phase transition is discussed. The hole-doping by F_4TCNQ contact is performed only on the surface of K-TCNQ. Thus it is impossible to compare the hole-doped crystal structure with the as-grown. An alternative method is required to estimate the hole-doping effect. For as-grown K-TCNQ, the overlap integral between LUMOs of TCNQ in low temperature region is different from that in high temperature region. This difference corresponds to the change of the band gap between the valence band and the conduction band, i.e. the change of the activation energy for conduction. The activation energy can be calculated from the slope of the plot of ln R vs. 1 / T [8]. Therefore it is expected that the slope of the plot will be different between low temperature region and high temperature region. If the overlap integrals in the TCNQ column change at the transition point, it can be detected by the resistivity or sheet resistance measurement. Thus the temperature dependence of the sheet resistance was measured for the F_4TCNQ contacted K-TCNQ surface and as-grown K-TCNQ surface.

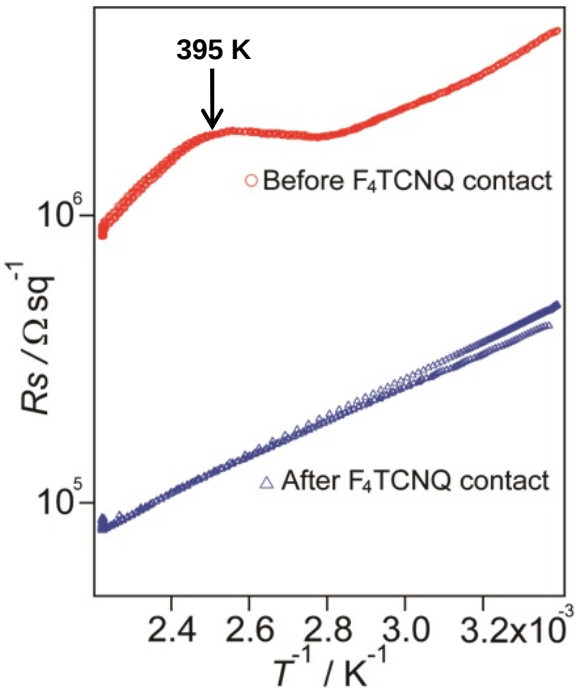

Figure 3.3.8. The sheet resistance of the K-TCNQ surface before and after the F_4TCNQ contact.

The results of the measurements are shown in Figure 3.3.8. For the surface of as-grown K-TCNQ, a peak was found at 395 K, and the slope of the plot changed at the peak. This clearly reflects the change of the band gap at the structural phase transition point. On the other hand, for the surface of K-TCNQ after the contact of F_4TCNQ, the peak which existed before F_4TCNQ contact disappeared, and the slope became constant. Based on these data, it is considered that the structural phase transition does not occur for the hole-doped surface.

The reason for the extinction of the phase transition will be discussed using the spin model of the TCNQ column. For as-grown TCNQ, the structural phase transition from a dimerized TCNQ structure to a uniform one occurs due to that the lattice vibration energy exceeds the on-site Coulomb repulsion energy by increasing temperature [9].

From the opposite point of view, i.e. if the structural phase transition is considered to be from the high temperature to low temperature, the lattice changes because of the transformation of TCNQ column from a uniform structure to a dimerized one. In this case, the energy gain for the spin dimerization exceeds the energy loss for the lattice transformation, leading to the structural phase transition. This type of phase transition is called spin-Peierls transition [10]. The hole-doping by the F_4TCNQ contact is performed for the low temperature phase, in which the TCNQ column dimerizes. Under such conditions, some TCNQ anions change to neutral, which may become a kink in the dimerized lattice. The neutral TCNQ at the kink can receive an electron from the adjacent TCNQ anion dimer, and in that case the position of the neutral TCNQ and the TCNQ anion will turn around. Providing this phenomenon continuously occurs, the neutral TCNQ can be regarded as a soliton [11], which is propagated through the TCNQ column, as described in Fig. 3.3.9. As a result, the lattice elastic energy gained by transformation to the uniform column is considered to be no longer dominant, thus the structural phase transition to the uniform column will not occur.

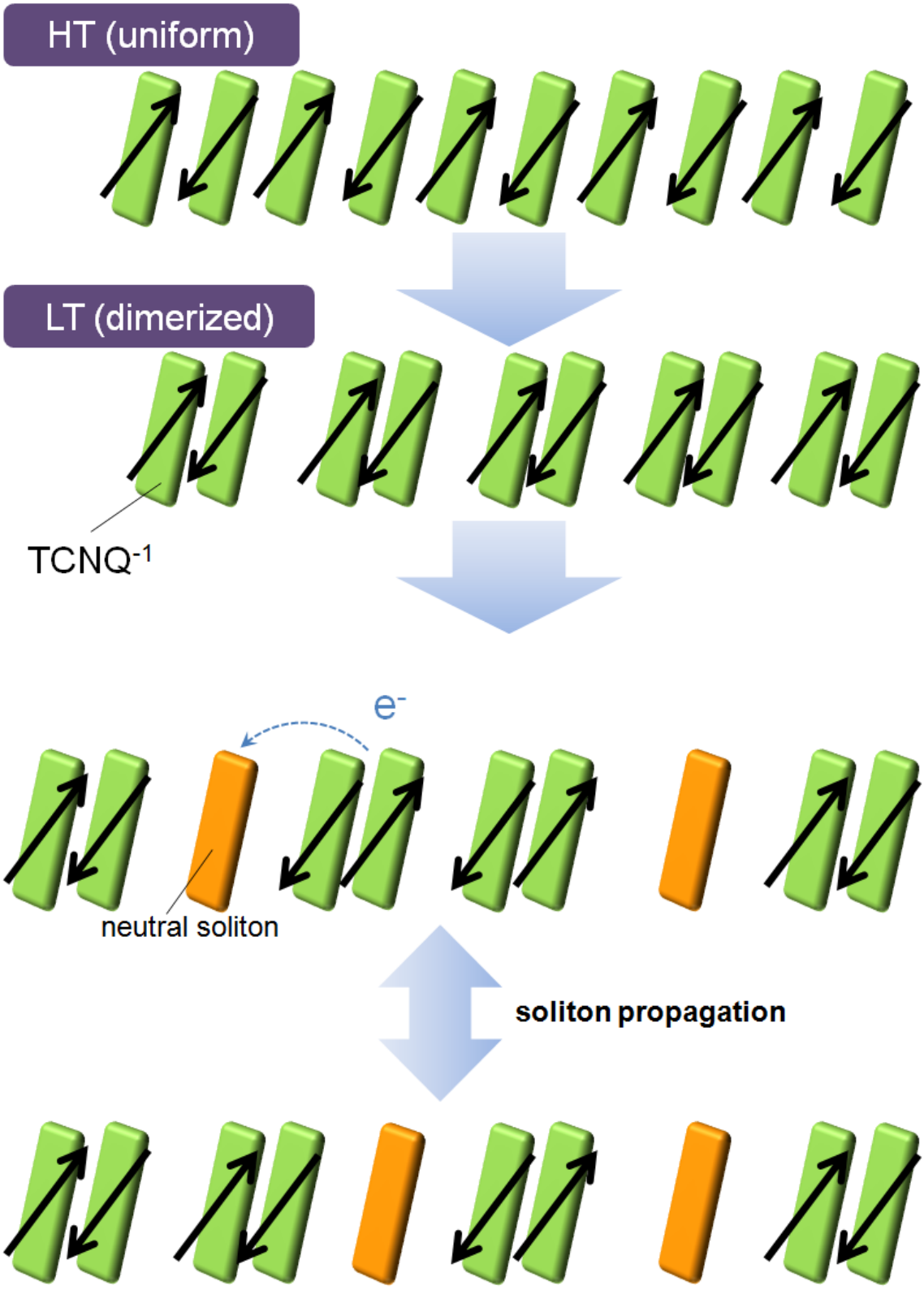

Figure 3.3.9. The effects of the hole-doping for the TCNQ column in K-TCNQ.

3.3.4. Effects on the current-voltage characteristics by the contact doping

Secondly, the effects of the hole-doping for the current-voltage characteristics at the low temperature region will be discussed. The results of the current-voltage measurements before and after the F_4TCNQ contact are shown in Fig. 3.3.10. For these two graphs, the same color indicates the results of the measurements at the identical temperature. Compared with the as-grown K-TCNQ, the negative differential resistance characteristics appear at the lower applying voltage after the F_4TCNQ contact.

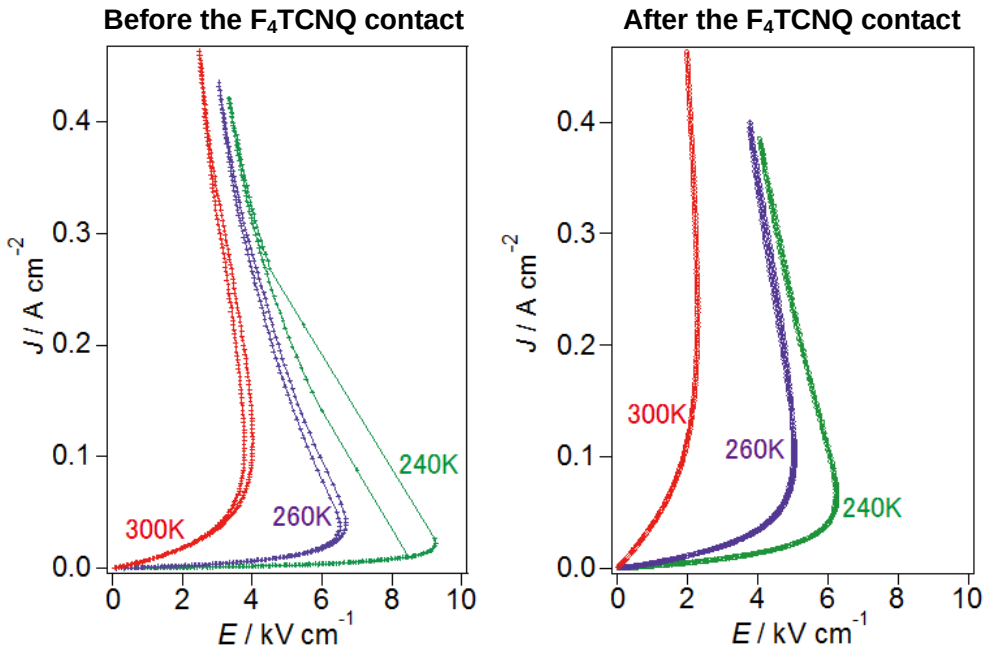

Figure 3.3.10. The negative differential resistance characteristics of the K-TCNQ surface before and after the F_4TCNQ contact.

This phenomenon will be discussed with the spin model of the TCNQ column, in the same way as the discussion about the conducting behavior at the high temperature region (Figure 3.3.11). At the low temperature region, TCNQ column is dimerized and each TCNQ molecule possesses one spin before the hole-doping. The negative differential resistance characteristics of the K-TCNQ can be explained as a result of

getting over the energy barrier for the electron transportation between TCNQ dimers; namely, the collapse of the insulation breakdown [12]. Before the hole-doping, the energy barrier is extremely large because of the Coulomb repulsion. After the hole-doping, partially generated neutral TCNQ will become solitons, by which the energy barrier will decrease, leading to transformation to the highly conducting state at lower applying voltage.

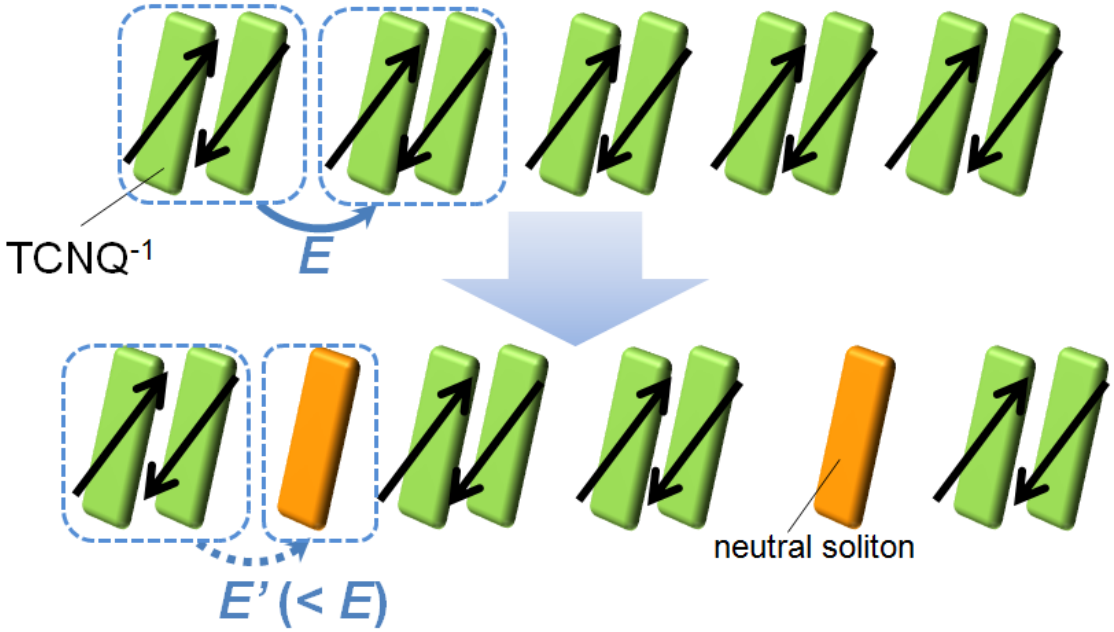

Figure 3.3.11. The effects of the hole-doping for the energy barrier against the electron transportation.

Providing hole is the major carrier and the hole densities before and after the F_4TCNQ contact are p and p', respectively, the doping amount of the hole will be p'- p. Since the mobility of K-TCNQ is unknown, the doping amount cannot be calculated precisely. Nevertheless, it can be approximately estimated from the J-E plot. Suppose the hole mobility of K-TCNQ is μ, p and p' can be described as follows.

$$p = \frac{J}{q\mu E}$$

$$p' = \frac{J'}{q\mu E'}$$

where J and E are the current density and the electric field before the F_4TCNQ contact, and J' and E' are the current density and the electric field after the F_4TCNQ contact [14]. Therefore, the doping amount of the hole can be described as follows.

$$p' - p = \frac{1}{q\mu}\left(\frac{J'}{E'} - \frac{J}{E}\right)$$

Considering only the linear part of individual *J-E* plot, *J/E* and *J'/E'* corresponds to the slope of the plot (σ), and the values were 9.36×10^{-6} and 4.26×10^{-5} S cm^{-1}, respectively. From these calculations, the doping amount of the hole is

$$\frac{1}{1.602\times10^{-19}\times\mu}(4.26\times10^{-5} - 9.36\times10^{-6}) = \frac{2.07\times10^{14}}{\mu}(\mathrm{cm}^{-3}).$$

For K-TCNQ, the electron density is the same as the number of TCNQ anions per 1 cm^3, and the value is 3.56×10^{21} cm^{-3}. If one assume μ = 1.0 cm^2 V^{-1} s^{-1}, the doping level is estimated to be 5.8×10^{-6} %.

3.4. Summary and conclusion

As a method for modifying the electric conductivity by changing the electronic structure of the organic material with already-known crystal structure, the contact doping is novel, simple, and effective for the carrier injection. In this study, the hole-doping for the TCNQ anion radical salt, K-TCNQ, was performed by F_4TCNQ contact. As a result, the sheet resistance of the surface of K-TCNQ decreased one order. From the SEM image and the IR spectra, K-F_4TCNQ was found to generate on the surface of K-TCNQ after the F_4TCNQ contact. On the basis of these results, the mechanism of the hole-doping was discussed. There existed two candidates for the current path; carrier doped K-TCNQ surface and K-F_4TCNQ generated on the contact interface. According to the conductive AFM data, current did not flow through the

K-F_4TCNQ, but through the surface of the carrier doped K-TCNQ.

Originally K-TCNQ has characteristic physical properties; the structural phase transition from band insulator to Mott insulator at 395 K, and the negative differential resistance characteristics in the low temperature region. The hole-doping by F_4TCNQ contact also affected these physical properties. On the hole-doped surface of K-TCNQ, the structural phase transition did not occur and the negative differential resistance characteristics appeared with lower applying voltage. This is because the neutral TCNQ molecules generated in the K-TCNQ surface after the hole-doping behave as solitons, through which the electron transportation becomes feasible. As described above, both the hole-doping for the two-component ionic system and the carrier doping for the crystal with segregated stack structure were accomplished for the first time, and then the modification of the electron transporting property at the contact interface after the hole-doping was discussed in detail.

References

[1] Alves, H.; Molinari, A. S.; Xie. H.; Morpurgo. A. F. *Nature mater*, **2008**, 7, 574-580.

[2] Takahashi, Y.; Hayakawa, K.; Naito, T.; Inabe, T. *J. Phys. Chem. C*, **2012**, 116, 700-703.

[3] Takahashi, Y.; Hayakawa, K.; Takayama, K.; Yokokura, S.; Harada, J.; Hasegawa, H.; Inabe, T. *Chem. Mater*, **2014**, 26, 993-998.

[4] Takahashi, Y.; Nakagawa, Y.; Hayakawa, K.; Inabe, T.; Naito, T. *Appl. Phys. Lett*, **2012**, 101, 103303.

[5] Konno, M.; Ishii, T.; Saito, Y. *Acta Crystallogr*, **1977**, B33, 763-780.

[6] Kumai, R.; Okimoto, Y., Tokura, Y. *Science*, **1999**, 284, 1645-1647.

[7] Okamoto, H.; Tokura, Y.; Koda, T. *Phys. Rev. B*, **1987**, 36, 3858-3867.

[8] Chappell, J. S.; Bloch, A. N.; Bryden, W. A.; Maxfield, M.; Poehler, T. O.; Cowan, D.O. *J. Am. Chem. Soc*, **1981**, 103, 2442-2443.

[9] Yasuzuka, S.; Murata, K.; Arimoto, T.; Kato, R.*J. Phys. Soc. Jpn*, **2007**, 76, 033701 (1-4).

[10] Itoh, K.; Itoh, H.; Naka, M.; Saito, S.; Hosako, I.; Yoneyama, N.; Ishihara, S.; Sasaki, T.; Iwai, S.*Phys. Rev. Lett*, **2013**, 110, 106401 (1-5).

[11] Hase, M.; Terasaki, I.; Uchinokura, K. *Phys. Rev. Lett*, **1993**, 70, 3651-3654.

[12] Ikezi, H.; Taylor, R. J.; Baker, D. R.*Phys. Rev. Lett*, **1970**, 25, 11-14.

[13] Sze, S.M. *Semiconductor Devices, Physics and Technology*, 2nd ed., John Wiley & Sons, Inc., New York, **2002**; 117-124.

[14] Sze, S.M. *Semiconductor Devices, Physics and Technology*, 2nd ed., John Wiley & Sons, Inc., New York, **2002**; 53-54.

Chapter 4.Overall summary and concluding remarks

In this study, controlling the electronic structure of the TCNQ anion radical salts was performed by two different approaches. One was the structural approach by modifying the size of the component, and the other was the electronic structure control by carrier injection. For the former, in Chapter 1, it was stated that the relative size of the components was considered to give some influence on the stoichiometry for two-component system. Thus, a series of the crystals in which the size of the components was systematically tunable was subjected to the study. As the candidate, TCNQ anion radical salts with dication components were selected. For the second approach, as mentioned in Chapter 1, the injection barrier, which has been the problem for the conventional carrier doping was pointed out. As an alternating method, the contact doping was proposed for the carrier doping. TCNQ Anion radical salts were again selected candidate as the object of the study.

Of the two approaches mentioned above, the former was described in Chapter 2. Initially, the features and the validity of the designed dications were explained. The variation of the stoichiometries and the degree of the overlap integrals of the TCNQ columns by the systematical size change of the dications were investigated and discussed. The stoichiometry was found to be changed from the more favorable 1:4 to an alternative 1:3 depending on the size of the dication. To explain the change of the stoichiometry, the concept of the “effective dication length” was proposed. Namely, a certain range of the effective dication length existed to form the stoichiometry of 1:4. In the case of too large or too small dication, the stoichiometry could change from 1:4 to 1:3.

Focusing on the dication-TCNQ salts with the same 1:4 stoichiometry, the more disadvantageous conformation of the dication occurred when the salts contained the larger dication, leading to the more obvious distortion of the TCNQ column. The diversity of the multimerization of the TCNQ columns was reflected in the magnetic behaviors. On the other hand, the decrease of the dication size induced the change of the stoichiometry (to 1:3) and the inclusion of the solvent. For the solvent-included salt, (C1BPy)$(TCNQ)_4CH_3CN$, the distortion of the TCNQ column was not obvious owing to its small dication size, resulting in the highest conductivity in this series. For more increase of the conductivity, a more uniform and a greater magnitude of overlap in the TCNQ column were required, thus the dication with more rigid alkyl chain was proposed for future works.

In Chapter 3, the contact doping was performed as a novel approach for the modification of the conductivity of the organic crystals. First of all, the concept and the previous studies of the contact doping were described, and then the possibility of the hole-doping for the two-component system and the carrier doping for the segregated structure, which has not been demonstrated, were discussed. To attain both of them, the hole-doping for K-TCNQ by contacting F_4TCNQ was carried out.

As a result, the increase of the conductivity was observed on the K-TCNQ crystal surface after the F_4TCNQ contact. In this case, both the carrier injection and the complex-formation occurred, and the carrier injected K-TCNQ surface was proved to be the conduction path from the conductive AFM image. Therefore, the hole-doping was confirmed and its mechanism can be elucidated. Owing to this hole-doping, some TCNQ anions changed to neutral TCNQ molecules. The neutral TCNQ molecules were considered to propagate through the TCNQ columns as solitons, causing the extinction

of the structural phase transition and the negative differential resistance characteristics at the lower applying voltage. At the present stage, the doping amount was not clarified, and no strategy of the control of the doping level was proposed. If the doping level could be systematically controlled in future, the electronic functionality of organic materials would be more valuable and more widely applicable.

Overall, the modification of the electronic properties of TCNQ anion radical salts was achieved by the structural design and the carrier doping. Thus TCNQ anion radical salts can be regarded as good objects of organic electronics and can be applied for a variety of research.